Graz University of Technology

Master Thesis

Institute of Applied Geosciences

Graz University of Technology

Contact-free measurement of rock–mass structures

Method comparison

Author

Dipl.-Ing. Carmen Jandrisevits

Advisor

Univ. Ass. Prof. Dr.phil Kurt Klima

Graz, May 2012

Erklärung

Ich erkläre an Eides Statt, dass ich die Arbeit selbstständig und ohne fremde Hilfe verfasst, andere als die angegebenen Quellen nicht benutzt und die den benutzten Quellen wörtlich oder inhaltlich entnommenen Stellen als solche erkenntlich gemacht habe.

Graz, Mai 2012

Acknowledgments

I have to thank my thesis advisor Univ. Ass. Prof. Dr.phil Kurt Klima. His continuous guidance, valuable suggestions, generous help and encouragement are greatly acknowledged.

Furthermore my thanks go to my co – advisor Ao. Univ.-Prof. Dr.phil Franz-Josef Brosch for his support, especially for providing me a wide range of appropriate literature.

This thesis is dedicated to my parents without whom I would not have been able to achieve so much: For their endless love, unremitting support and never – ending encouragement through my entire life.

Abstract

Remote sensing techniques are gaining increasingly importance in geological investigations trying to complete or even replace traditional geological field methods. Digital photogrammetry provides 3D measuring of geological structures. At the quarry site Angenofen in Western Styria photogrammetry and traditional field mapping techniques were applied for structural assessment of rock face. Photogrammetric investigations were performed with digital photogrammetry package ShapeMetriX^{3D} which provides geological mapping facilities. Discontinuities were quantified in terms of their orientation and roughness. With both methods comparable results were achieved. Roughness investigations have shown that discontinuity surface roughness strongly influences the variability of discontinuity orientations. Different imaging configurations were tested for modeling of the exposed rock face. Models generated from stereo image pairs taken from ideal imaging positions deliver reliable results for orientation measurements. For configurations where imaging parameters (base length, distance) lie wide above tolerance range models were not completely reconstructed.

Kurzfassung

Fernerkundungsmethoden werden vermehrt zur geologischen Kartierung eingesetzt. Sie stellen eine Alternative bzw. einen Ersatz für die klassische geologische Aufnahme dar. Digitalphotogrammetrie ermöglicht die dreidimensionale Messung von geologischen Strukturen. Zur Erfassung des Trennfächengefüges im Steinbruch Angenofen in der Weststeiermark kamen klassische Verfahren der geologischen Kluftaufnahme und auch terrestrische Photogrammetrie zum Einsatz. Photogrammetrische Untersuchungen wurden mit dem bildbasierten Messsystem ShapeMetriX^{3D} durchgeführt. Die Untersuchungen dienten der Ermittlung der Trennflächenorientierungen und der Oberflächenbeschaffenheit der Trennflächen. Mit beiden Methoden konnten vergleichbare Ergebnisse erzielt werden. Untersuchungen der Trennflächenrauigkeiten ergaben, dass die Streuung kleinräumiger Orientierungsmessungen auf den Einfluss der Oberflächenrauigkeit zurückzuführen ist. Photogrammetrische Aufnahmen wurden aus unterschiedlichen Positionen und Perspektiven zur Felswand vorgenommen. Modelle, die aus Stereobildern mit idealer Aufnahmegeometrie zur Felswand generiert wurden, liefern zuverlässige Resultate für Trennflächenorientierungsmessungen. Für Konfigurationen bei denen Aufnahmeparameter (Basislinie, Distanz) beträchtlich über den angegebenen Toleranzen liegen wurden die Modelle nicht mehr vollständig dargestellt.

CONTENTS

1. INTRODUCTION

Describing the orientations of the geological structures is an integral part during any engineering geological investigations. Mapping of visible structural features that are found on outcrops or excavated faces is currently done with traditional field measurement methods including geological compass, tape measures and field notes of observations on site.

In recent years, new innovative technologies for geological in situ – data collection and analyzing methods have progressed. Techniques, such as photogrammetric survey (e.g. Gaich, 2006), laser scanning (e.g. Feng, 2006) and total station (e.g. Feng, 1999) have been tested for structural mapping of rock faces.

These techniques should provide rapid spatial measurements of discontinuity orientation and location and therefore give more comprehensive information on geological outcrops. Surveying of inaccessible rock cuts is facilitated and user's safety is increased due to that there is no need of direct measurements on hazardous sites. Beside of all these positive effects indirect measurement methods have some limitations especially when taking also physical properties of discontinuities into account or when there are no suitable conditions for data capturing on site.

In this thesis the traditional geological method and the close range terrestrial photogrammetry are compared with respect to data acquisition and evaluation, reliability, influencing factors and limitations for the purpose of orientation measurements.

Therefore a case study of a plattengneis quarry near Stainz in the Western Styria, Austria has been carried out where traditional discontinuity measurement techniques and terrestrial photogrammetric surveys with the product ShapeMetriX^{3D} were used for discontinuity orientation measurements.

2. STUDY AREA

2.1 GEOGRAPHICAL OVERVIEW

Geographically the investigation area is located in West Styria (Austria) in the eastern part of the Koralpe. The Koralpe makes up a natural N – S orientated border between the provinces of Styria and Carinthia. The area is bordered to the north by the Pack mountain saddle, to the south by the Soboth mountain saddle. To the west the Koralm complex is limited by the Styrian basin, to the east it is bordered by the Lavant basin. Investigations were carried out in the Angenofen rock quarry (Fig. 2) adjacent to Stainz in the southwest of Graz (Fig. 1).

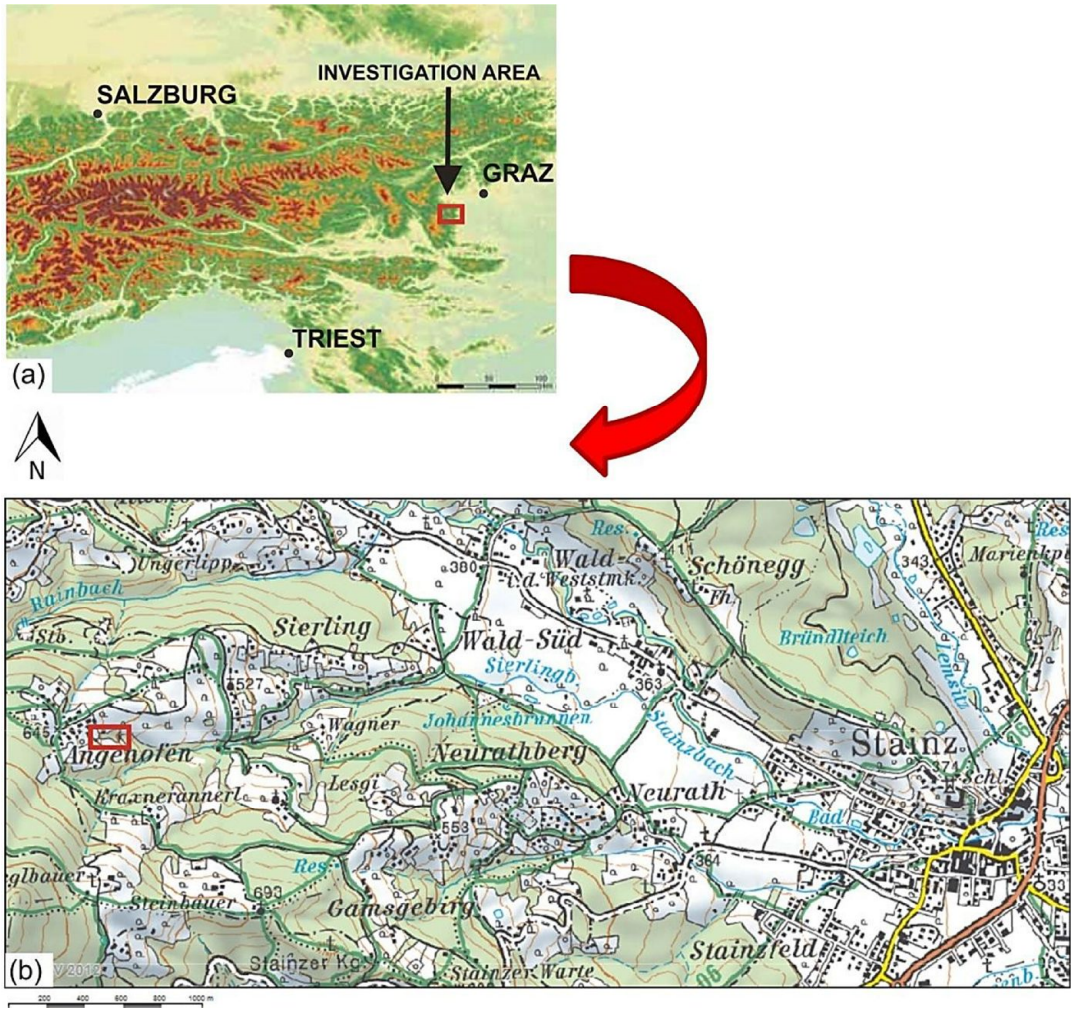

Figure 1: (a) Map of Austria; (b) topographic map of Austria – section of ÖK 200 (BEV) showing the investigation area outlined by red rectangles in Fig 1(a) and Fig 1(b)

Figure 2: Angenofen rock quarry near Stainz

2.2 GEOLOGICAL OVERVIEW

The Koralm Complex is surrounded by distinct faults and shear zones along it's margins. In particular, low-angle normal faults form the northeastern and southern margins of the Koralm Complex (Pischinger et al, 2008a). The western margin of the Koralm Range is formed by a NNW-trending strike slip fault, the Lavanttal fault (Fig. 3). This fault is part of the Pöls-Lavanttal fault system which is still regarded active with dextral sense of shear (Reinecker, 2000; Reinecker and Lenhardt, 1999). Near its southern termination the Lavanttal fault cuts and offsets the Periadriatic lineament by about 20 km (Frisch et al, 2000). The eastern boundary of the range is characterized by sets of normal faults which, for the major part, are hidden below Neogene sediments (Pischinger et al. 2008a). The boundary between the crystalline and the tertiary rocks generally trends approx. NNE to SSW, tracing the given morphology of the crystalline basement (Pischinger et al, 2008b).

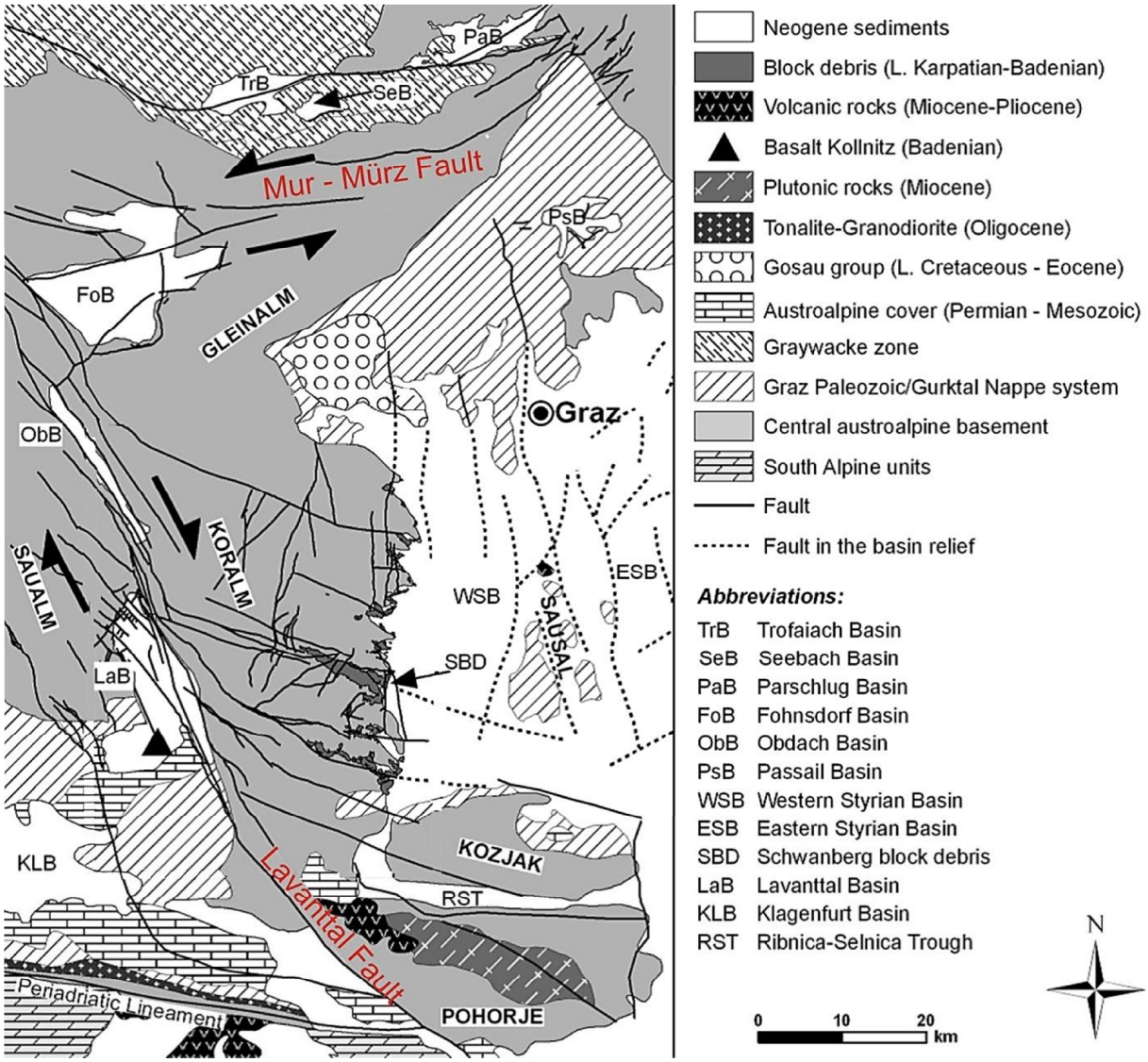

Figure 3: Tectonic map of Koralm region (modified after Pischinger et al, 2008a)

The area investigated belongs geologically to the Plattengneis of the Koralm complex .The Koralm complex is part of the Koriden Unit within the Middle _ Austroalpine nappe complex in the Eastern Alps incorporated into the Austroalpine nappe stack during the Lower Cretaceous (Kurz et. al, 2002). During the collisional event a number of regionally important shear zones have been developed, i.e. the Plattengneis shear zone which represents one of the major shear zones in the Eastern Alps. The Plattengneis shear zone is about 250-600 m thick and extends over almost 1000 km^2 in the Koralpe region along the eastern margin of the Alps (Putz et al, 2006). This major mylonite zone consists of predominantly metapelitic sediments and was synchronously metamorphosed and deformed in the Cretaceous (Thöni & Jagoutz, 1992). A Plattengneis is thick mylonic gneiss of dark-grey to grey-brown color. At the Angenofen quarry the Stainzer Plattengneis is exposed.

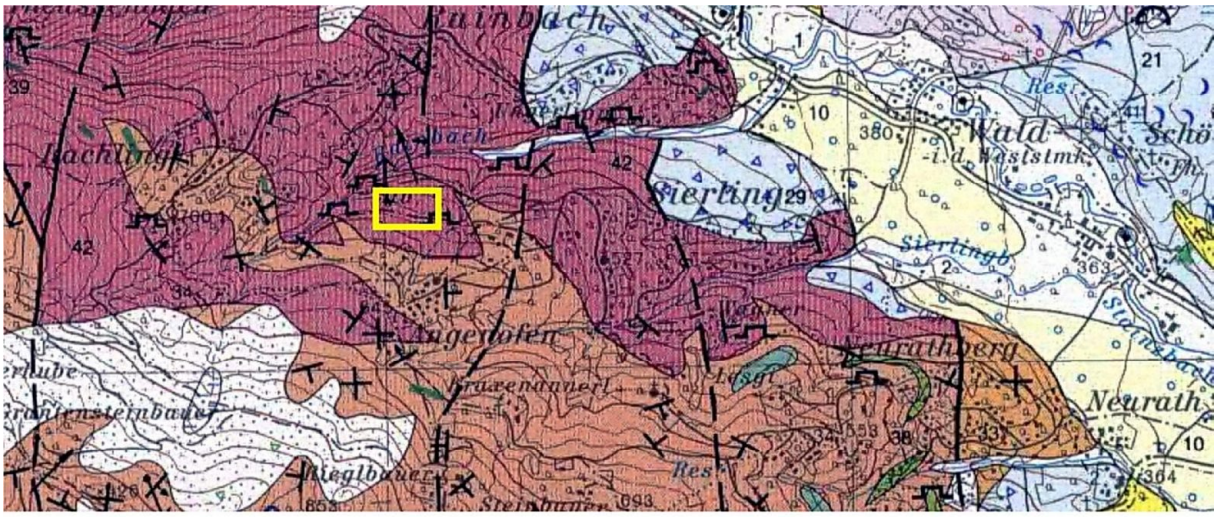

Figure 4: Section from geological map Mo. P. 189 (ÖK 500); investigation area outlined with yellow rectangle

3. METHODS

3.1 QUANTIFYING DISCONTINUITY ORIENTATION

The investigation of geological outcrops involves the evaluation and characterization of discontinuity orientation measurements. After Priest and Hudson (1976) a geological discontinuity, is a mechanical break or physical interruption of a continuous rock material. A discontinuity typically appears in a rock outcrop as a fault, joint, bedding surface, or as a damage fracture. The orientation of discontinuities is expressed as the dip and dip direction (or strike) of the surface (Fig.5).

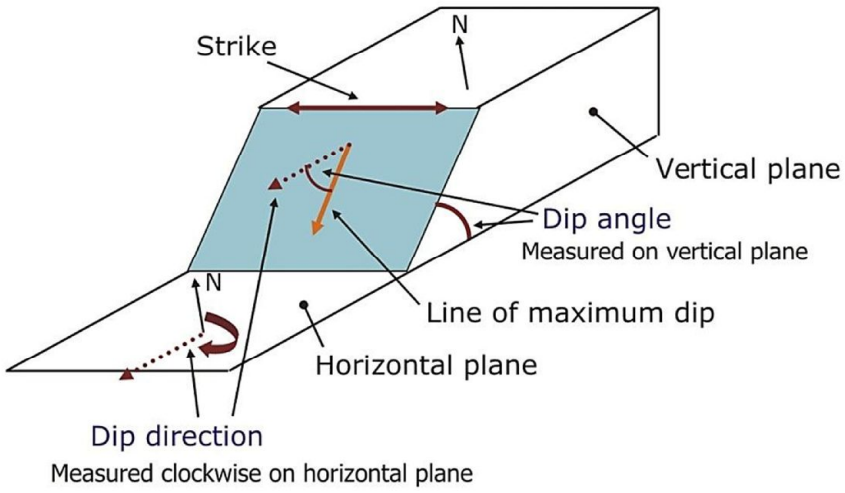

Figure 5: Illustration of strike, dip direction and angle of dip (modified after ZHAO J, 2008)

The dip of the plane is the maximum angle of the plane to the horizontal, while the dip direction is the direction of the horizontal trace of the line of dip, measured clockwise from north (Duncan, Wyllie & Mah, 2004). Strike is an alternative mean of defining the orientation of a plane. It is the angle between the Northern direction and the trace intersection of the discontinuity plane with a horizontal reference plane (Giani, 1992). The strike direction is perpendicular to the dip direction. It is defined as the compass direction, relative to north, of the line formed by the intersection of a planar feature with an imaginary horizontal line.

3.1.1 TRADITIONAL DISCONTINUITY MAPPING

A traditional way of discontinuity mapping at rock faces is typically performed by using a geological compass and documentation by recording measurements and information on a notebook.

3.1.1.1 DATA ACQUISITION USING A GEOLOGICAL COMPASS

The geological compass has been in use since 1896. It is not just a compass, it combines the principles of a surveyor's compass, a prismatic compass, a clinometer, a hand level and a plumb (Kliche, 1999). Geological compasses according to the measuring method of Prof. Dr. Clar facilitate mapping because they allow measuring of dip and dip direction in one single operation. Here the dip is read off a graduated scale on the lid hinge, while the dip direction is read of the compass scale that is graduated from 0° to 360° (Fig. 6).

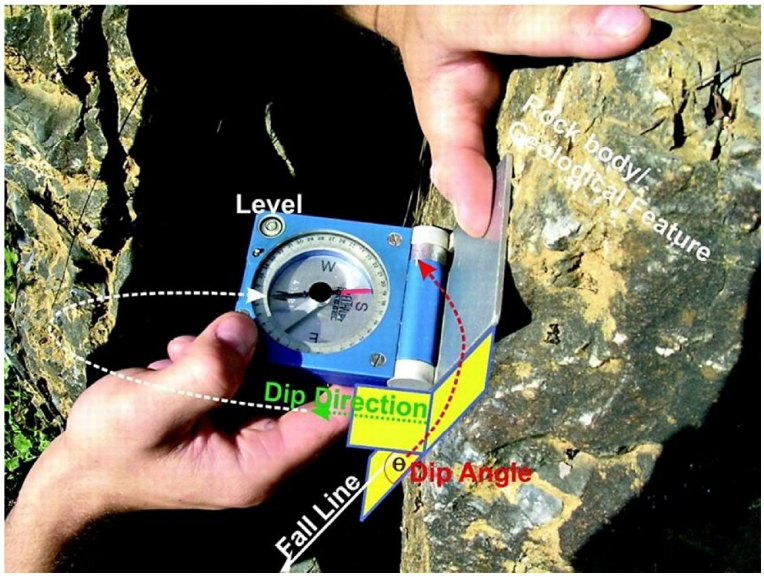

Figure 6: Measuring of dip direction and dip angle with a geological compass (after Zobl et al, 2009)

Since geological compasses are attracted to the magnetic North Pole measurements have to be corrected for the magnetic declination. The declination is the angle, in degrees between the magnetic North Pole and the true North Pole. Values of magnetic declination vary across the earth and also over time.

3.1.1.2 DATA PROCESSING AND ANALYSIS

3.1.1.2.1 HEMISPHERICAL PROJECTION

Orientation measurements can be represented graphically using hemispherical projections. These techniques offer a graphical method for analyzing three – dimensional problems involving planes, lines and points in a convenient and easily interpreted two – dimensional form. The method is often referred to as stereographic projection, which literally means the projections of solid or three – dimensional drawings (Priest, 1985).

The stereographic projection consists of a reference sphere in which its equatorial plane is horizontal, and its orientation is fixed relative to north (Fig. 7). Planes are positioned in an imaginary sense so that the axis of the feature passes through the center of the reference sphere. There are many different types of hemispherical projections, whereby in structural geology the equal area (Schmidt) lower – hemisphere projection is the most common one. Equal – area means that the area on the surface of the reference is projected as an equal area on the stereonet.

The intersection of the feature with the lower half of the reference sphere defines a unique line on the surface of the reference hemisphere. For a plane, this intersection with the reference sphere in a circular arc called a great circle, while for a line the intersection with the reference sphere is a point (Duncan, Wyllie & Mah, 2004).

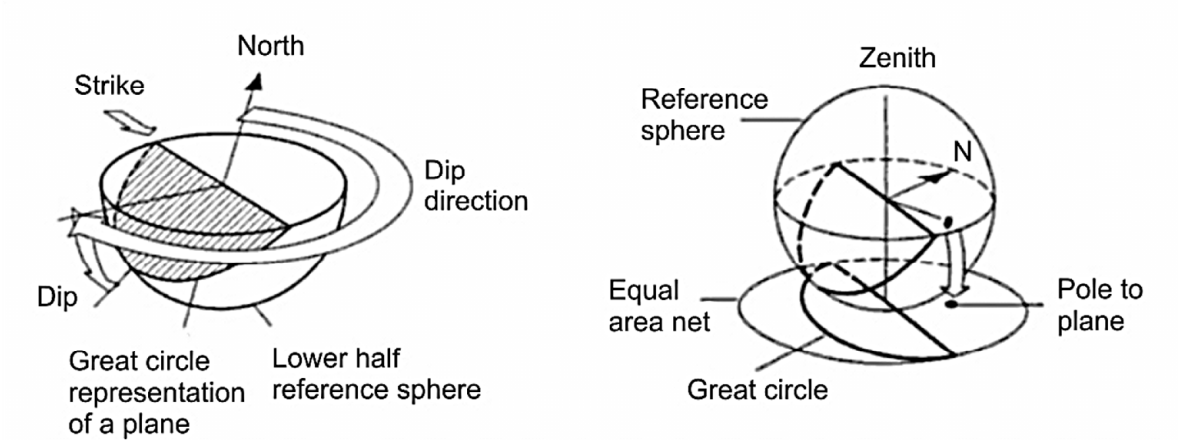

Figure 7: Hemispherical projection (modified after Duncan, Wyllie & Mah, 2004)

An alternative means of representing the orientation of a plane is the pole to the plane. The pole is point on the surface of the reference sphere that is pierced by a radial line in a direction normal to the plane. The use of poles facilitates the analysis of a larger number of planes compared with the use of great circles (Duncan, Wyllie & Mah, 2004).

3.1.1.2.2 PLOTTING POLES ON STEREONETS

There are many different types of hemispherical projections, whereby in structural geology the equal area (Schmidt) lower – hemisphere projection is the most common one. Figure 7 shows the stereonet for the equal – area stereographic lower hemisphere projection. The North Pole of the stereonet is the upper point where all lines of longitude converge. The South Pole is the equivalent lower convergence point. Lines that run from the North to South Pole of the stereonet are termed great circles and are analogous to lines of longitude on a globe. Circular arcs that run east-west are termed as small circles. The dip direction scale (0 - 360°) around the periphery has the zero mark at the bottom of the vertical axis and the 180° mark is at the top of end (Wyllie and Mah, 2004). A dip is counted along the east - west direction from the outer radius of the stereonet towards the point of interest. Pols can be plotted by hand on a stereonet or stereographic computer programs can be used to generate a plot

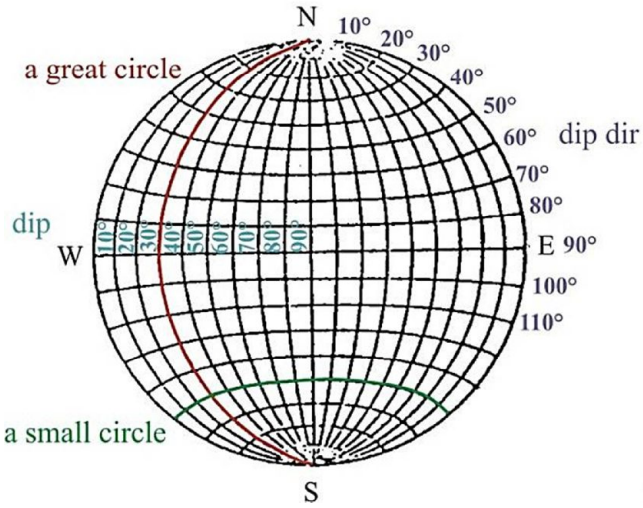

Figure 8: Equal - Area Stereonet

The manual procedure for plotting a pole on a stereonet using dip direction and dip is described briefly (Fig. 8). Therefore a plane dipping 50° in the dip direction of 150° is assumed (Hoek and Bray, 1981).

Step 1:

- A tracing paper is positioned over the stereonet by means of a centre pin
- As a first step the north is marked on the tracing paper
- The dip direction of 130° is measured clockwise around the outer circumference of the stereonet and marked on the tracing paper

Step 2:

- To project the dip angle the tracing paper is rotated until the marked dip direction lies on the west – east line of the stereonet.
- Then the dip angle of 50° is counted from the outer circle of the stereonet towards the center and marking on the tracing paper.
- A great circle is drawn to the to this corresponding dip angle
- The pole to a plane is 90 degrees away from every point on the great circle. The location of the pole can be found by counting 90 degrees from the great circle along the west –east line.

Step 3:

- The tracing paper is rotated back to the original position again so that the north mark of the tracing paper coincides with north mark on stereonet. The final appearance of the great circle and the pole representing a plane dipping at 50° in a dip direction of 130° is illustrated.

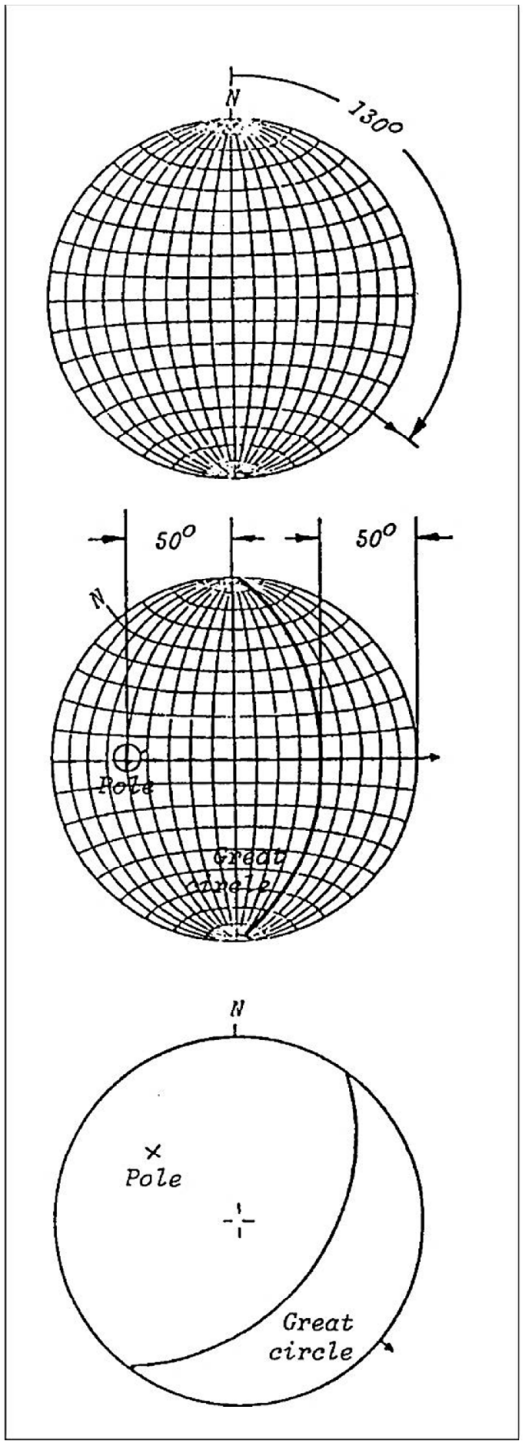

Figure 9: Stereographic plots (after Hoek and Bray, 1981)

3.1.1.2.3 STATISTICS OF ORIENTATION DATA

The purpose of plotting poles on stereonet is to find concentrations of poles and to conclude on preferred orientations. Plotted poles can be grouped into clusters or sets in order to perform

statistical analysis. The Fisher distribution also called spherical normal distribution is used to describe the distribution of orientation data (Wallbrecher, 1986). It is assumed that orientation measurements are distributed about some true "value "with rotational symmetry (Priest, 1993).

The probability density function of the Fisher distribution has the following form (Fisher 1993):

$$f(\theta,\varphi) = \frac{k}{4\pi.\sinh k}.exp[k\ (\sin\theta\ \sin\alpha\ \cos(\emptyset-\beta\ ) + \cos\theta\ \cos\alpha\ )]\ .\sin\theta$$

where α is the θ - pole coordinate (latitude) of the main orientation direction, β is the $\emptyset$ - pole coordinate (longitude) of the main direction and k is the concentration parameter

Wallbrecher (1986) has suggested some statistical measures that can be used to describe the dispersion of orientation data:

Concentration

describes the concentration around the mean orientation. A larger K equals a stronger concentration. For K equals 0 the orientations describe a uniform distribution.

Degree of Preferred Orientation

is a measure for the alignment of orientation, whereby 0 percent stands for uniform distribution and 100 percent means parallel alignment.

Cone of Confidence

Is used to calculate the probability P, that the actual mean pole of a discontinuity set lies outside the cone measured from the calculated mean pole

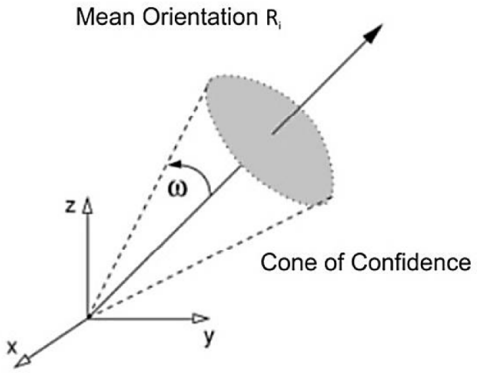

Figure 10: Cone of Confidence

Measures for cone of confidence are spherical variance and spherical aperture.

Spherical Variance

is defined as

$$S^* = \frac{n - |R_i|}{n}$$

where n is the sample size and $|R_i|$ is the length of the mean resultant orientation

Spherical Aperture

the confidence angle around the mean direction is known as spherical aperture. The spherical aperture for the Fisher distribution is equivalent to the standard deviation of the Gaussian normal distribution.

$$\omega = \arcsin\sqrt{2\frac{1-\frac{1}{n}}{k}}$$

a confidence level for the deviator angle needs to be established for this to define the allowable deviation in dip direction and dip angle from mean. In addition, measures of reliability need to be included.In the stereolplot the cone of confidence plots as the small circle and the spherical aperture as the larger circle around the main orientation (Fig. 11).

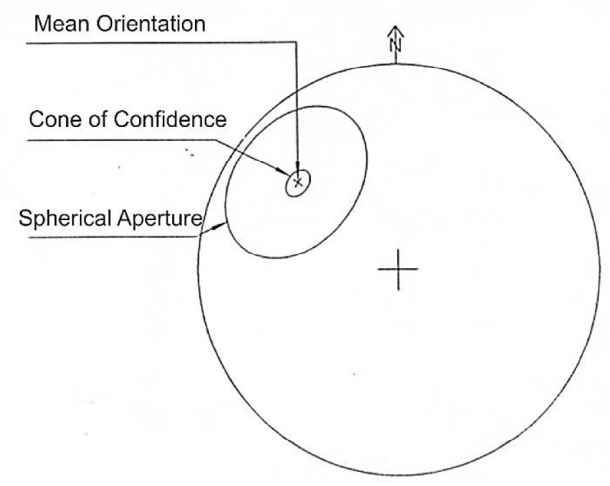

Figure 11: Statistical Orientation Analysis – Parameters (after Wallbrecher, 1986)

3.1.2 PHOTOGRAMMETRIC SYSTEM ShapeMetriX^{3D}

3.1.2.1 PHOTOGRAMMETRY BACKGROUND

Close range terrestrial digital photogrammetry provides an alternative approach to traditional discontinuity mapping that allows to measure orientations of inaccessible or hazardous rock faces and it facilitates the collection of a large number of measurements which is prerequisite for statistical analysis of orientations data. The system ShapeMetriX^{3D} which was developed by the Austrian company 3G Software & Measurement provides the facility of indirect discontinuity mapping using close range terrestrial photogrammetry. It is designed to acquire surfaces with three-dimensional images based on the principle of stereoscopic photogrammetry. Stereoscopic photogrammetry is a science of obtaining three – dimensional information from two or more overlapping two – dimensional images. If taking pictures from at least two different positions (viewpoints) of the same object of interest, the intersection of the lines of sight from two matching image points determines a point in 3D space (Fig. 12). There are several important variables involved in photogrammetry. First of all it requires the essential knowledge of to the camera interior and exterior orientation parameters. The interior orientation determines the internal geometry of the camera, including location of the principal point, focal length and lens geometric distortion characteristics in order to define the camera projection system. For this purpose, a special type of camera, called a metric camera with completely known internal characteristics was developed. The exterior orientation of the camera defines its position (location in space) and its orientation (viewing direction). In order to calculate the exterior orientation control points, i.e. points with known coordinates are necessary.

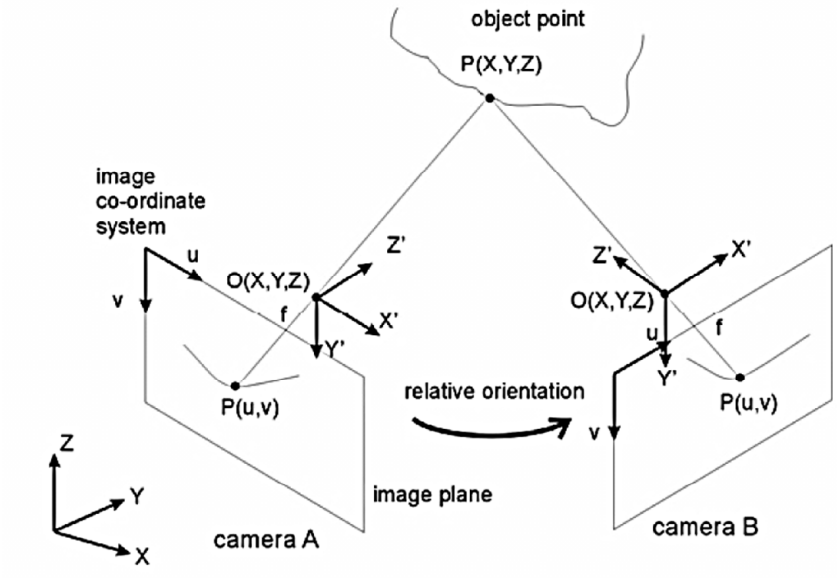

Figure 12: Stereoscopic principle (after Gaich, 2006)

ShapeMetriX^{3D} combines methods and technology of Digital Photogrammetry and Computer Vision. Digital photogrammetry is concerned with capturing, processing and analyzing digital input data, i.e. digital images or scanned photographs. Methods and tools developed in Computer Vision prove to be useful for increasing the degree of automation in digital photogrammetry (Schenk et al, 1991). ShapeMetrix3D is based on this approach providing highly automated 3D – modeling. The relative orientation of the images among each other is determined automatically and there is no need of control points anymore. Pattern matching algorithms are used to match characteristics from the images.

3.1.2.2 DATA AQUISITION

For data aquisition off-the- shelf digital single reflex (DSLR) cameras pre - calibrated by software from 3G Software & Measurement are used in order to take two pictures from different standpoints. The virtual connection between the two camera standpoints is referred to as baseline and the SMX documentation recommends base – lengths of about 1/5 -1/8 of the mean imaging distance. However the chosen base - length is compromise due to the fact that the theoretically achievable accuracy can be increased by larger base – lengths on the one hand when regarding the intersection angle of image rays and intersection precision, but on the other hand larger base – length also lead to greater perspective changes between corresponding images and therefore complicates the automatic identification of corresponding points (Fig. 13) (Gaich, 2006).

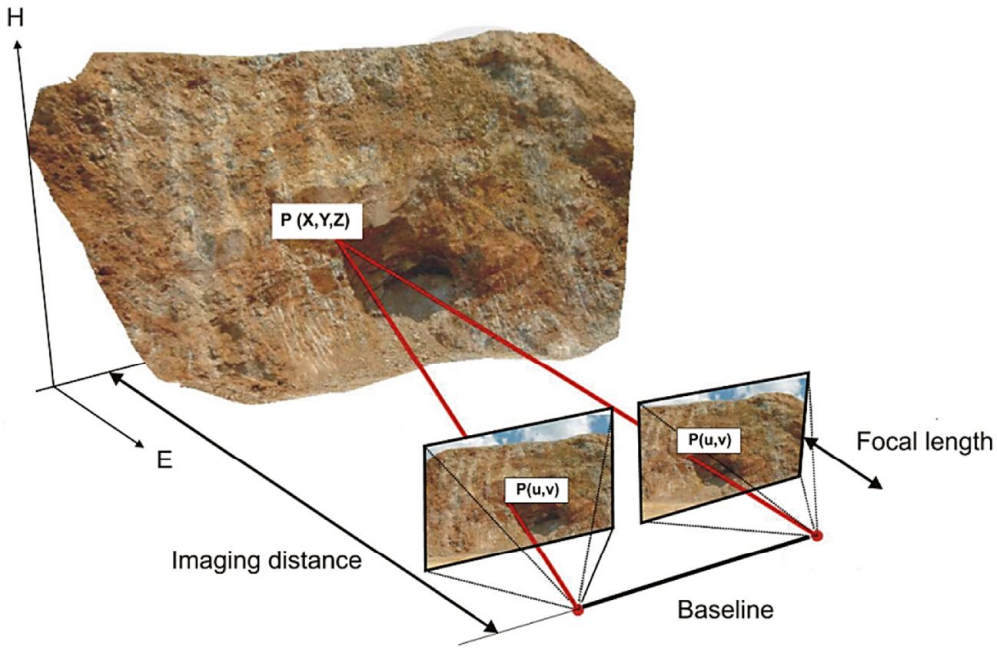

Figure 13: Principle of three – dimensional modeling by means of stereo photogrammetry (ShapeMetrix^{3D} User Manual)

If measurements should be related to a local coordinate system a vertical range pole has to be established in the imaging area. For a coarse referencing to north a manual compass reading can be used. In case of measurements related to a global coordinate system so – called reference points are placed somewhere in the image scene. The three- dimensional coordinates of these points are determined by means of geodetic measurements i.e. total station or Real Time Kinematic GPS.

3.1.2.3 DATA PROCESSING

After data acquisition on site the digital images are transferred on a standard PC where the SMX software is used for further processing to create 3D – models. The modeling process is mostly done automatically, however some “hands – on” and user interaction is required. It starts with the user specifying the two overlapping images defining the stereo image pair, the used camera and lens and the region of interest on the images (Gaich, 2006). A generic 3D image is generated by wireframe triangulation and automatic image matching. Figure 14 illustrates the progression from a 3D point cloud to a 3D image:

A: A point cloud is a series of points with grayscale information that represent points on the outcrop surface (prominent rock mass structures are partly visible in the 3D point cloud)

B: The wirframe is created when all measuring points are connected among each other to reconstruct the outcrop surface (Delaunay – Triangulation is used to create a Triangulated Irregular Network (TIN)).

C: A 3D image is generated by merging of wireframe and digital image

For developing metric 3D images scaling and orientating is crucial. This is done by identification and measurement of conjugate points which is the most fundamental process in photogrammetry (Lennox, 2009). Within the SMX software two methods are realized for incorporating scaling and orientation information measurements. For matching of conjugate image points the “Normalizer” or “Referencer” mode is used. “Normalizing” refers to local orientated models and the user has to mark the range pole targets representing vertical in the image with a known length in both images. For “Referencing” at least three surveyed reference points are needed. The points have to be selected on the corresponding image pair and the surveying points can be incorporated either as local (x, y, z) or global (E, N, elevation) coordinates. Metric 3D – models can be used for geometric measurements. When larger areas have to be analyzed distinct models can be combined into mosaics.

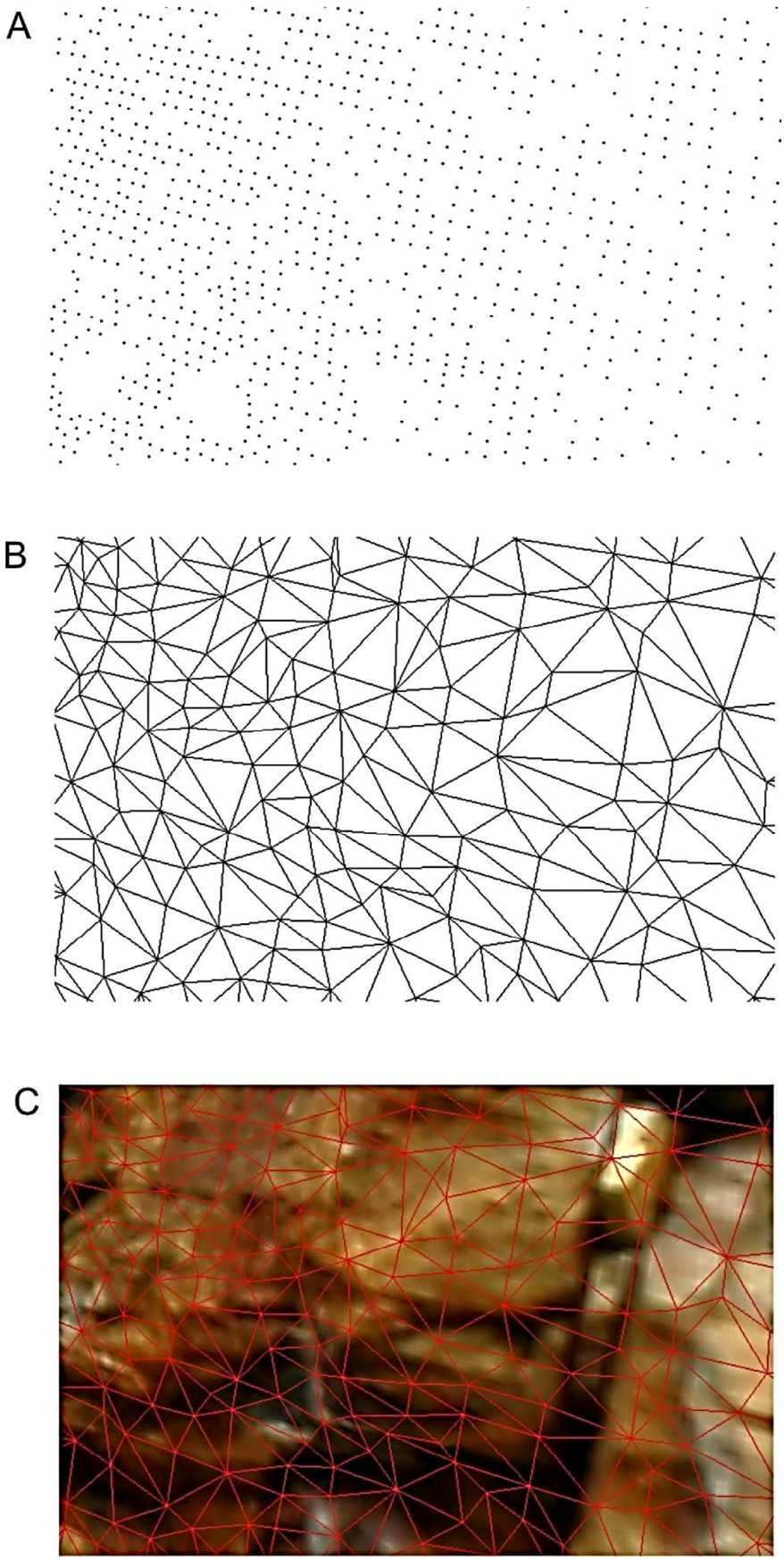

Figure 14: Modeling procedure (A: 3D point cloud, B: wireframe , C: 3D image)

3.1.2.4 DATA ANALYSIS

3D images can be viewed from any designated perspective and measurements are carried out interactively with the help of a computer mouse and a special kind of cursor. The cursor can be placed freely on a designated position on the 3d image and when moving the cursor measurement values are instantaneously updated and shown in a status bar.

The SMX software provides different kind of tools to carry out metric measurements (lengths, distances and areas), orientation measurements, scan line mapping and linear profile measurements.

In this thesis discontinuity orientation measurements are of particular interest.

Individual orientation measurement

Orientations can be measured at arbitrary locations. Therefore this position has to be marked by the cursor and an arrow is set which shows the upward normal vector of the measured orientation. If the arrowhead is visible the surface is dipping towards the observer, whereas a visible arrow end indicates an overhanging surface (Fig. 15). The SMX software calculates the mean orientation of the surface which is made up of the triangles underlying the base disc. The base disc size depends on the point density and determines the minimum size of an orientation measurement (ShapeMetriX^{3D} User Manual). The closer surface points are to each other the smaller is the area patch for orientation measurements.

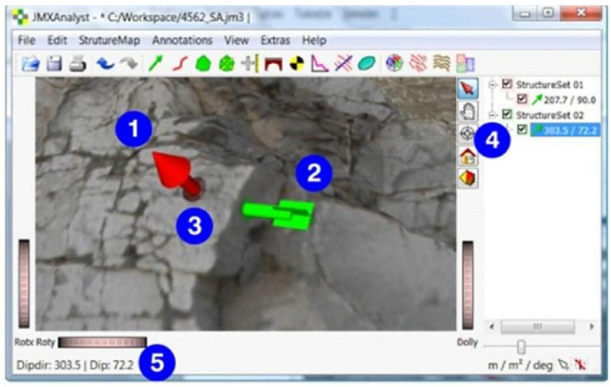

1 Arrow points in direction of the upward surface normal vector
2 Tail indicates overhang
3 Base disc corresponds to compass flap - minimum patch
4 Dip direction and dip angle in StructureList
5 Dip direction and dip angle in status bar

Figure 15: Individual orientation measurement (ShapeMetriX^{3D} User Manual)

Area orientation measurements

For an area orientation measurement a closed polyline on the 3D surface is drawn (Fig. 16) . The software calculates then the mean orientation values dip direction and dip angle of the marked surface (ShapeMetrix^{3D} User Manual).

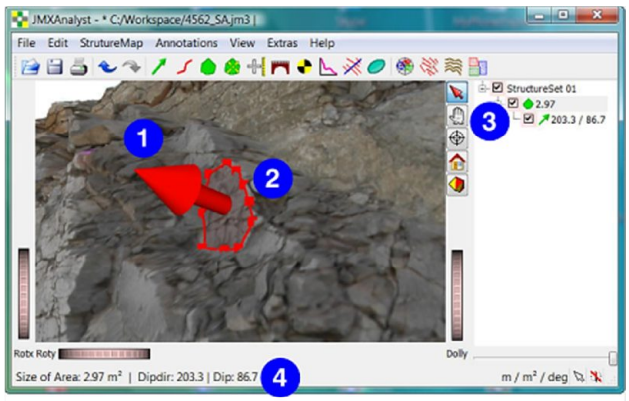

1 Mean upward normal vector of the area
2 Clicked polygon follows the surface of the 3D image
3 Size of area (rough) with assigned mean dip direction and dip angle in the StructureList
4 Display of area size, dip direction and dip angle in the status bar

Figure 16: Area orientation measurement (ShapeMetrix^{3D} User Manual)

Joint trace measurements

Joint traces are intersections of joints with the rock face. In ShapeMetrix3D the joint trace measurements are performed by marking traces on the 3D image. The result of these markings is a three –dimensional polyline. A plane can be fitted automatically if the 3D polyline shows a significant change in depth (Fig. 17) (Gaich, 2006). The trace length is given in terms of the Euclidean distance and along the rock surface. (ShapeMetriX^{3D} User Manual).

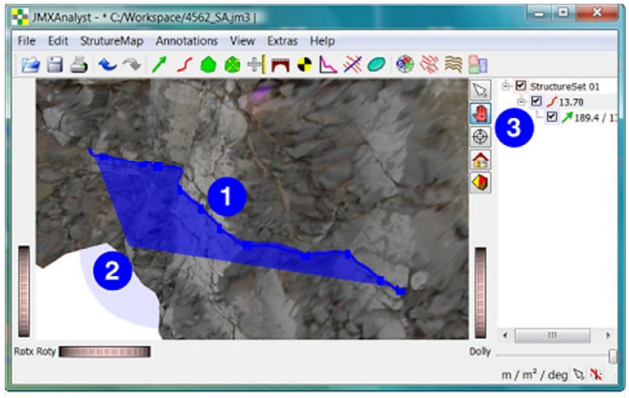

1 Joint follows trace along the surface
2 Square indicates joint plane and orientation
3 Length along surface, dip direction, and dip angle

Figure 17: Trace measurement (ShapeMetrix^{3D} User Manual)

Hemispherical plot

The orientation measurements can be grouped into cluster sets either by the user or by automatic clustering where the user only has to decide for the number of cluster sets. The cluster sets are visualized in a stereonet and statistical parameters such as mean value for dip direction and dip angle, cone of confidence, spherical aperture are provided for each cluster set.

3.1.2.5 QUALITY MEASURES

The quality of a 3D model has a substantial influence on measurement results. After Gaich (2006) several issues have to be taken into account:

Geometric accuracy

High precise surveyed reference points or control points can improve the geometric accuracy of the 3D model.

Geometric image resolution

One of the key parameters which influence the quality is geometric image resolution. It refers to the number of pixels within a certain area, and thus the amount of detail an image can contain and structural information is visible. The higher the number of pixels that map an area, the higher is geometric image resolution and the better the quality.

3D Point density

3D Point density is a measure of how accurate and detailed shapes can be described. This parameter is specified by points/m^2 or by the mean distance between surface measurements in mm.

Radiometric image resolution

The radiometric image resolution determines how finely differences of intensity can be visualized and distinguished. It is an indicator for the amount of color information per image point. For geological/geotechnical applications at least 3 × 8 bit/pixel is recommended.

Field of view (FOV)

The field of view of a camera is defined as the angle over which objects are recorded on a sensor in a camera. It is determined by the focal length of the lens and the size of the image sensor area (Fig. 18). With a short focal length the size of the image which is projected onto a camera sensor area is reduced and more of a scene is captured. Therefore the field of view is increased. This can also be done by increasing the image sensor area where a larger area of the projected image canbe captured. There are two different views: the horizontal FOV and the vertical FOV. For geological/geotechnical

applications the space to take photos is often limited. Changing the focal length allows to come closer to an object or to move away. Being close a geological outcrop wide angle lenses (short focal length) are used because they can capture more due to that they have a wider picture angle. For locations with larger distances to rock faces tele lenses (long focal length) are required. Digital cameras with zoom lenses provide a flexible wide operational range.

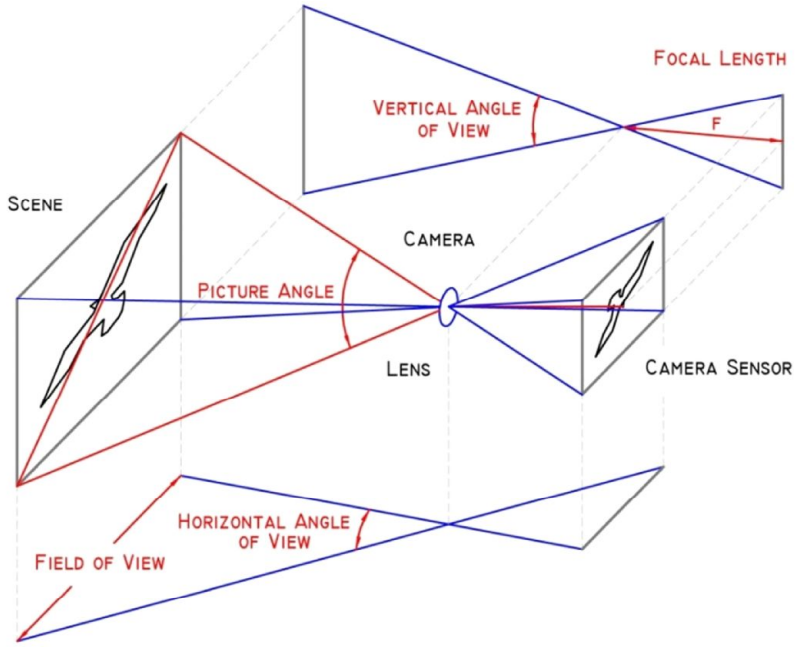

Figure 18: Camera field of view

Application range

There is a large application range of close range terrestrial digital photogrammetry for geological/geotechnical applications going from large scaled applications of slope failure analysis to small scaled discontinuity roughness investigations. The main limits are related to taking pictures at visibly acceptable quality. A free sight to the object of interest is essential. Bad atmospheric conditions (clouds, fog and rain) as well as vegetation on the rock face should be avoided when imaging the stereo pair. For taking pictures a suitable perspective has to be chosen in order to prevent shadows in the picture (Fig. 19).

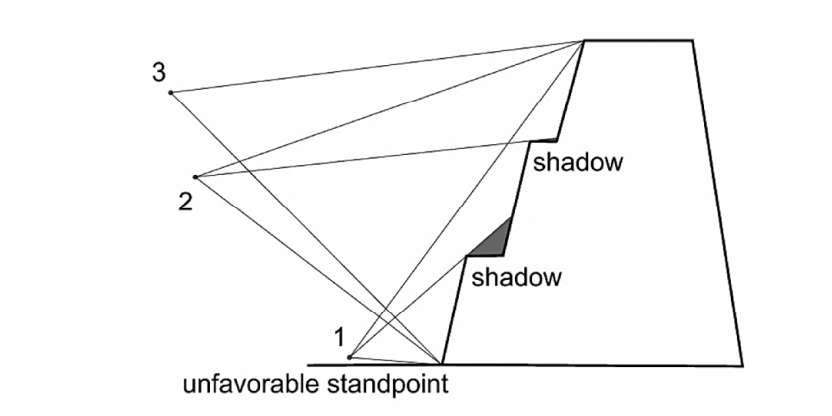

Figure 19: Perspectives for taking pictures (modified after Pötsch and Gaich, 2009)

3.2 QUANTIFYING DISCONTINUITY ROUGHNESS

When analyzing orientation measurements the variability of discontinuity orientation is assessed. According to Priest (1993) it should be recognised that the variabilty of discontinuity orientation measurements is often simply a refelection of irregular discontinuity geometry.

3.2.1 DEFINITION OF ROUGHNESS

The geometry of a discontinuity surface can be described by two distinct components: one that may be referred to as the shape in terms such as waviness or curvature and a random component referred as unevenness (ISRM, 1978). The term “roughness” is used to describe both aspects. Different discontinuity roughness scales are sampled at different test scales (Giani, 1992). Small scale roughness (unevenness) measurement involves a several centimeter sample size and large scale roughness (waviness) involves a sample size of several meters (Fig. 20).

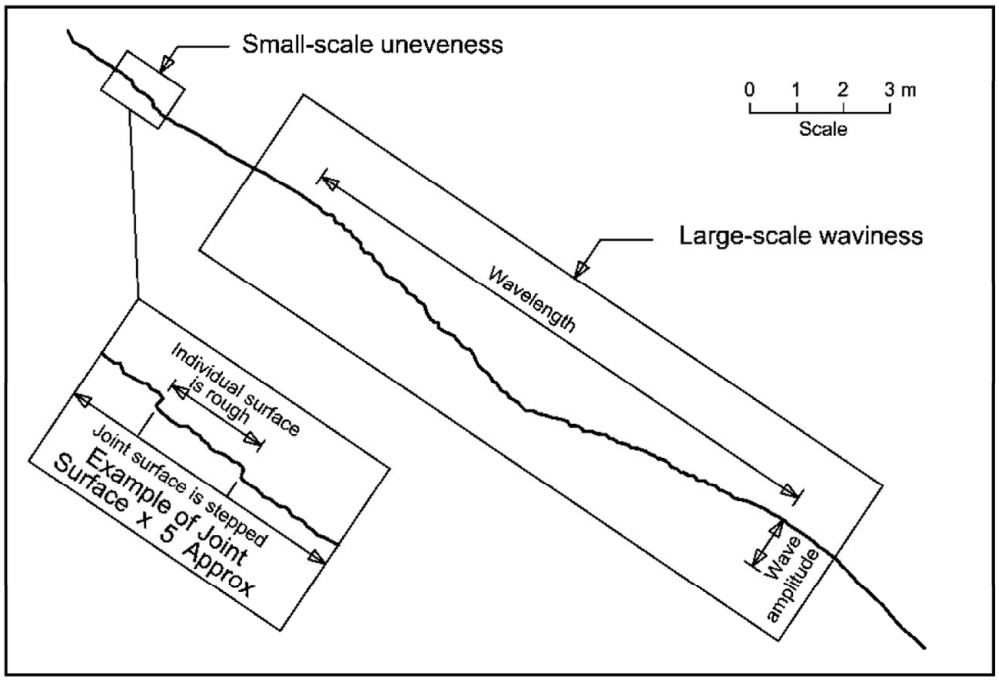

Figure 20: Small and large scale roughness

3.2.2 ROUGHNESS MEASUREMENT

Discontinuity roughness can be measured by enclosing the entire exposed discontinuity surface or an axis that is set in the direction of potential sliding and a line on the rough surface (Unal et al, 2000).
A variety of techniques have been used to assess discontinuity roughness in different ways:

- by direct contact to the discontinuity surface, by mechanical profilographs (Barton and Choubey, 1977), electronical profilographs (Beer et al, 2002) or by measuring with plates of variable diameter fitted to a geological compass (Fecker and Rengers, 1971)
- without direct contact with the discontinuity surface, by photogrammetric techniques, interferometry and laser scanning (Feng et al, 2003)

In this thesis following techniques have been used:

3.2.2.1 LINEAR PROFILING - BARTON COMB

Roughness profiles can be surveyed by measuring the heights (y_i) of asperities along the axis at various points (Δx) at constant interval (Fig. 21) (Giani, 1992).

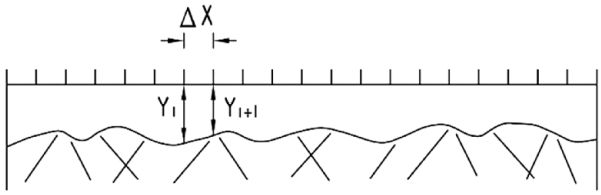

Figure 21: Linear profiling

One mean, probably the most commonly used method of making roughness profile measurements is to use a Barton comb (Fig. 22). With this method profiles with length 10 to 20 cm can measured. A direct contact to the discontinuity surface is required to carry out the measurements. The comb consists of a serious of metal rods, which are usually uniformly spaced and they are positioned in a way that they can slide relative to each other. If the comb is pressed against the discontinuity surface, the rods will slide to conform to the shape of the surface (Wyllie and Mah, 2004). The profile can be transferred to a piece of paper. For quantification of the discontinuity surface the measured profile can be compared with standard profiles by visual inspection or the Joint Roughness Coefficient (JRC) can be estimated by measuring the distance of each rod from a reference line.

Figure 22: Barton comb

3.2.2.2 DIGITAL PHOTOGRAMMETRY

Discontinuity surface roughness characterization by means of digital photogrammetry has already been successfully tested. Highly accurate and high resolution 3D point clouds can be obtained for small – scale and large scale roughness measurements. This method likewise requires accessible rock surfaces for taking photos in very close proximity to surface. The evaluation processes of discontinuity roughness can be carried out as well with ShapeMetriX3D. There are three important steps for modeling of discontinuity surfaces in order to carry out roughness profile measurements:

- Taking stereo photos by a digital camera
- Evaluation of digital photo pairs by computer software and determination of corresponding surface points and adding scaling information
- Obtaining a three – dimensional model of discontinuity surface for linear profiling by using graphics software

For three – dimensional modeling of a discontinuity surface the following points listed below have to be considered when taking the photos on site (Seker ve Tavil, 1996: Unal vd., 2000):

- Using a suitable camera to the aim of this study
- Denoting and determination the object points on sample surface for the evaluation process
- Arranging photo pairs by taking photos from different points for three – dimensional modeling
- Taking photos so as to take, to capture all the details of the surface

The obtained roughness profiles with the help of graphics software can be used for Joint roughness coefficient (JRC) estimates.

3.2.3 ROUGHNESS QUANTIFICATION

Many methods can be found in literature for the quantification of roughness from surface profiles. Among these, the JRC coefficient proposed by Barton (1973) is probably the most widely used method in rock engineering. JRC stands for Joint Roughness Coefficient and it's an index that is used to describe the roughness of a surface. Due to the fact that discontinuity surfaces are three – dimensional features and roughness profiles are only two – dimensional representations of them it is suggested to take several linear profiles of a discontinuity surface for evaluating the Joint Roughness Coefficient.

3.2.3.1 JOINT ROUGHNESS COEFFICIENT (JRC)

3.2.3.1.1 COMPARING MEASURED PROFILES TO STANDARD PROFILES

Barton & Choubey (1977) proposed ten standard roughness profiles (Fig. 23) The JRC values range from 0 to 20 in steps of two starting from a smooth flat surface to a very rough surface. A roughness profile is measured with a Barton comb and the obtained profile is visually compared with the standard profiles afterwards. A value of JRC is assigned for characterization of discontinuity roughness. The method is very simple and quick, but deciding for a JRC value only due to visual inspection is often difficult and subjective.

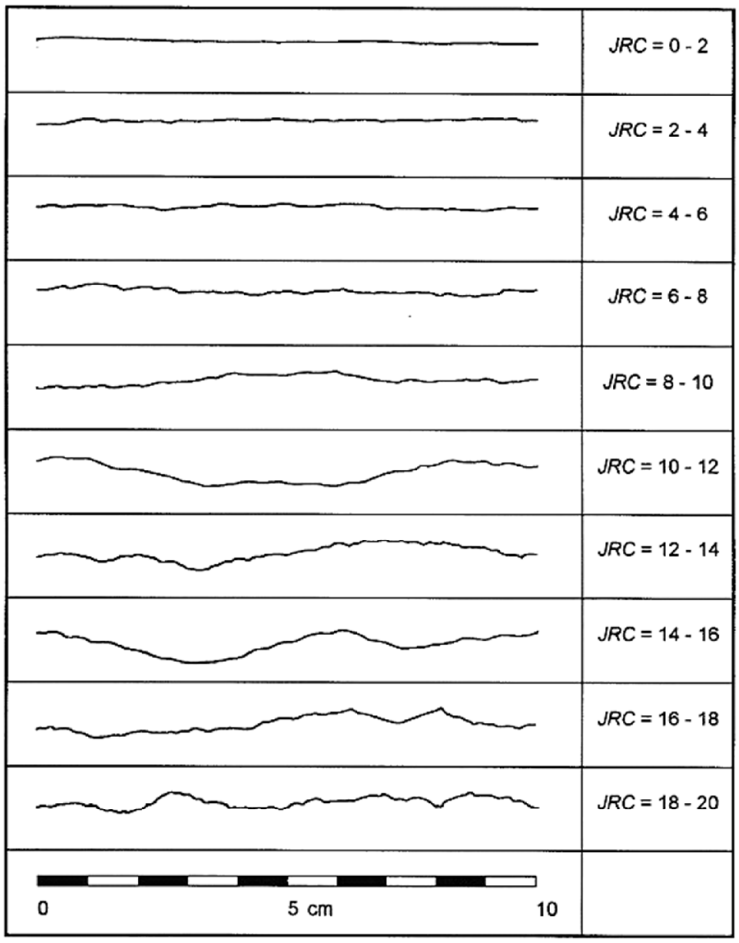

Figure 23: Standard roughness profiles (after Barton & Choubey , 1977)

3.2.3.1.2 MEASURING ASPERITY PROFILE LENGTH AND AMPLITUDE

There is an alternative method for estimating the JRC from surface profile measurement. Therefore the length and the maximum amplitude of the asperity profile have to be measured and with the help of graphic correlation the corresponding value of the Joint Roughness Coefficient can be evaluated (Fig. 24).

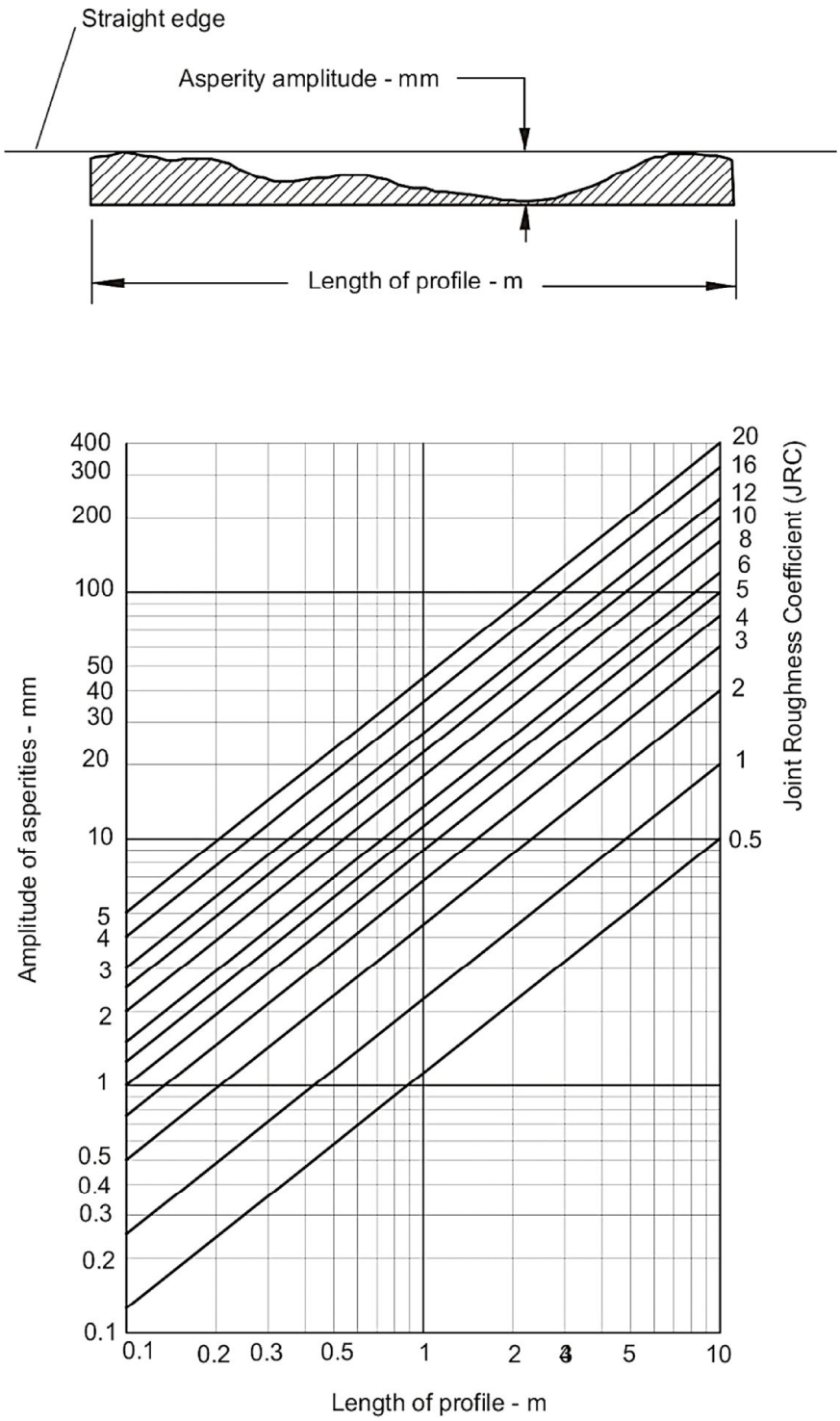

Figure 24: Estimating JRC coefficient from measuring roughness amplitude for various measuring length (after Barton, 1982)

4. APPLICATION

4.1 QUARRY INVESTIGATIONS

To gather discontinuity measurements on the quarry site the stereography – based ShapeMetriX^{3D} technique and traditional manual field survey methods were used.
The results of manually measured and model- derived discontinuity orientations were compared. With both methods the main structure sets were evaluated. For a direct comparison of single discontinuity surface orientation measurements selected surfaces were marked on site to identify the same surfaces on the digital image.
In order to test the limits for obtaining accurate 3D models several stereoscopic image pairs were taken of the same area but with

- different distances and resolutions
- different base- lengths while constant distance
- different perspectives

For testing these different configurations several camera standpoints were selected and marked on the ground before starting imaging the stereoscopic pairs. The choice of the standpoints was geared to test optimal as well as bad geometrical configurations for image acquisition and was somehow limited to the space at the quarry.

Discontinuity roughness measurements were performed on site by means of a Barton comb and three - dimensional photogrammetry was as also used to quantify discontinuity roughness.

4.2 COMPASS MEASUREMENTS

The manual discontinuity orientation measurements were carried out by means of the compass GEOKOM No.3019 by Breithaupt. It is a robust stratum compass according to the measuring method of Prof. Dr. Clar. For the dip direction a graduation interval of 2° is given on the horizontal circle and for the dip readings a graduation interval of 5° is applied on the lid hinge (vertical circle). Through estimation, a reading precision of 1° is specified for the azimuth and a reading precision of 2° for the dip (Breithaupt). The compass measurements have been corrected for the magnetic declination which is about 3° at the investigation site (Fig. 25) (exact value for Graz 3° 5' for 1.1. 2011 (ZAMG)).

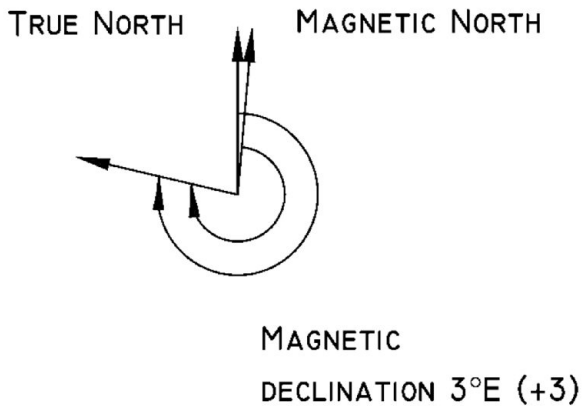

Figure 25: Magnetic declination

Performing measurement by using compass was restricted only to accessible parts of the quarry. Orientations were recorded on a notebook during the investigations on site and transferred to a PC later on. For visualization and statistical evaluation of orientation measurements the software package SPHAIRA2.0 was used.

4.3 MANUAL ROUGHNESS AQUISITION

The procedure for estimating discontinuity roughness of manually measured 2D profiles can be divided into three steps. It involves: (1) acquisition of 2D profiles, (2) digitizing of the profiles (3) evaluation and analysis of roughness for the obtained profiles.

Two dimensional profiles were measured directly by means of a carpenter (Barton) comb. With the 0.13 m long comb continuous measurement points at a interval of 1 mm can be obtained over a discontinuity surface. Thus, features on the surface with a size less than 1 mm are neglected. Profiles were measured in horizontal and vertical (potential sliding) directions on the discontinuity surface and traced to a piece of paper in the field. Papers were scanned and saved as images in GIF format which were imported into AutoCAD 2010 for digitization. First images were scaled to real - world dimensions and polylines were then used to the trace the profiles. By measuring maximum amplitude and length of the roughness profile JRC coefficient were determined for different discontinuity surfaces.

4.4 SURVEYING

4.4.1 FIELD WORK

Geodetic measurements were performed with twofold aim. The first one was to determine the 3D coordinates of reference points to be used for the georeferencing process of 3D models generated by means of ShapeMetriX3D. Second for the surveying of camera standpoints to examine the location of standpoints with respect to rock face. Therefore a surveying equipment of a total station Leica Geosystems TCR 1203 (Fig. 26 (a)) and Leica GPS 1200 (Fig. 20 (b)) was used.

(a)   (b)

Figure 26: Surveying equipment: Leica TCR1203 total station (a) and Leica GPS 1200 (b)

The Leica TCR1203 total station has a angular accuracy of 3" and provides dual mode electronic distance measurements. In normal IR (infra-red) mode distances of up to 3000 m to a single prism are measured with 1mm + 1.5ppm accuracy. The "reflectorless" (visible red laser) mode allows to measure distances of up to 1000 m with 2mm + 2ppm accuracy on shots under 500m and 4mm + 2ppm over 500m. The GPS1200 was used as rover for RTK data logging. Measurement precision and accuracy in position and accuracy in height are dependent upon various factors including number of satellites, geometry, observation time, ephemeris accuracy, ionospheric conditions, multipath etc. Centimeter accuracy positions are available continuously at rates of up to 20 Hz (Leica Geosystems).

Prior to fieldwork fixed points were ascertained in the near surrounding of the quarry. In the field the coordinates of the fixed points were determined by means of RTK - GPS in order to perform a coordinate transformation with the GPS controller. GPS - RTK transformation is used to transform the GPS ETRS-89 coordinates into the Gauss - Krüger M34 system. In the quarry area three points (PP1 - PP3) were stabilized by driving a surveyor's nail into the ground. The coordinates of these points were already calculated in field by means of RTK GPS (Fig. 27). The total station was set up at PP3 and measurements of predetermined point PP1 were taken to orientate the total station's position. Point PP2 was used for controlling issues.

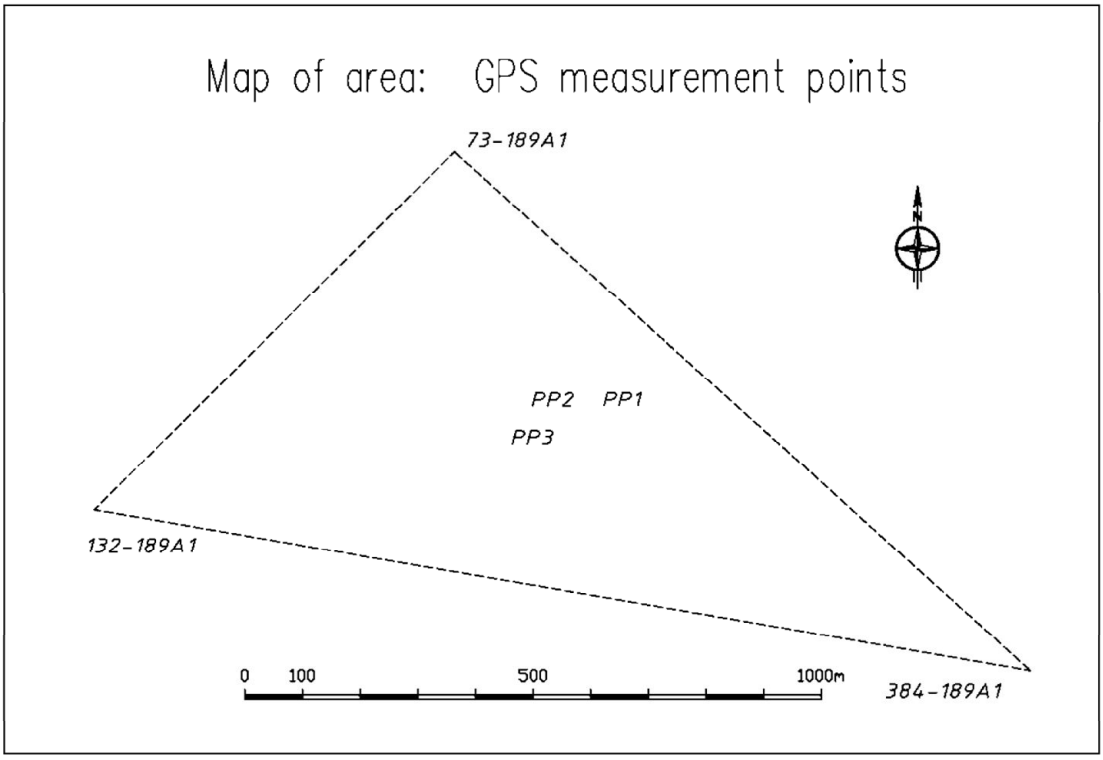

Figure 27: Map of investigation area (fixed points and GPS measurement points)

For complete stereoscopic coverage of the entire rock face at the quarry the area was divided into three sections (Model A, Model B, Model C) (Fig. 28). ShapeMetriX^{3D} equipment contains reference target discs. In each section three reference targets (A1- A3, B1 - B3, C1 - C3) were installed in front of the rock face. The coordinates of the reference points were determined by means of total station. The exact alignment of central position of the reference targets was achieved by laser targeting with reflector less mode.

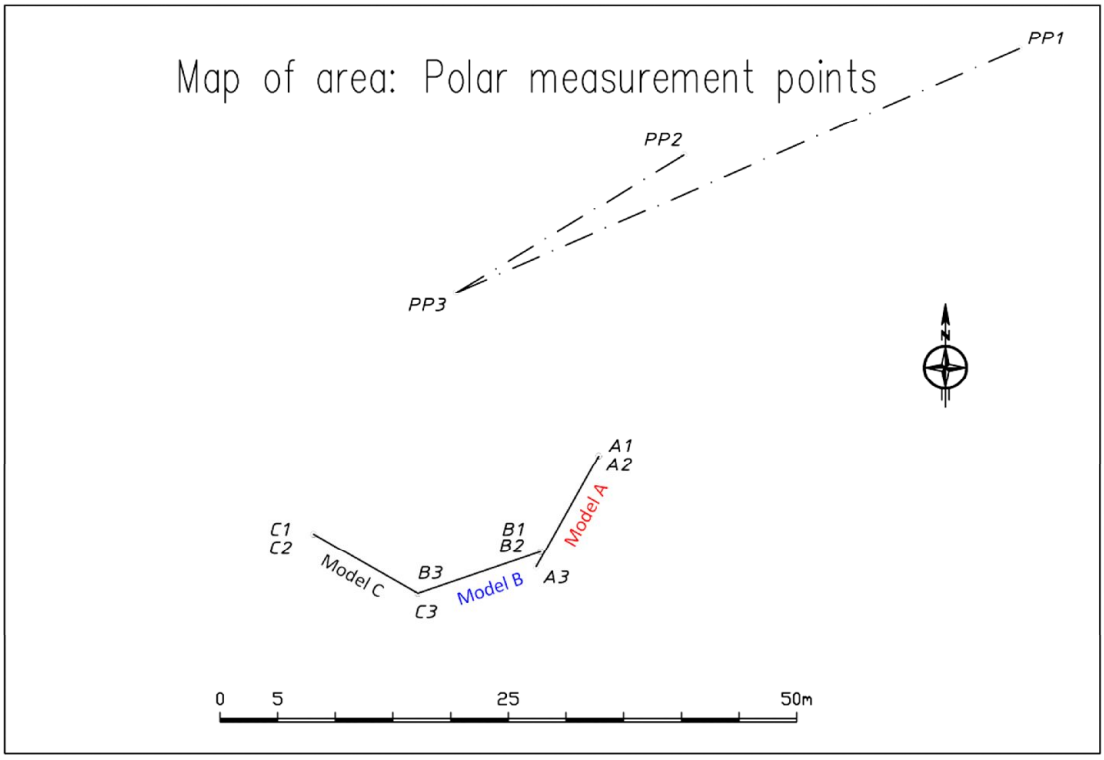

Figure 28: Map of area (Rock face and polar measurement points)

Due to the aim to test different configurations for imaging and modelling the rock face with respect to imaging distance, base - lenghts and perspectives camera standpoints were accurately chosen and marked by a spray print on the ground . To determine coordinates of the camera standpoints a standard Leica prism pole was used to perform IR mode measurements.

4.4.2 DATA PROCESSING AND ANALYSIS

The measurement data that is gathered with a total station is stored in an internal database was exported to an ASCII file on a memory card. Measurement data was transferred to a computer and the ASCII File was imported into AutoCAD2010 where a map of the investigation area was created.

4.5 ShapeMetriX^{3D}

4.5.1 FIELD INVESTIGATIONS

Images for rock face modeling have been acquired with a standard off-the shelf Nikon D70s and with calibrated zoom lens (10 - 20 mm and 18 - 70 mm). The camera is a 6 Megapixel camera which has a 3008 × 2000 pixels resolution. Due to the average height of 5 m of modeled rock face a geometric image resolution of 2.5 mm/pixel and a point density of 16000 points/ m^2 is achieved. For imaging distances from 10 up to 25 m between camera standpoint and rock face different zoom lens positions between 18 and 45 mm were chosen. For modeling of the entire rock face it was taken care that the imaged sections of the rock face have an overlap of approximately 0.25 of the image width.

The stereoscopic images for discontinuity surface modeling were taken with the Sigma (10 - 20 mm) wide angle zoom lens. The geometric image resolution for discontinuity surface images is about 0.1 mm/pixel. Before imaging three control points were marked by permanent marker on the discontinuity surface. Two points were marked vertical about each other having a distance of 13 cm. A third point was tagged about 20 cm away from these two vertical arranged points on the surface. Camera standpoints for imaging stereo pairs were varied only some centimeters.

4.5.2 ROCK FACE MODELING AND DISCONTINUITY ORIENTATION MEASUREMENT

Photograph files were downloaded from the camera to the computer. For processing of the images and for determining geometrical discontinuity properties, particularly their orientation and roughness the software package ShapeMetrX^{3D} v3.5 is used

The software component “Reconstruction assistant” was used to generate a three dimensional generic image. After the import of left and right image information about camera type, zoom lens and reconstruction area was added. A special feature of the software is that there is no need of knowing the actual position and viewing direction of the camera when taking images. In order to transform the 3D image into a global coordinate system based on the observation of control (reference) points the tool “SMX Referencer” was used. For modeling of the entire rock wall three overlapping individual 3D images were connected into a large 3D image using the “Model Merger”. Therefore three overlapping 3D images were chosen. The combination of the individual images is based on the common information which are corresponding points in overlapping regions. Georeferenced 3D models were then used to carry out interactive discontinuity orientation measurements with the 3D assessment tool “JMX Analyst”.

4.5.3 DISCONTINUITY SURFACE MODELING AND ROUGHNESS MEASUREMENT

High resolution images of discontinuity surfaces were first uploaded to the SMX Reconstructor to produce generic 3D images. For setting scale and orientation the “Normalizer” tool was used. The mode requires defining three points to provide scale and orientation. Therefore a upper and lower point were marked on both images and the true distance between these two points was entered. A third point is tagged defining the plane to the discontinuity surface (Fig. 29).

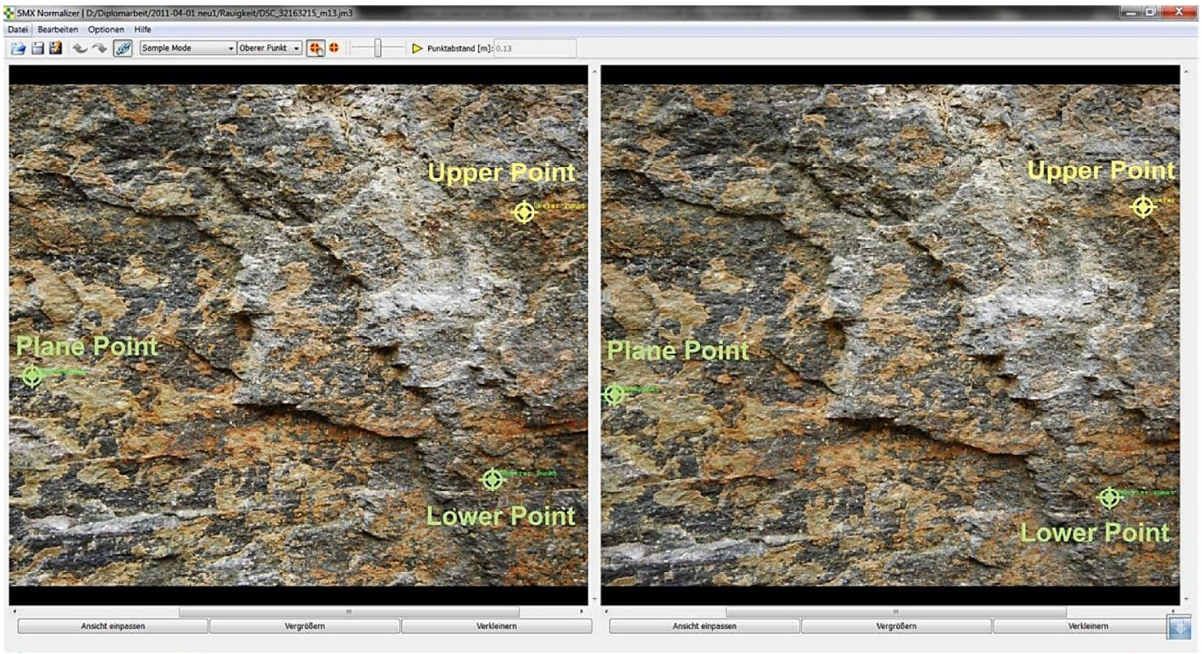

Figure 29: SMX Normalizer - Sample Mode for definition of corresponding points of discontinuity surface image pairs

For selected discontinuity surfaces profiles were measured to get an objective description of discontinuity roughness. The JMX analyst allows do define profiles in arbitrary directions by marking starting and endpoint of profile. Three profiles, two in vertical and one in horizontal direction, were extracted for each modeled discontinuity surface.

5. RESULTS

5.1 GENERAL STRUCTURAL ANALYSIS

The investigated rock face at the quarry covers approximately a vertical area of extension 33 m in width and 5 m in height. Results of discontinuity orientation measurements obtained with ShapeMetriX^{3D} are similar to manually measured orientations. With both methods five structure sets have been identified. Pole concentration plots of discontinuity orientations are shown in Fig. 30 derived by digital (a) and manual measurement methods (b).

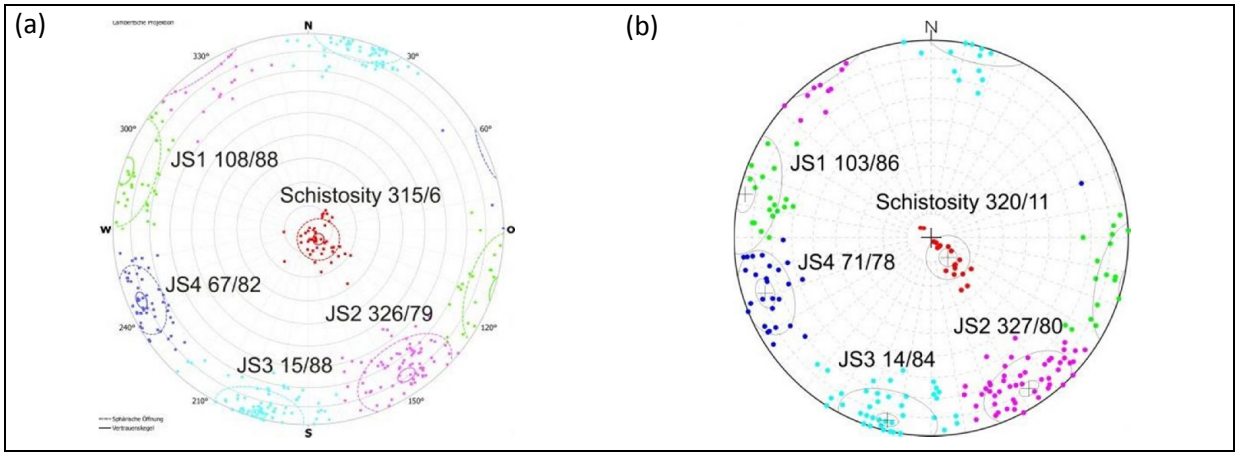

Figure 30: Lambert projection of digital (a) and manually (b) measured discontinuity orientation data (poles with centers of gravity)

Joints dipping almost vertically (88° WE for digital and 86° WE for manual measurements) are belonging to JS1. The NW dipping joints (JS2) are inclined at 79° (digital) to 80° (manual). A third joint set (JS3) is dipping about 84° (manual) to 88° (digital) NE . Joint set (JS4) dipping with 79° (digital) to 80° (manual) is orientated to ENE. The schistosity planes are sub – horizontal inclined, having a centre of gravity of 315/6 for digital and 320/11 for manual measurements.

The dominant strike directions of discontinuities are plotted on compass rose diagrams (Fig. 28). They are orientated NNE - SSW (JS1) , NE - SW (JS2), NWW - SEE (JS3) , NNW - SSE (JS4) for the four major joint sets. The strike direction of schistosity planes is NE – SW.

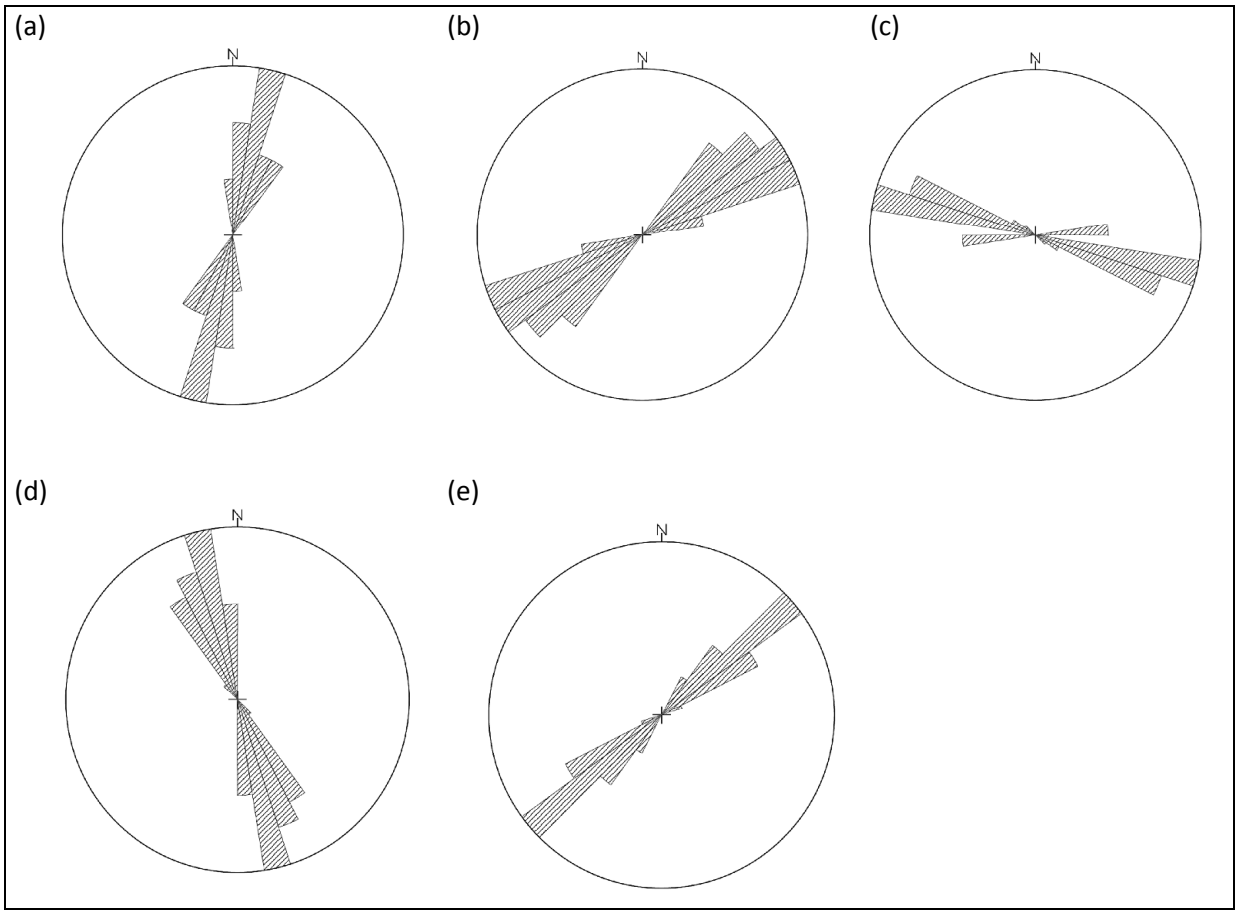

Figure 31: Rose digrams showing the dominant strike direktions for JS1 (a), JS2(b), JS3(c), JS(d) and Schistosity (e)

5.2 STRUCTURAL ANALYSIS OF ROCK FACE SECTIONS

The entire modeled rock face is composed of three individual models (Model A, Model B, Model C). The results of structural analysis of this individual sections obtained by SMX and manual measurements are displayed below. In section A the NE – dipping joint set (JS3) is absent, it hasn't been measured neither by SMX (Fig. 32 (a) nor by manual measurements (Fig. 32 (d)). Orientation data for section B is shown in Fig. 32 (b) for SMX and in Fig. 32 (e) for compass measurements. The ENE – dipping joint set (JS4) is only present for SMX orientation data. As these joints are not day lighting in this section only SMX trace measurements were possible. Rock mass in section C (Fig. 32 (c) for SMX and Fig 31 (e) for compass data) is less fractured than in section A and B. Schistosity orientation data was only gathered by SMX trace measurements.

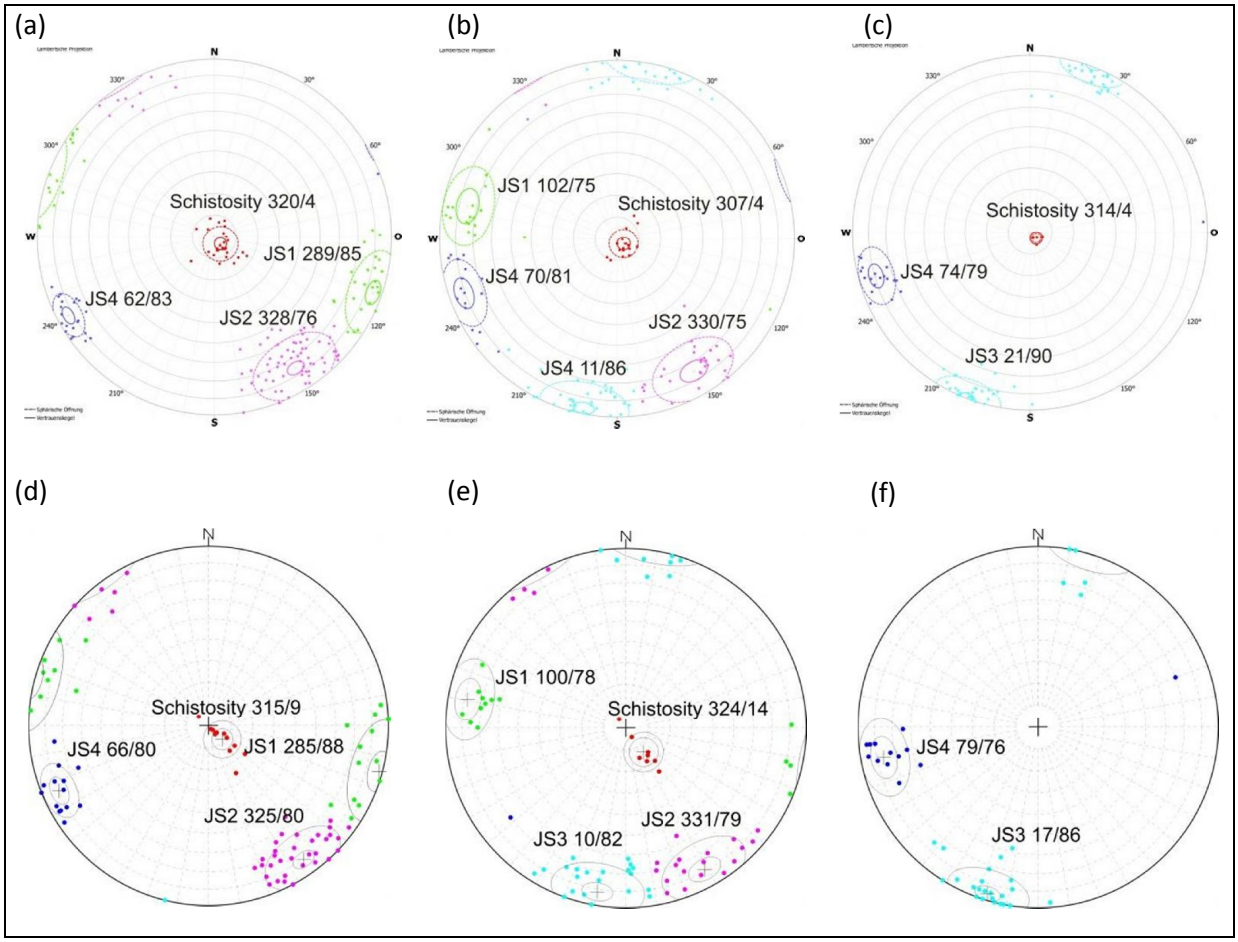

Figure 32: Lambert projection of discontinuity orientation data (poles with centers of gravity) for (a) SMX – measurements of Model A, (b) SMX – measurements of Model B, (c) SMX – measurements of Model C, (d) manual– measurements of Model A, (e) manual– measurements of Model B, (f) manual– measurements of Model C

5.3 INDIVIDUAL ORIENTATION MEASUREMENTS

5.3.1 COMPARISON OF MANUAL AND DIGITAL INDIVIDUAL ORIENTATIONS

Individual orientations measured using SMX software were compared to orientations measured manually by means of a geologic compass. Therefore forty nine joint surfaces were selected (Fig. 33 – Fig. 35). For digital orientation measurements 3D models with best quality were chosen.

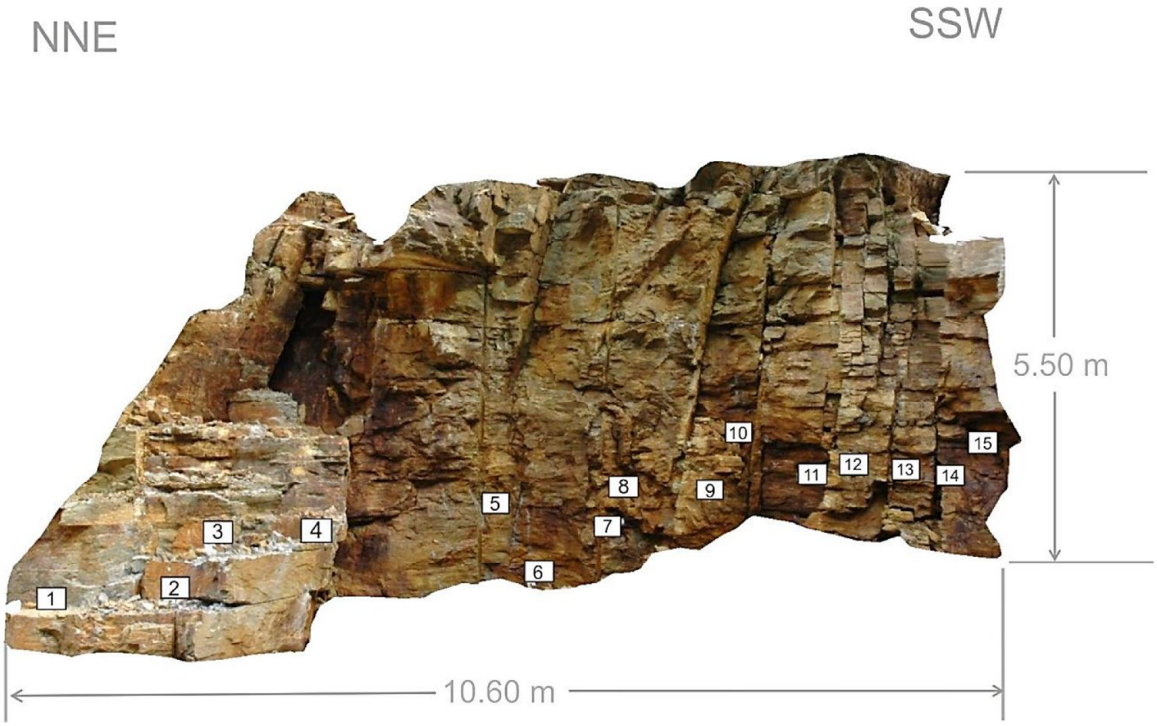

Figure 33: Model A - location of joint planes 1 to 15

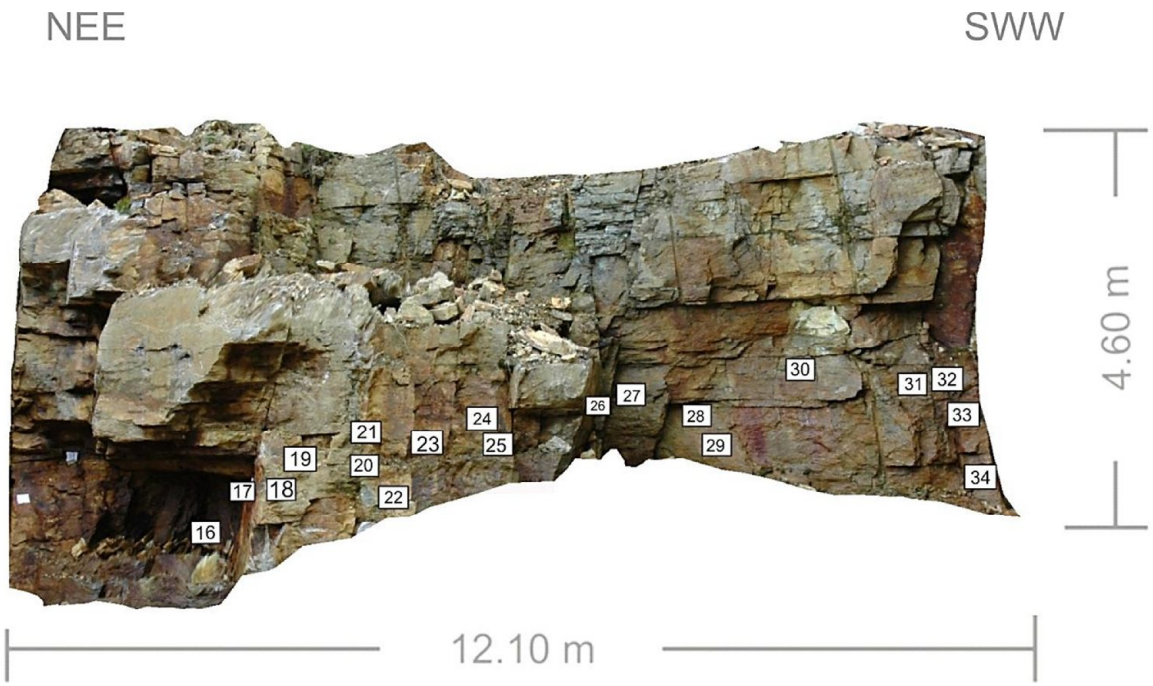

Figure 34: Model B - location of joint planes 16 to 34

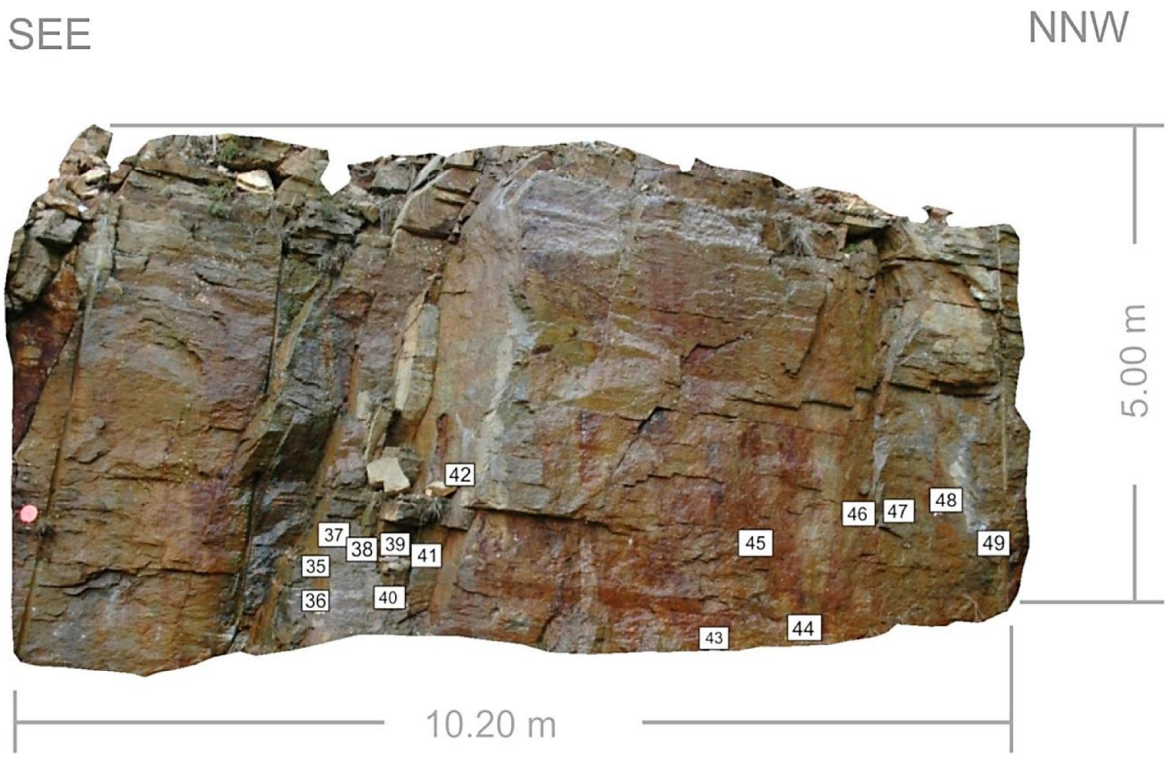

Figure 35: Model C - location of joint planes 35 to 49

An important aspect that has to be considered when comparing orientation results of the two methods is the size of reference plane used for orientation measurements. For compass measurements the size of the reference plane is 0.006m^2 (compass dimensions: 86 mm × 70 mm). The size of the reference plane used for individual SMX measurements is shown in statistics output of SMX software (Tab. 1). The used reference size depends on the 3D point density spacing of the model stored in the central memory (total number of points) which is more densely space than the point density shown on screen (reduced model). The minimal area patch size is the area used for individual orientation measurements. The denser the point spacing the smaller is the area patch size. For Model A having an average 3D point spacing of 0.04 m the minimal area patch size is 0.006 m^2 which equals the size of reference plane for compass measurements. The minimal patch size area for model B lies with 0.007 m^2 within the range of compass reference plane size. Rock mass in model C is less jointed than in two other models A and B which allows denser 3D point spacing and therefore a smaller patch size area used for orientation measurements. The reference plane used for SMX measurements for Model C is half of the size used for compass measurements.

	Model A	**Model B**	**Model C**
3D point spacing [m]	0.04	0.04	0.02
Geometric image resolution [m/Pixel]	0.0048	0.005	0.0038
Minimal area patch size for orientation [m^2]	0.006	0.007	0.003
Number of 3D points	96365	89349	134958
Surface size of whole 3D model [m^2]	120.9	169.8	79.1

Table 1: Statistics of SMX Models

On each joint surface one manual measurement and five SMX measurements were carried out. For SMX measurements the average orientations (centers of gravity) were estimated as a dipline resultant calculated by SMX software. Differences between manual and SMX measured joint orientations are quantified in Tab. 2, where the absolute deviations of dip directions and dips and as well the angle θ separating the two unit normal vectors (manual and digital measurement) are shown.

Discontinuity orientations can be converted into vector form by adopting Cartesian coordinate system and calculating the Cartesian components of the downward directed unit normal vector to ta discontinuity plane v_i (Priest, 1993).

If dip direction (α_d) and dip angle (ϕ_d) are known the trend and the plunge of the line normal to a mean orientation can be found by

$$\alpha_n = \alpha_d \pm 180° \qquad 0 \le \alpha \le 360°$$

$$\varphi_n = 90° - \varphi_d \qquad 0 \le \varphi_d \le 90°$$

Global x, y and z-axes are defined in terms of the “right handed” Cartesian axis system (Fig. 36). :

- x - axis is horizontal to the north of trend/plunge
- y - axis is horizontal to the east of trend/plunge
- z- axis is vertical downwards of trend/plunge

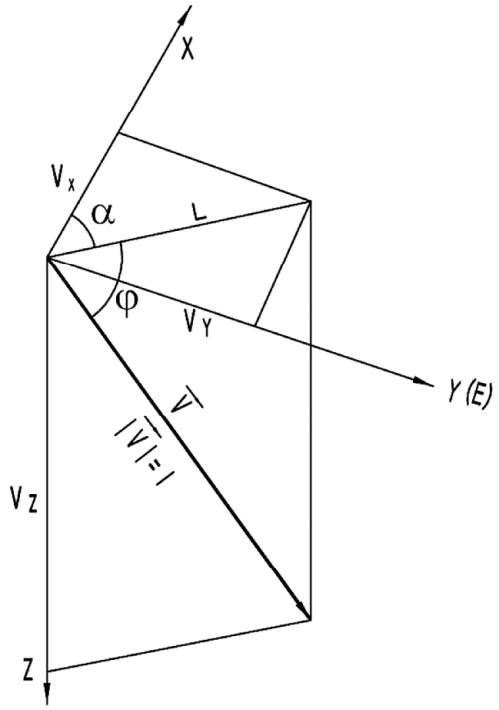

Figure 36: Unit normal vector relative to a Cartesian coordinate system

Cartesian components a referred to as direction cosine (Priest, 1993). The components of the vector v = (V_x, V_y, V_z) can be calculated with

$$V_x = \cos\alpha_n * \cos\varphi_n$$
$$V_y = \sin\alpha_n * \cos\varphi_n$$
$$V_z = \sin\varphi_n$$

The orientation of the vector sum of normal vector (v_i) is called the resultant R.

$$R = \sum_{i=1}^{n} v_i$$

To derive the vector mean (average orientation) R is divided by the number of measurements:

$$\overline{R} = \frac{R}{n}$$

The separating angle θ between manual measured surface normal ($\overline{R}_{compass}$) and mean normal resultant calculated by SMX ($\overline{R}_{SMX}$) is calculated with:

$$\cos\theta = \frac{\overline{R}_{compass} \bullet \overline{R}_{SMX}}{\left\|\overline{R}_{compass}\right\| \left\|\overline{R}_{SMX}\right\|}$$

Separating angles θ of 0° to 27° have been calculated for the selected discontinuity planes indicating both, partly a very good agreement and as well large dispersions between manual measured and digital obtained orientations on 3D models (Tab. 2).

	Compass Measurement		SMX Measurement		Absolute deviations		Separating
Joint ID	dip dir [°]	dip [°]	dip dir [°]	dip [°]	Δdip dir [°]	Δdip [°]	angle [ϑ]
1	314	90	311	85	3	5	6
2	311	85	308	82	3	3	4
3	318	90	313	84	5	6	8
4	312	80	314	80	2	0	2
5	268	90	274	83	6	7	9
6	332	90	330	83	2	7	7
7	272	80	278	85	6	5	8
8	284	75	290	79	6	4	7
9	110	80	107	87	3	7	8
10	332	90	327	84	5	6	8
11	120	85	147	82	27	3	27
12	334	90	331	85	3	5	6
13	322	80	326	75	4	5	6

14	314	80	321	74	7	6	9
15	14	90	10	83	4	7	8
16	30	80	no measurement possible				
17	52	70	28	66	24	4	23
18	338	75	339	75	1	0	1
19	352	80	354	80	2	0	2
20	282	80	282	79	0	1	1
21	316	75	314	80	2	5	5
22	334	70	330	70	4	0	4
23	330	75	327	76	3	1	3
24	358	70	355	64	3	6	7
25	340	70	335	75	5	5	7
26	358	65	350	77	8	12	14
27	18	85	15	87	3	2	4
28	14	85	12	82	2	3	4
29	359	68	2	68	3	0	3
30	10	75	10	79	0	4	4
31	146	80	164	87	18	7	19
32	172	90	174	86	2	4	4
33	11	90	11	84	0	6	6
34	20	90	16	89	4	1	4
35	78	80	77	77	1	3	3
36	76	75	73	71	3	4	5
37	11	90	15	84	4	6	7
38	80	85	75	85	5	0	5
39	190	70	193	75	3	5	6
40	192	90	187	86	5	4	6
41	9	90	9	86	0	4	4
42	84	80	80	80	4	0	4
43	20	80	25	80	5	0	5
44	18	90	17	86	1	4	4
45	20	85	17	80	3	5	6
46	356	90	356	87	0	3	3
47	18	90	18	85	0	5	5
48	12	85	11	87	1	2	2
49	190	90	193	85	3	5	6

Table 2: Individual orientation measurements of selected joints

5.3.2 DISCUSSION OF POSSIBLE SOURCES FOR ERRORNEOUS ORIENTATION MEASUREMENTS AND NATURAL VARIABILITIES IN ORIENTATIONS

Different aspects have to be considered which may be responsible for measurement errors and the natural variability in discontinuity orientation. Sources of error can be introduced by manual and digital measurements. By using geological compass orientation measurements can be performed at least with an accuracy of 1°. However sampling difficulties and human bias can lead to erroneous orientation measurements and affect the accuracy of the data. As joints surfaces are never perfectly planar and characterized of irregularities a certain amount of scatter in orientation measurements has to be anticipated (Anonymous, 1977). A source of error has to be considered when measuring the orientation of an irregular discontinuity surface with a compass and the size of compass is relatively small to roughness wavelength (Sturzenegger & Stead, 2009). Depending on where the compass is located on the discontinuity surface the orientation varies due to different obtained surface normal vectors. To estimate the influence of roughness on discontinuity orientation measurements discontinuity roughness was quantified, the results are shown in 5.3.3.1.

For digital photogrammetry orientation biases occur if the discontinuities are unfavorable orientated with respect to camera position. These are discontinuities which are inclined parallel to the vertical line of sight of the camera and therefore leading to the so called vertical orientation bias (Fig. 37) (Sturzenegger & Stead, 2009). Occlusion phenomena occur if the vertical – line of sight of the camera has a steeper angle than the discontinuity inclination. Therefore parts of the rock face cannot be fully represented on the digital image and results in a shadow zone.

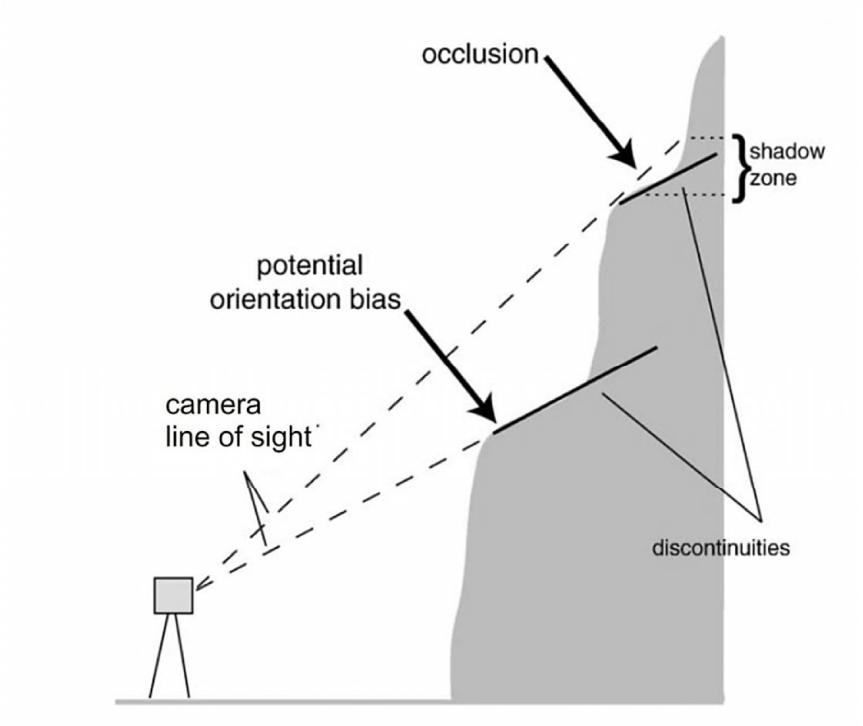

Figure 37: Illustration of occlusion and vertical orientation bias (modified after Sturzenegger et al., 2007)

5.3.3 INFLUENCE OF DISCONTIUNUITY ROUGHNESS ON ORIENTATION MEASUREMENT

5.3.3.1 JOINT ROUGHNESS QUANTIFICATION

For all four joint sets one joint surface (JS1 – JS4) was selected and used to quantify roughness (Fig. 38, Fig. 40, Fig. 42 and Fig. 44). The roughness profiles obtained by manual measurement and by the use of analytical photogrammetry are shown below (Fig. 39, Fig. 41, Fig. 42 and Fig. 43). Out of each 3D joint surface two vertical and one horizontal profile were extracted. On same surfaces two manually measured profiles, one in horizontal and one in vertical direction were plotted. An average plane was fitted to each profile line and the maximum peak height of the profiles and profile length were measured to estimate the JRC coefficient after Barton (1983). Only from visual inspection of roughness profiles it is evident that joints JS1 and JS3 have the most irregular surfaces which is confirmed by estimated JRC. For the digital as well as for manually measured profiles the highest JRC have been evaluated for JS1 and JS3. In general higher roughness amplitudes are obtained for photogrammetric produced profiles. This is due metallic rods of a carpenter comb are arranged at 1 mm intervals, compared to photogrammetric measured profiles where the 3D image of the joint surface has a geometric image resolution of 0.1 mm/pixel the rods of the comb have a less penetration depth.

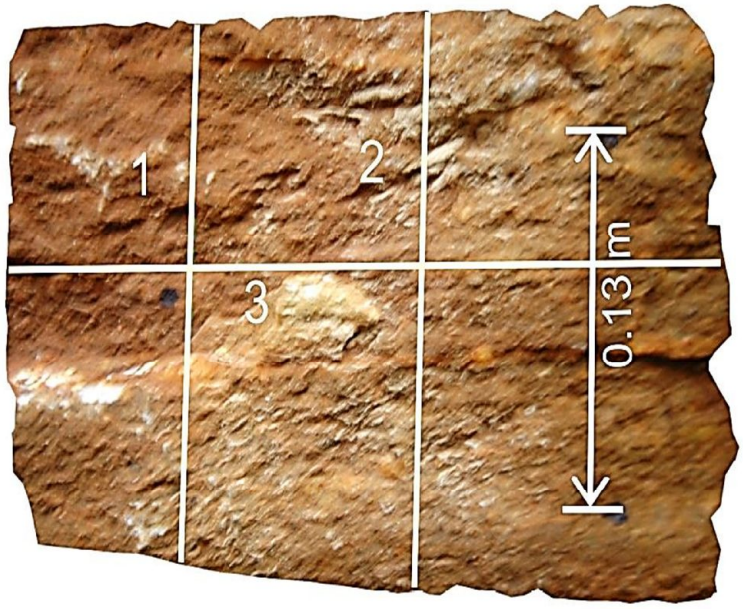

Figure 38 : Modeled joint surface of JS1 with locations of the measured profiles

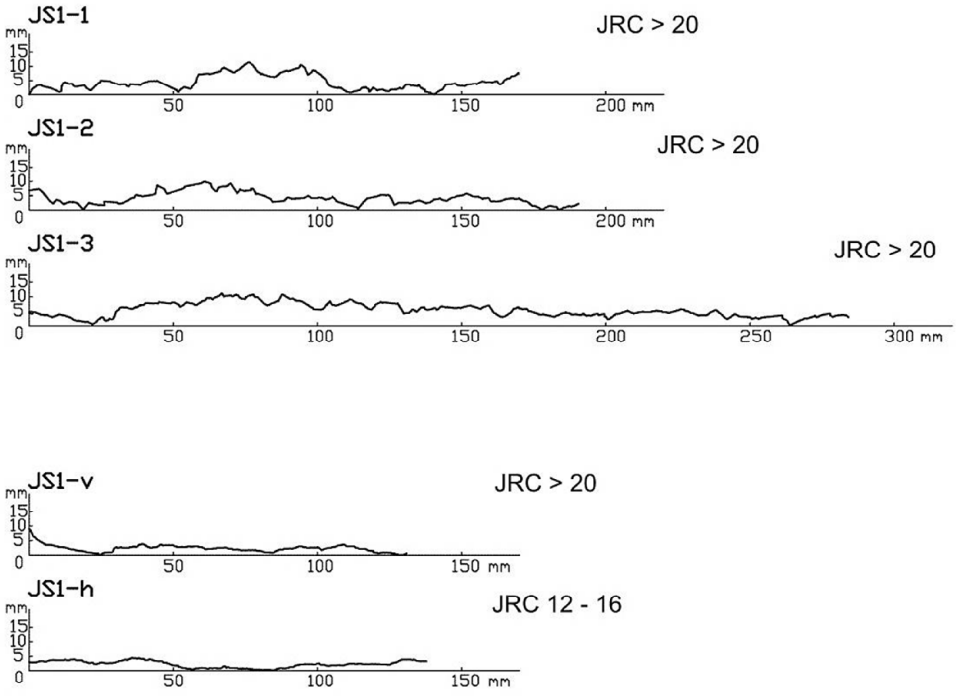

Figure 39 : Roughness profiles obtained for a joint surface of JS1 (Digital measured profiles: JS1 – 1 and JS1 – 2 in vertical direction, JS1 – 3 in horizontal direction; manually measured profiles: JS1 – v in vertical direction, JS1 – h in horizontal direction (both profiles measured in middle of the sampled joint surface))

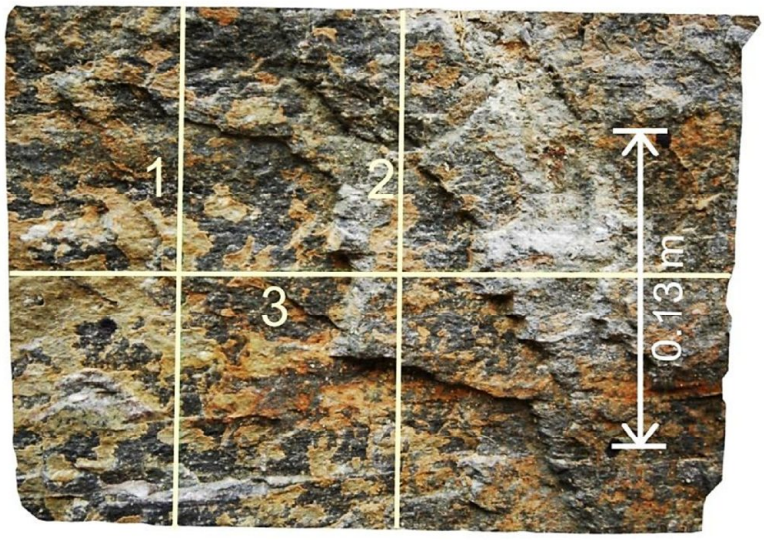

Figure 40 : Modeled joint surface of JS2 with locations of the measured profiles

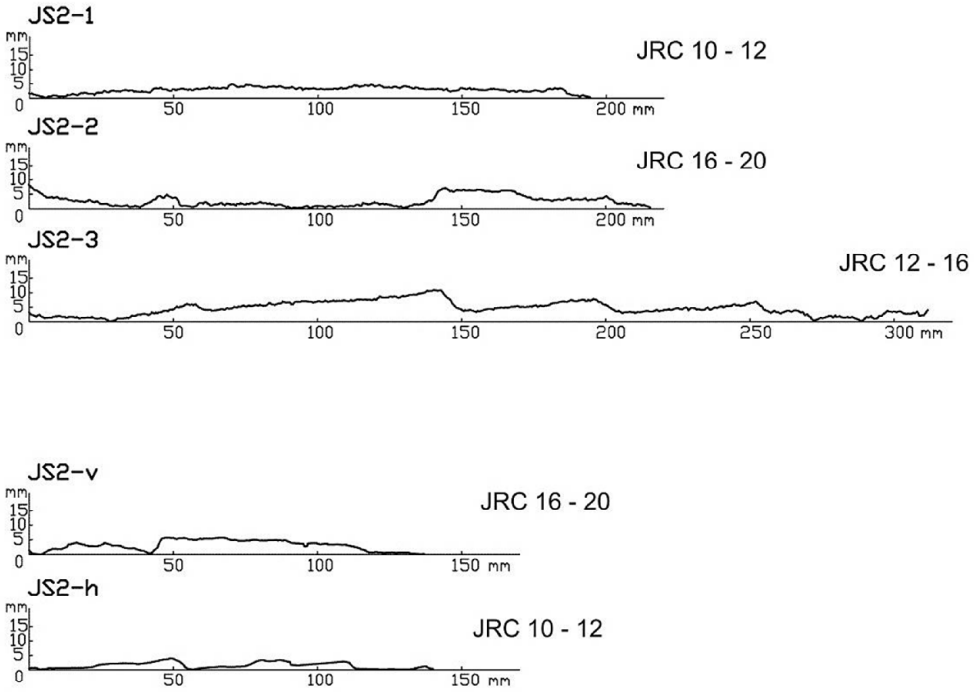

Figure 41: Roughness profiles obtained for a joint surface of JS2 (Digital measured profiles: JS2 – 1 and JS2 – 2 in vertical direction, JS2 – 3 in horizontal direction; manually measured profiles: JS2 – v in vertical direction, JS2 – h in horizontal direction (both profiles measured in middle of the sampled joint surface))

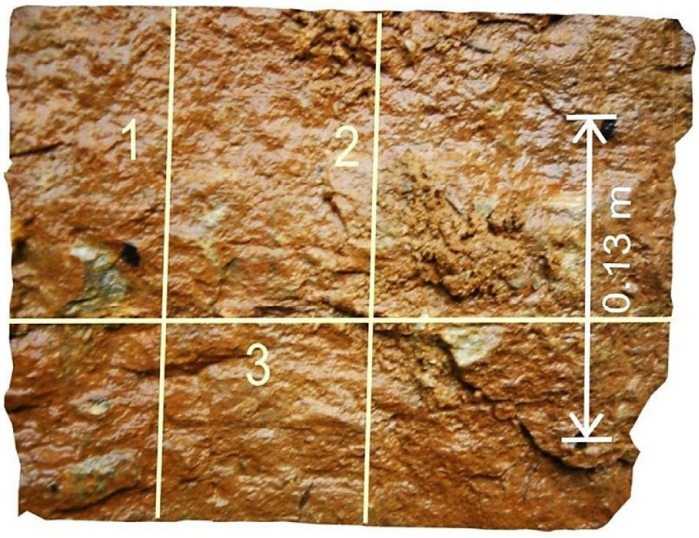

Figure 42: Modeled joint surface of JS3 with locations of the measured profiles

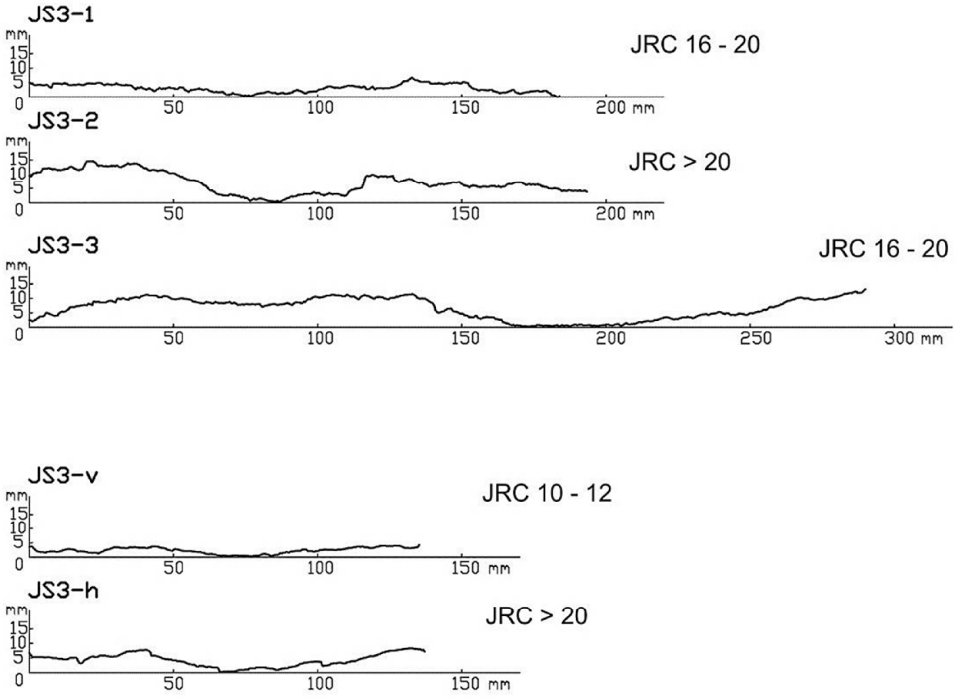

Figure 43: Roughness profiles obtained for a joint surface of JS3 (Digital measured profiles: JS3 – 1 and JS3 – 2 in vertical direction, JS3 – 3 in horizontal direction; manually measured profiles: JS3 – v in vertical direction, JS3 – h in horizontal direction (both profiles measured in middle of the sampled joint surface))

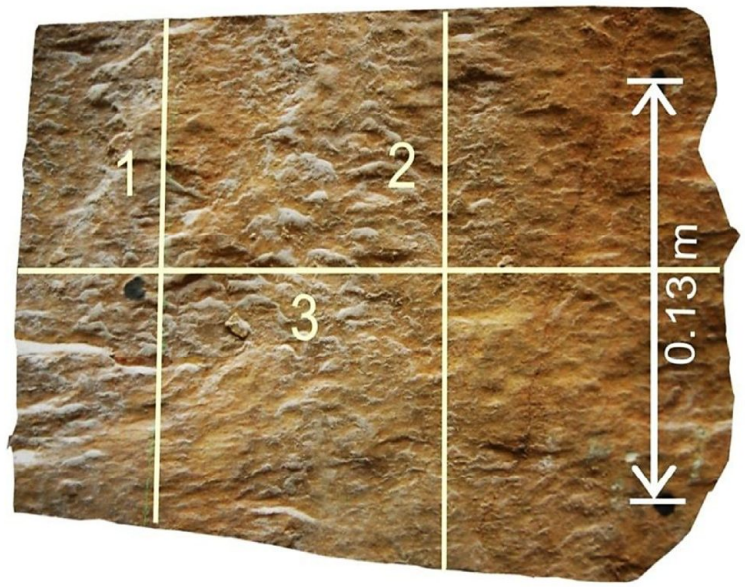

Figure 44: Modeled joint surface of JS4 with locations of the measured profiles

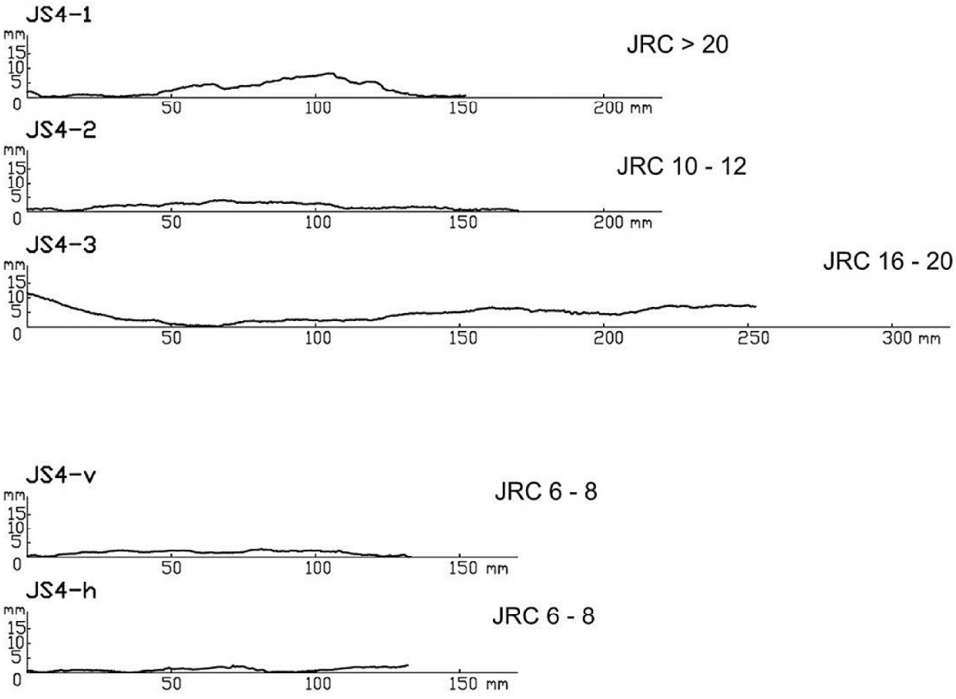

Figure 45: Roughness profiles obtained for a joint surface of JS4 (Digital measured profiles: JS4 – 1 and JS4 – 2 in vertical direction, JS4 – 3 in horizontal direction; manually measured profiles: JS4 – v in vertical direction, JS4 – h in horizontal direction (both profiles measured in middle of the sampled joint surface))

5.3.3.2 ESTIMATING AMOUNT OF INFLUENCE OF IRREGULAR SURFACES ON DISCONTINUITY ORIENTATION

The most irregular shaped profiles were used to simulate “virtual” compass measurements on different locations and to estimate the amount of influence of irregular discontinuity surfaces on orientation measurements. Fig. 46 illustrates this attempt. Tangents to profiles are representing different “virtual” compass locations on the discontinuity surface and tangents normal illustrate surface normal vectors. As shown below, depending on the location of the compass on discontinuity surfaces orientation measurements will scatter only few degrees for slightly undulating surfaces, for rougher surfaces however a higher degree of scattering has to be expected.

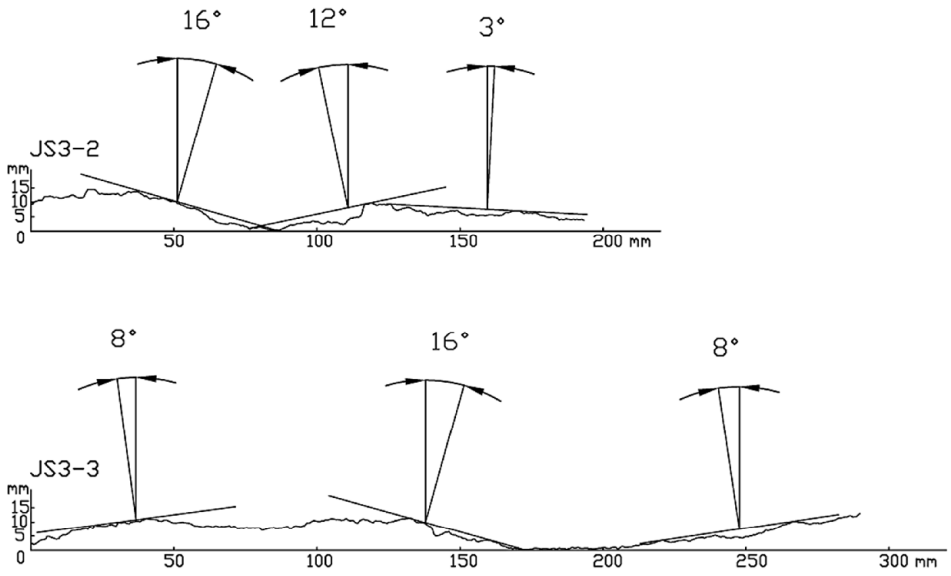

Figure 46: “Virtual” compass measurements on different locations on discontinuity surface (Illustrates the natural amount of scatter for manual orientation measurements: Compass measurements on this arbitrary selected joint surface will scatter from 3° up to 16°)

5.3.4 DISCUSSION OF RESULTS OF INDIVIDUAL ORIENTATION MEASUREMENTS

For slightly irregular joint surfaces where roughness amplitude is small compared to compass size the deviations of manually measured and digital observed orientations are low ($\theta < 3°$) (Tab. 2). Larger dispersions are observed due to different origins. Joints 11, 16, 17 and 26 are located in shadow zones which explain the large discrepancy of orientation results of 11, 17 and 26 for manual and digital measurements. At the location of joint 16 no measurement was possible for this designated model with ShapeMetriX^{3D} due to the very unfavorable imaging perspective for this joint surface. Larger deviations between orientation measurements can also result from natural irregular surfaces as for joint 31.

5.4 TESTING OF DIFFERENT GEOMETRICAL CONFIGURATIONS FOR ROCK FACE MODELING AND ORIENTATION MEASUREMENTS

To account for the influence of different geometrical imaging configurations on orientation results several image pairs were combined and orientation measurements were carried out using SMX software. Since rock mass in Model C is less fractured than in other sections only Model A and Model B were used for these investigations.

5.4.1 VARIATION OF DISTANCE TO ROCK FACE

As a first aspect the influence of different imaging distances was evaluated. Therefore stereoscopic image pairs were taken from different distances (FA1: D=10m, FA2: D=15m, FA3: D=18m, FA4: D=24m; FB1: D=10m, FB2: D=17m, FB3: D=23 m) by varying of focal length (FA1: f=18 mm, FA2: f=27mm, FA3: f=35mm, FA4: f=46mm; FB1: f=18mm, FB2: f=30mm; FB3: f=46mm) (Fig.47).

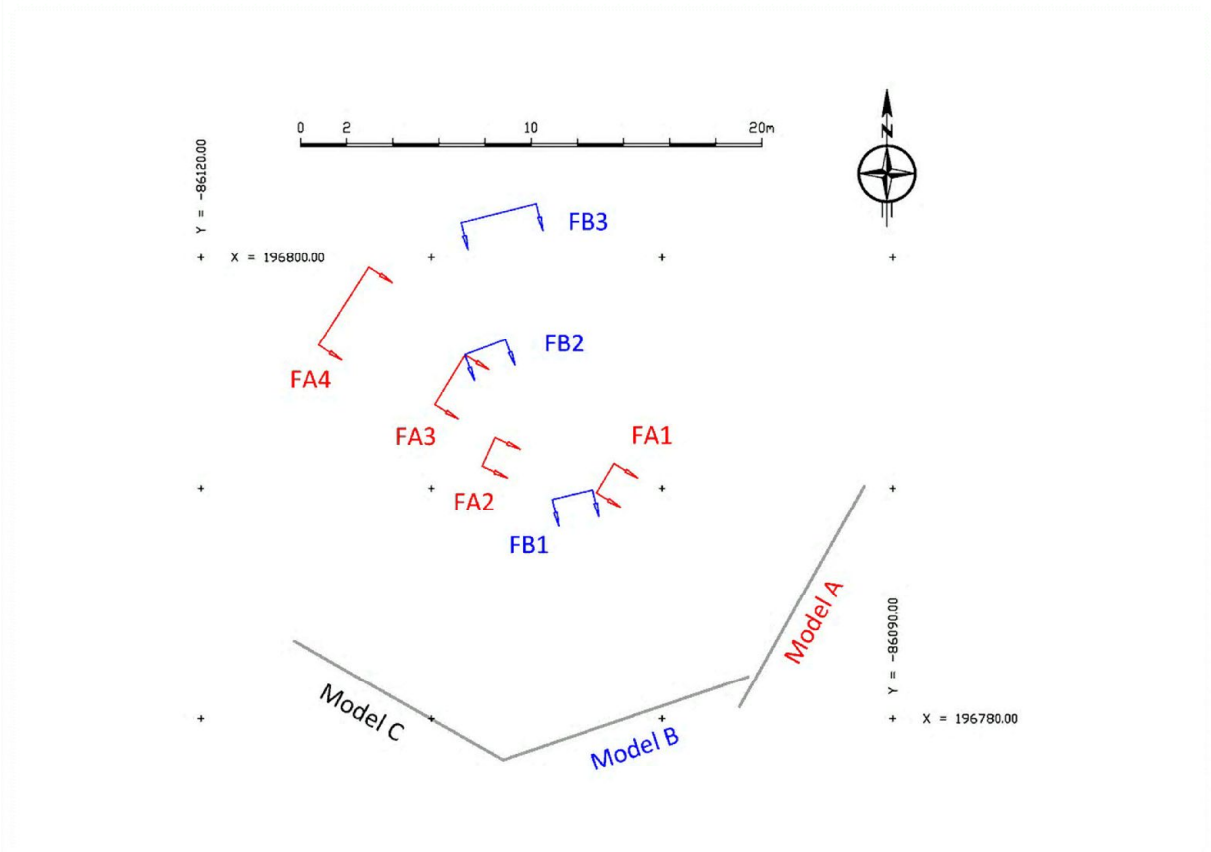

Figure 47: Location of camera standpoints for testing of variable imaging distances

The different models for rock face section A are shown in Fig. 48. The added colorbar is a measure for the quality of the modelled rock face. If the pointer is in the green section it indicates a good quality and quality gets worse towards the red section. The colorbars show that quality of the models FA1 – FA3 is very good and also satisfactory for model C.

MODEL A

FA1

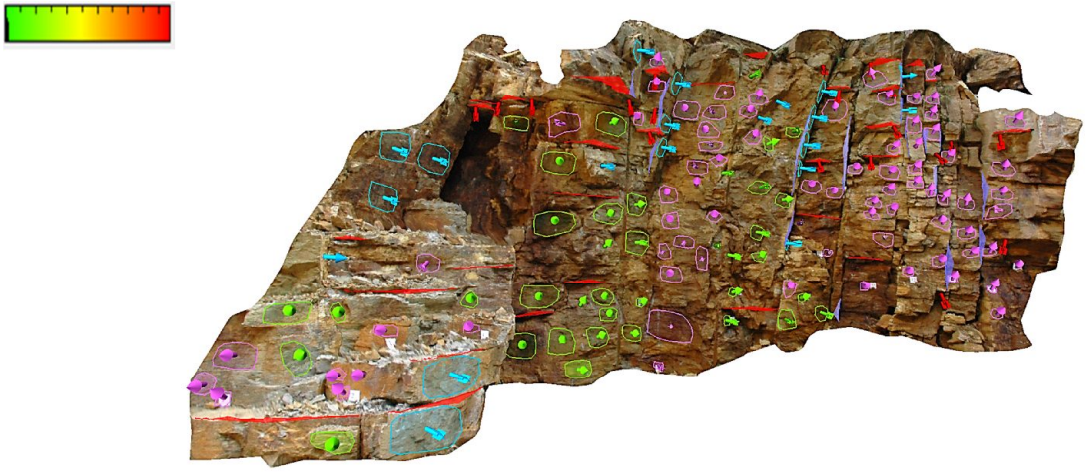

FA2

FA3

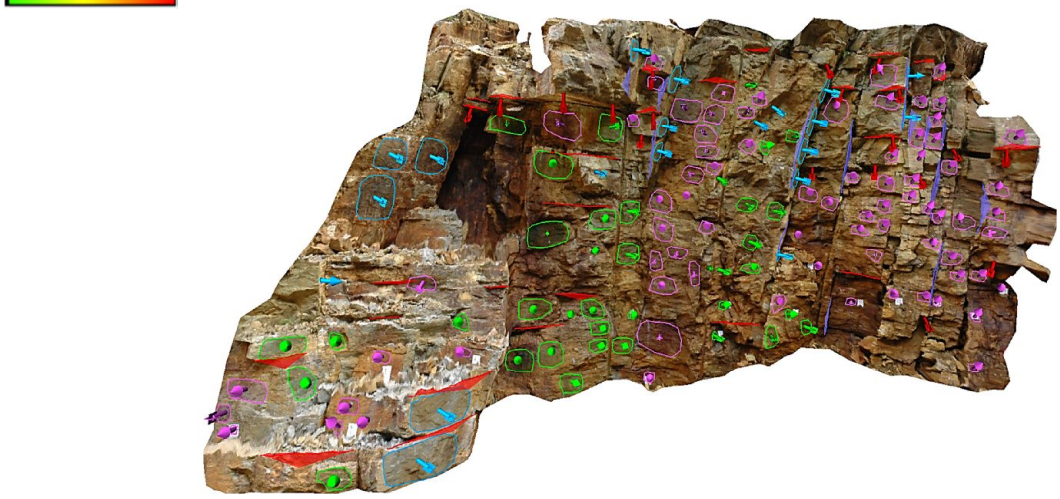

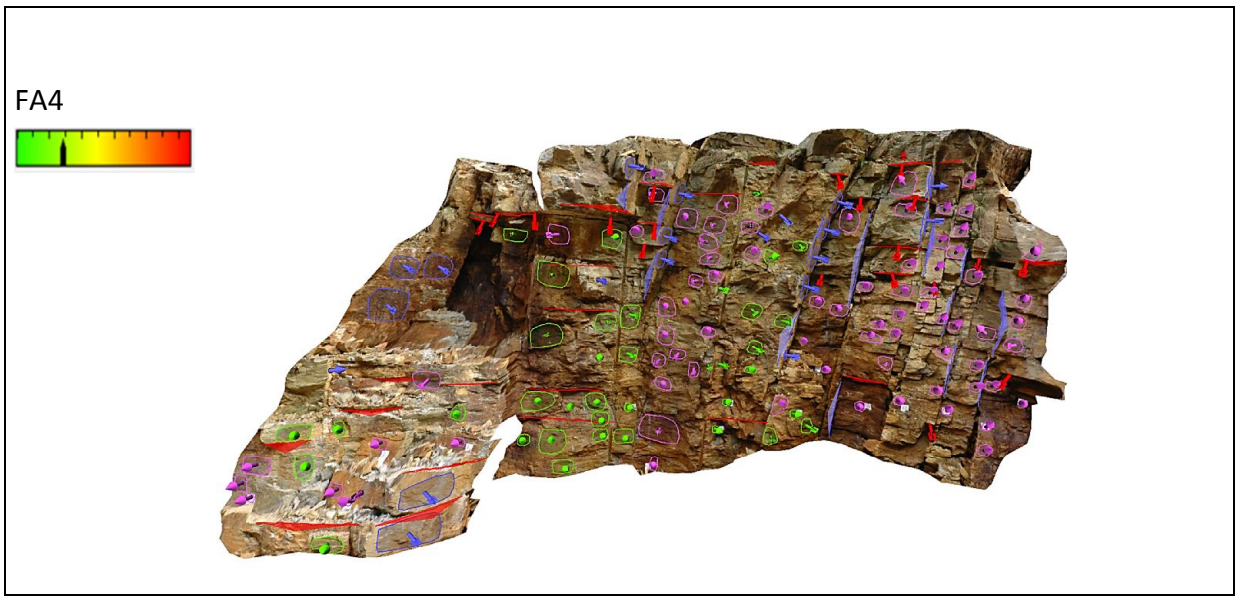

Figure 48: Rock face models for section A with variable imaging distances: (a) FA1, (b) FA2, (c) FA3 and (d) (FA4)

5.4.1.1 DISCONTINUITY PLANE MEASUREMENTS (FA1 – FA4)

The evaluation of discontinuity orientation was performed by outlining of discontinuity planes and discontinuity traces on digital 3D models.

The orientation results for all models (FA1- FA4) are shown in Fig. 49. As orientations of joint sets are similar imaging distance for these configurations has no influence on the results. Generally, there is a good agreement for orientation results of JS1, JS2 and JS4. The closest agreement of mean orientation is achieved for JS1 and JS2. As JS1 and JS2 developed almost parallel to the strike direction of the rock face the largest number of measurement data is obtained for these two joint sets. Sub – horizontal inclined schistosity planes cannot be fully sampled in digital images, thus leading to shadow zones on images. Therefore schistosity orientation obtained by individual orientation measurement spread most.

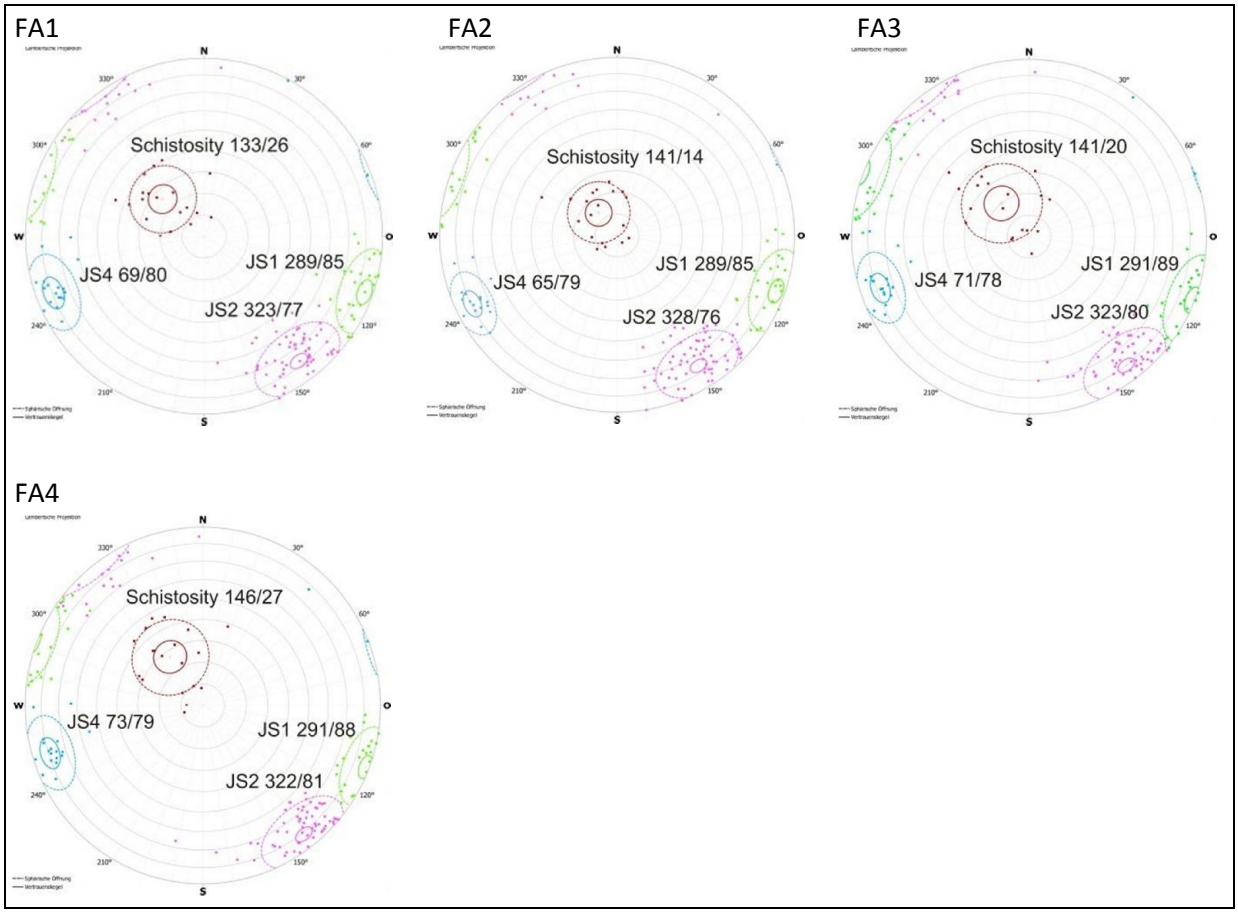

Figure 49: Lambert projection of discontinuity orientation data (poles with centers of gravity) of section A obtained by discontinuity plane measurements for variable imaging distances

5.4.1.2 DISCONTINUITY TRACE MEASUREMENTS (FA1 – FA4)

Trace measurements were possible for schistosity planes and for planes of JS4. The results from interactive mapping are shown in Fig. 50. Discontinuities trace lengths analysis is dislplayed in Tab. 3.

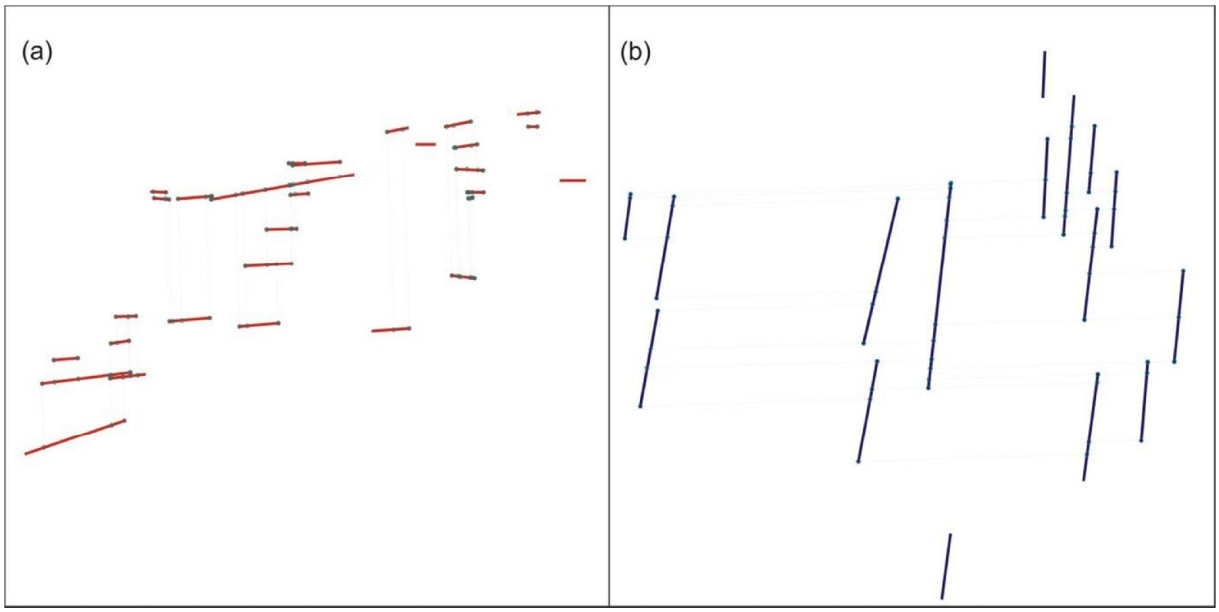

Figure 50: Discontinuity trace map of schistosity planes (a) and planes of JS4 (b) for model FA2

	Schistosity	**JS4**
Total joint trace length	17.36 m	13.72 m
Mean joint trace length	0.60 m	0.86 m
Standard deviation of joint trace length	0.34 m	0.37 m
Number of samples	29	16

Table 3: Results of discontinuity trace length analysis for model FA2

Discontinuity orientations obtained by trace measurements are shown in Fig. 51. Compared to plane measurements schistosity results spread less for trace measurements). While dip angles of schistosity are very similar dip direction values fluctuate for the different configurations. As most joint traces for schistosity planes are not long, measured dip directions vary for slightly different positioned traces on 3D image. Orientation results of JS4 are comparable to plane measurements. Dip directions are few degrees lower than for trace measurements.

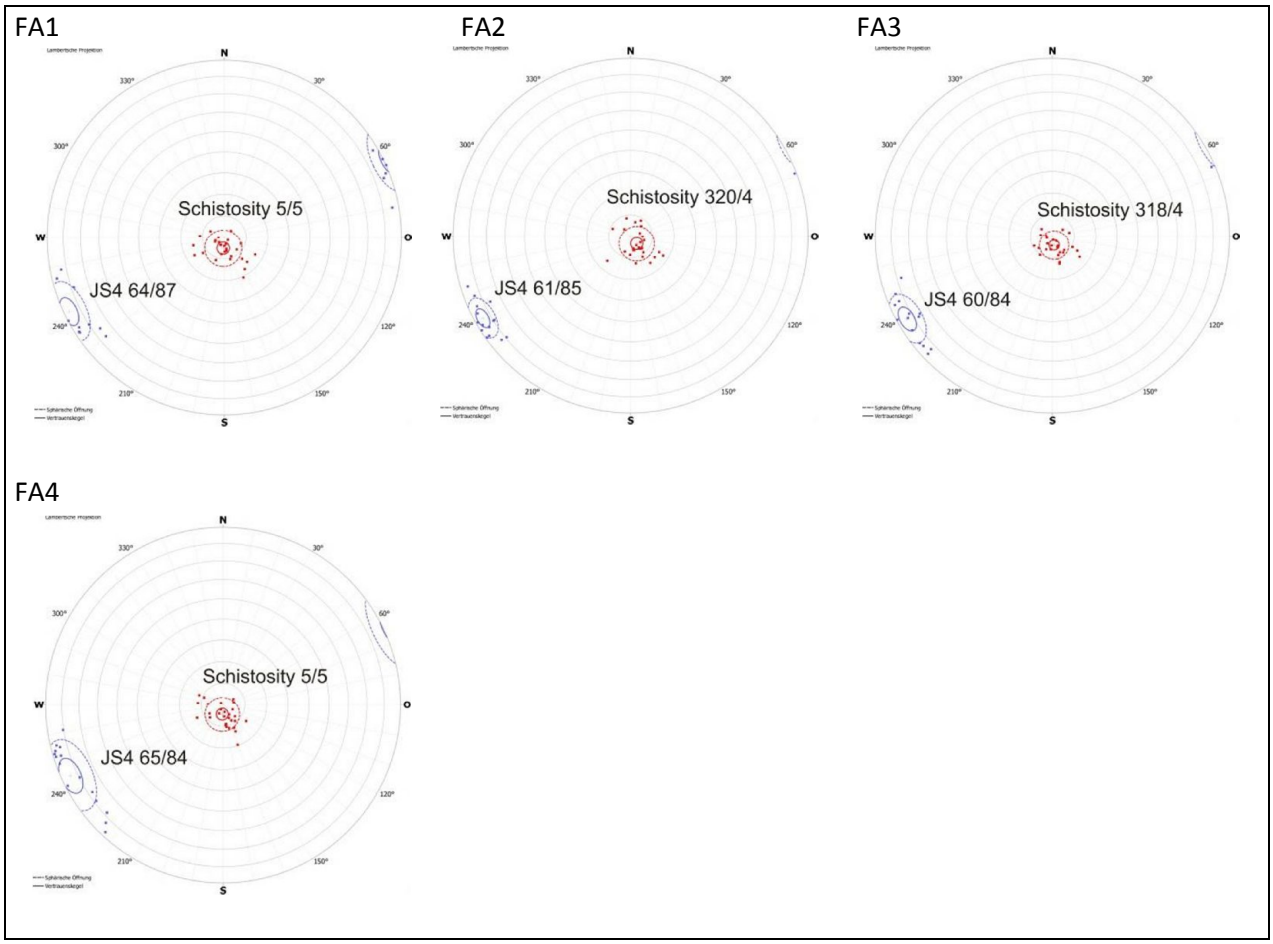

Figure 51: Lambert projection of discontinuity orientation data (poles with centers of gravity) of section A obtained by discontinuity trace measurements for variable imaging distances

MODEL B

The models for rock face section B (FB1 – FB3) are shown in Fig. 52. For the imaging distance of 24 m the quality of Model FB3 is bad and it should be used for precise measurements.

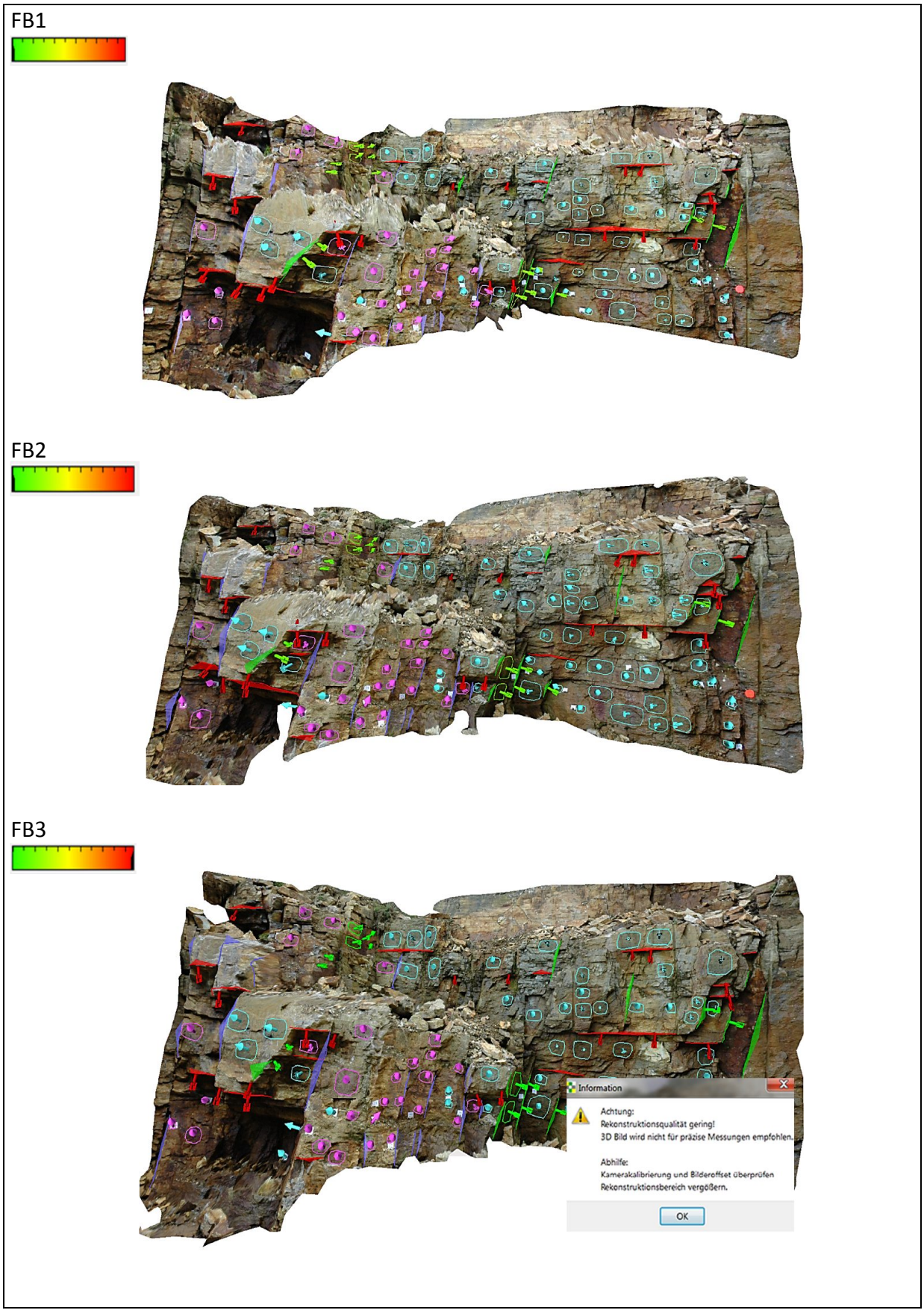

Figure 52: Rock face models for section A with variable imaging distances

5.4.1.3 DISCONTINUITY PLANE MEASUREMENTS (FB1 - FB3)

Fig. 53 shows the results of orientation measurements for models FB1 – FB3. There is a good agreement of mean orientation for JS2 for all models and as well for results of JS3 for configuration FB1 and FB2. These two joint sets (JS2 and JS3) are dipping nearly normal to camera line of sight. Despite of schistosity orientations (reasons for dispersion have already been discussed above) the largest spread of orientation measurements is observed for JS1. There are fewer measurements for JS1 and the orientation of this joint set is unfavorable related to imaging position as these joints are orientated nearby parallel to the vertical line of sight of camera for this configurations.

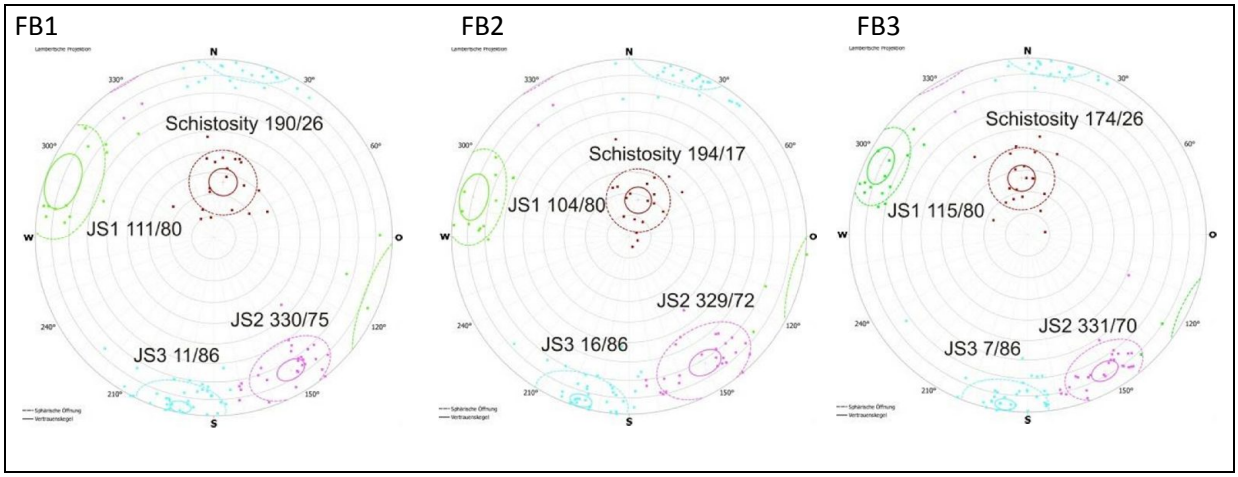

Figure 53: : Lambert projection of discontinuity orientation data (poles with centers of gravity) of section B obtained by discontinuity plane measurements for variable imaging distances:

5.4.1.4 DISCONTINUITY TRACE MEASUREMENTS (FB1 - FB3)

Trace measurements were performed for schistosity planes and for planes of JS1 and JS4. Their trace maps are displayed in (Fig. 54). The results of discontinuity trace length analysis are shown in Tab. 4. Schistosity planes measured by traces deliver more reliable results (Fig. 55) as they are more similar to compass measurements (Fig. 32 (b)) and they scatter less than results obtained by plane measurements (Fig. 53). Fewest trace measurements were possible for JS1.

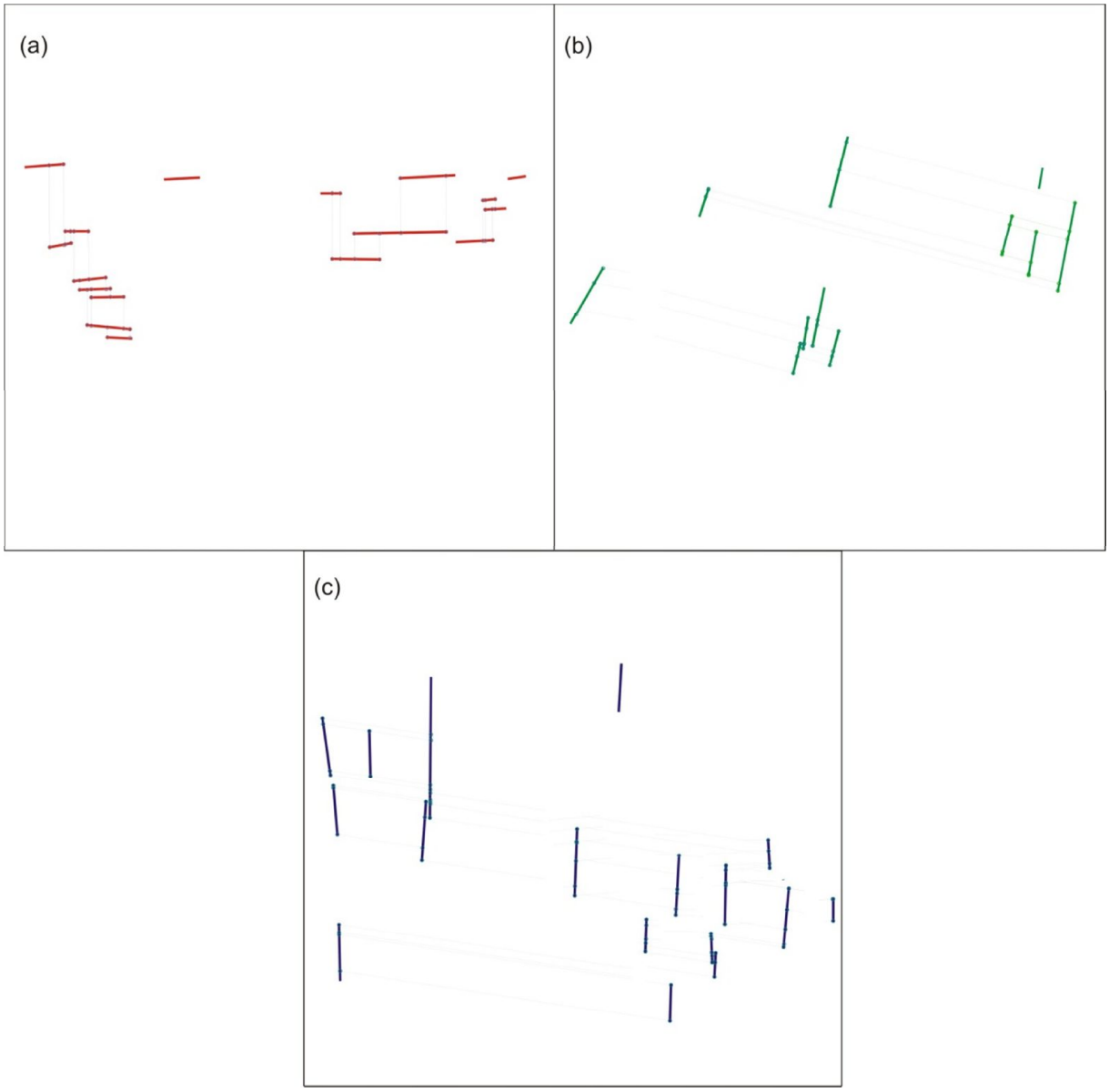

Figure 54: Discontinuity trace map of schistosity planes (a), planes of JS1 (b) and planes of JS4 (c) for model FB2

	Schistosity	**JS1**	**JS4**
Total joint trace length	12.70 m	8.17 m	11.71 m
Mean joint trace length	0.75 m	0.74 m	0.69
Standard deviation of joint trace length	0.45 m	0.37	0.3
Number of samples	17	11	17

Table 4: Results of discontinuity trace length analysis for model FB2

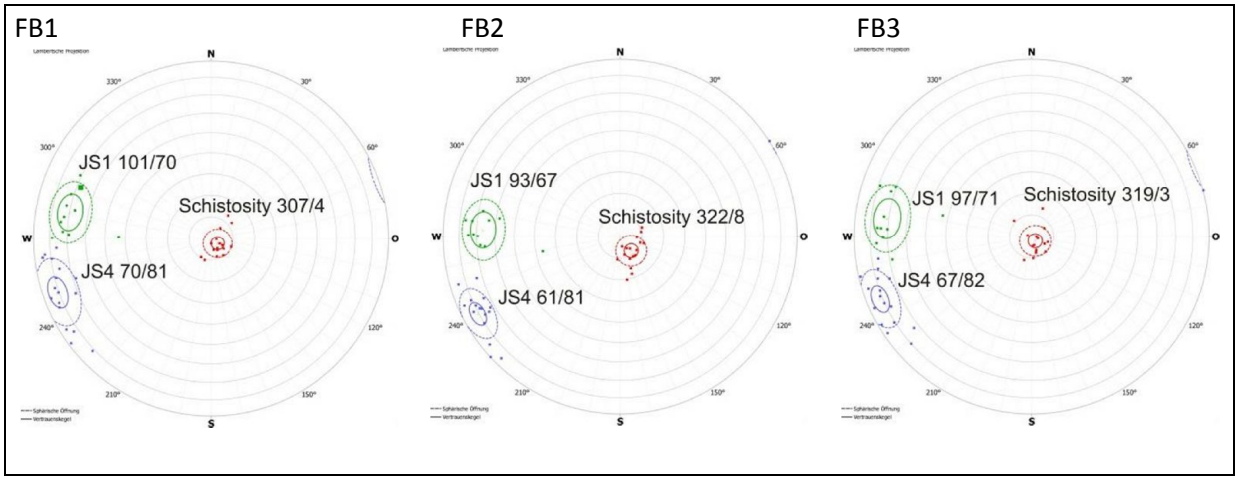

Figure 55: Lambert projection of discontinuity orientation data (poles with centers of gravity) of section B obtained by discontinuity trace measurements for variable imaging distances

5.4.2 VARIATION OF BASELENGTH

For obtaining accurate models it is recommended to use base - lengths in the order of 1/8 to 1/5 of the imaging distance. To test how sensitive the choice of base - length is with respect to construction of rock face model and orientation measurements recommended base – length as well as less appropriate configurations were chosen (Tab. 5). Fig. 56 shows the configurations for modeling of rock face A. Rock face models are displayed in Fig. 57 (BA1 – BA3) and Fig. 58 (BA4 – BA6).

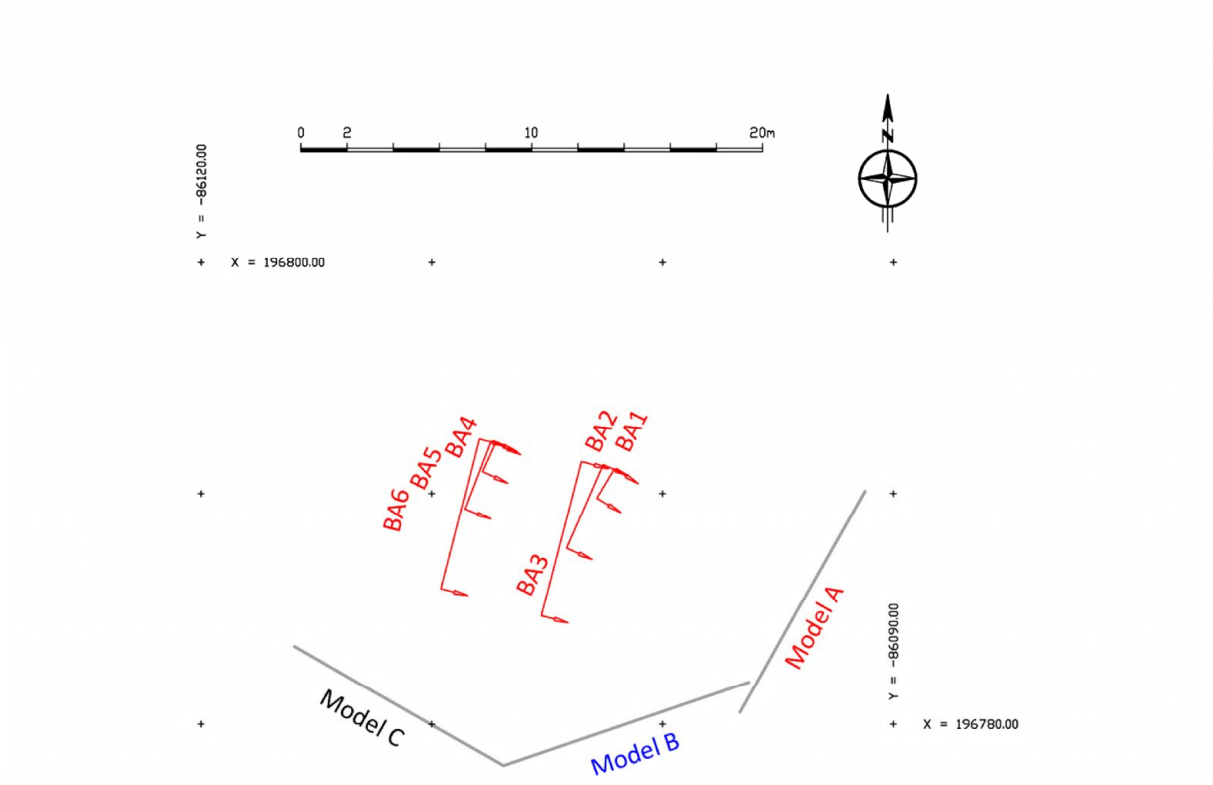

Figure 56: Location of camera standpoints for testing of variable base - lengths (section A)

Model	B [m]	D [m]	Tolerance range for base length (D/8 -D/5) [m]
BA1	1.4	10.0	1.3 - 2.0
BA2	4.0	10.3	1.3 - 2.1
BA3	6.9	10.8	1.4 - 2.2
BA4	1.4	15.0	1.9 - 3.0
BA5	3.1	15.0	1.9 - 3.0
BA6	6.7	15.3	1.9 - 3.1

Table 5: Base lengths configurations for model A

Models BA1 and BA5 were created from stereo pairs with ideal base lengths. For BA4 base lengths is 0.5m shorter than recommended. Configurations BA2 and BA6 are having base lengths already twice as long as recommended. It was not possible to create a model for configuration BA3. Here base length is already three times larger than D/5. The added colorbar in Fig. 57 and Fig. 58 indicates the quality of the model. Quality of the model is good in green section and it gets worse towards red section. For configuration BA6 the model hasn't been completely reconstructed. Marginal regions were not reconstructed (Fig. 58).

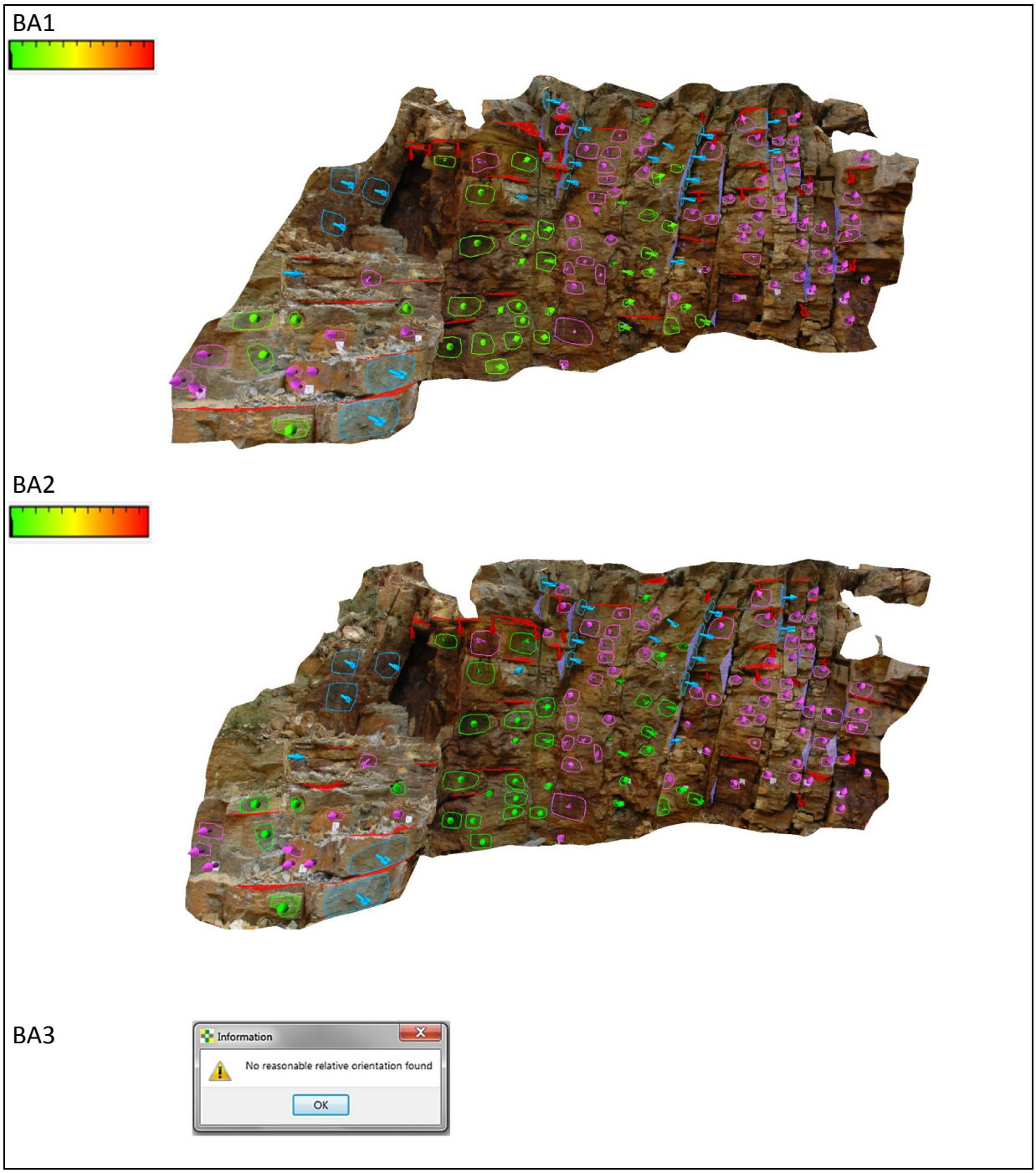

Figure 57: Rock face models for section A with variable base – lengths

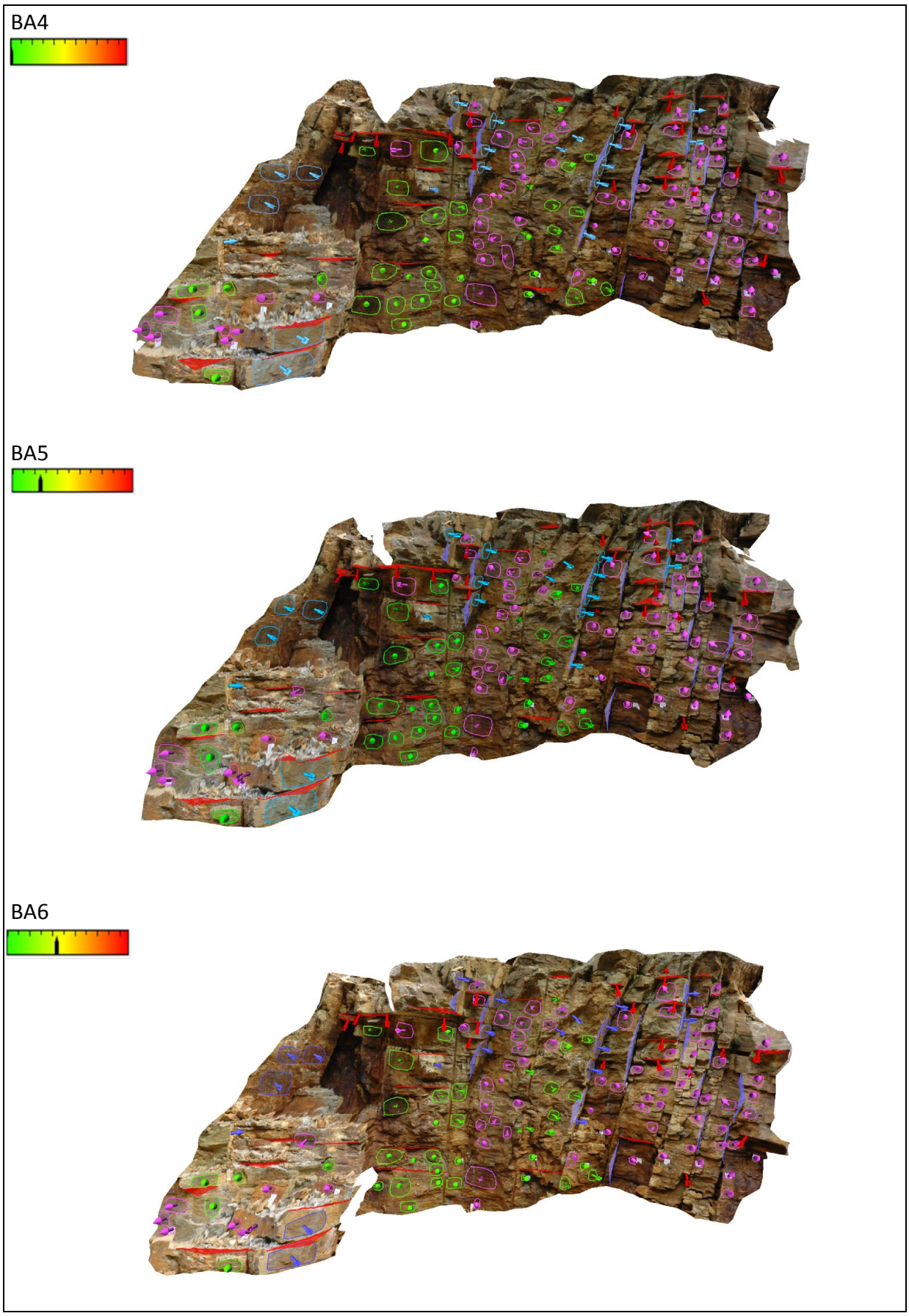

Figure 58: Rock face models for section A with variable base – lengths

5.4.2.1 DISCONTINUITY PLANE MEASUREMENTS (BA1 – BA6)

Orientation results for models BA1 – BA2 and BA4 – BA6 obtained by discontinuity plane measurements are shown in Fig. 59. Variation of base lengths doesn't affect results for JS1, JS2 and JS4. Although configuration BA2 uses base length twice as large as recommended, the mean orientations of JS1, JS2 and JS3 are very similar compared to results obtained for model BA2 It is also the case for orientation results of model BA5 and BA6. Comparable results are achieved. Again model BA6 uses a 50% larger base length than model BA5. It has already been pointed out that individual measurements do not deliver accurate orientation data for sub horizontal inclined schistosity planes. Schistosity orientations spread even more with increasing base length.

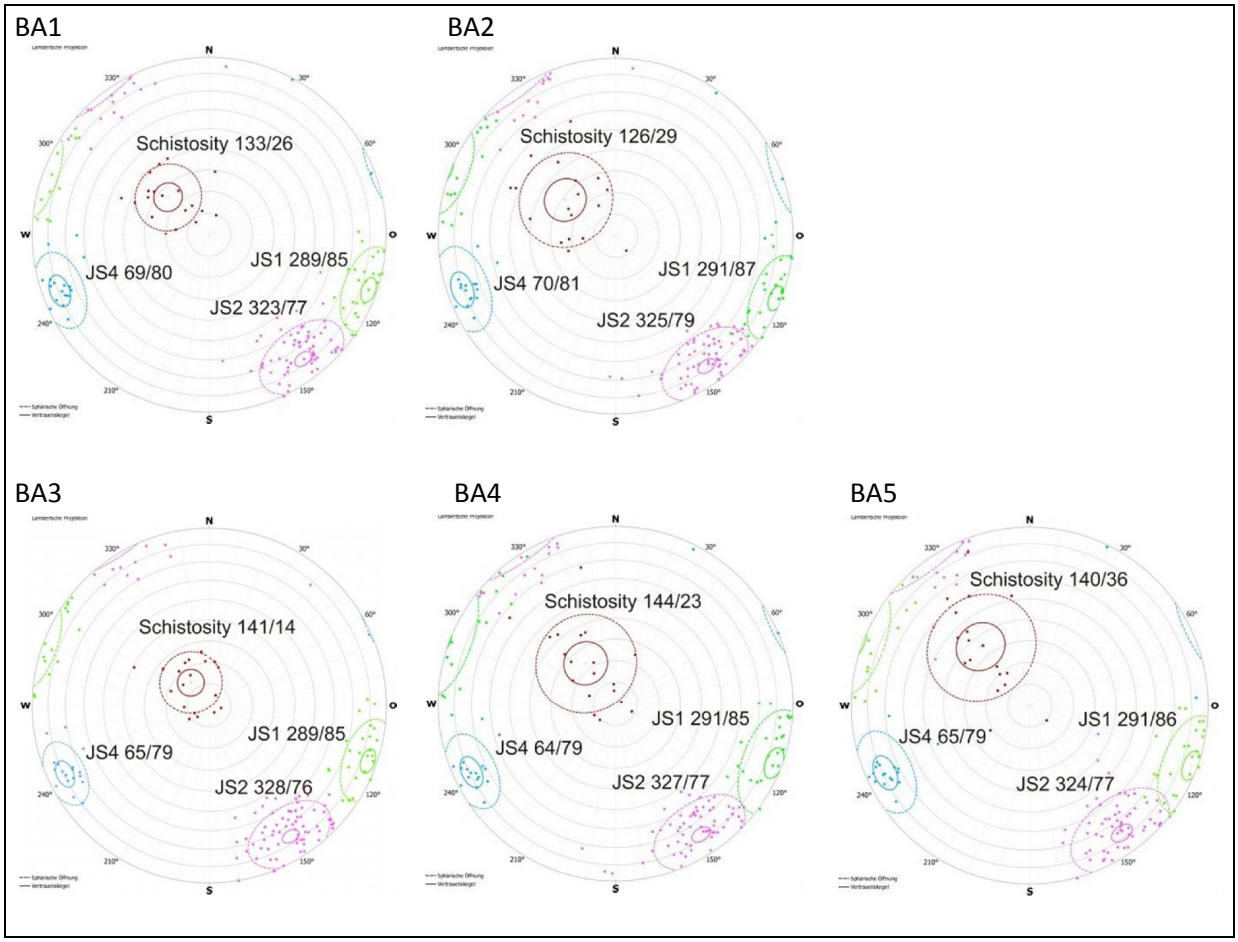

Figure 59: Lambert projection of discontinuity orientation data (poles with centers of gravity) of section A obtained by discontinuity plane measurements for variable base - lengths

5.4.2.2 DISCONTINUITY TRACE MEASUREMENTS (BA1 – BA6)

Fig. 60 shows the orientation data obtained by discontinuity trace measurements performed on models BA1 - BA6. Like for discontinuity plane measurements, orientation for JS4 is similar for configurations with different base – length.

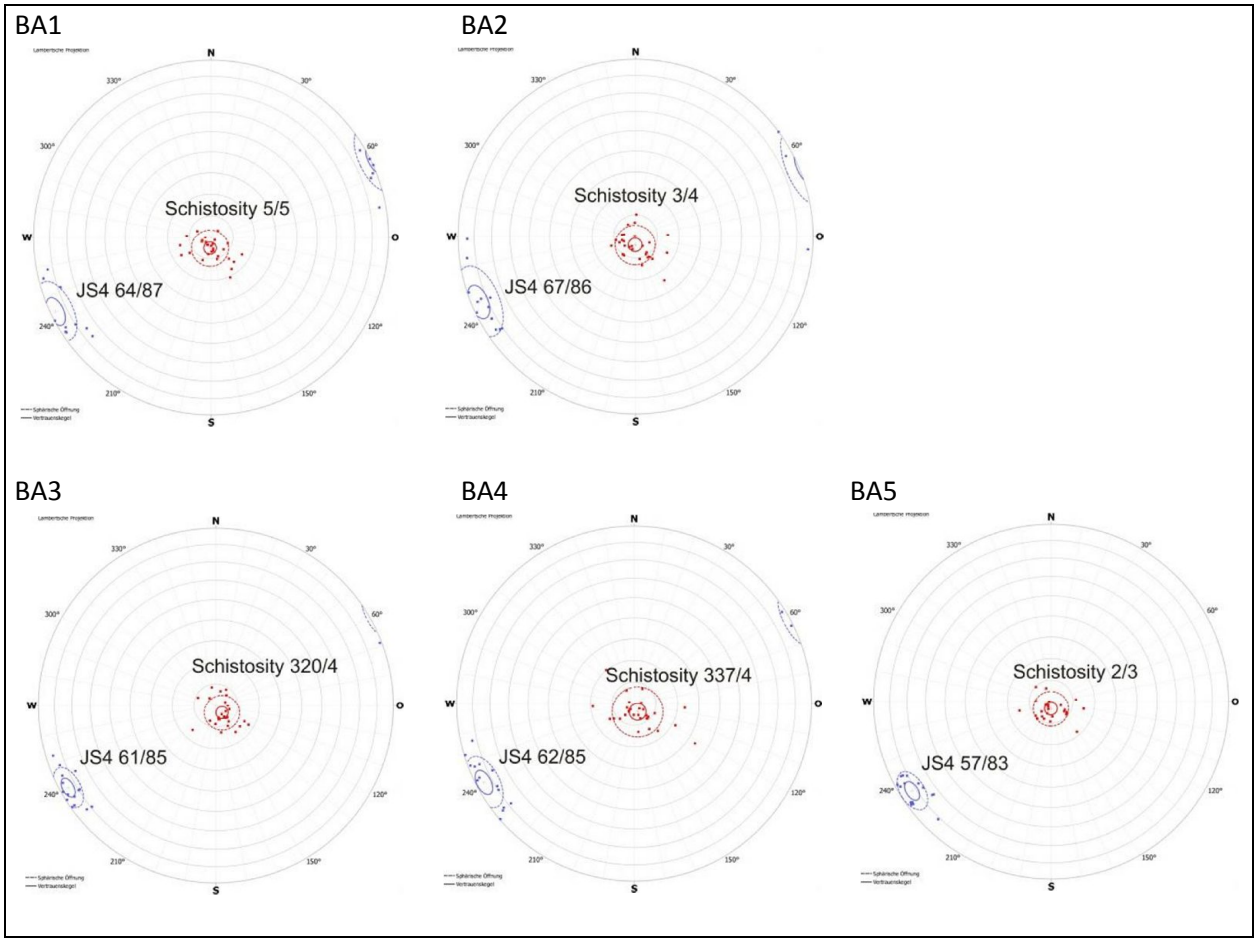

Figure 60: Lambert projection of discontinuity orientation data (poles with centers of gravity) of section A obtained by discontinuity trace measurements for variable base - lengths

MODEL B

Image pairs with variable base – lengths were also taken for modeling of rock face section B (Fig. 61). Base lengths configurations are displayed in Tab. 6.

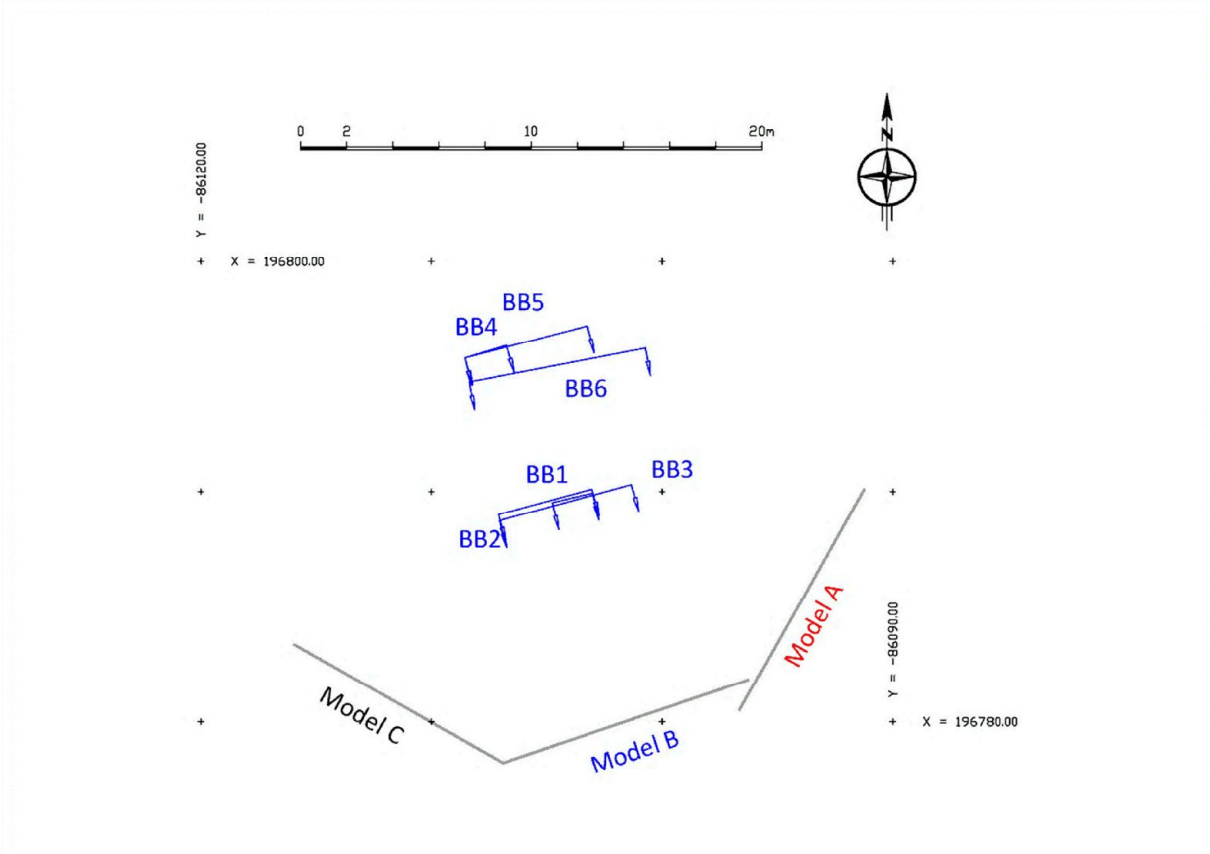

Figure 61: Location of camera standpoints for testing of variable base - lengths (section B)

Rock face models are shown in Fig. 62 (BB1 – BB3) and in Fig. 63 (BB4 – BB6). Recommended base – length was used for model BB1. Also base length for model BB4 is acceptable. Base lengths for BB2 and BB6 are more than twice times larger than recommended. For configurations with too long base lengths (BB2, BB3, BB5) models were not completely reconstructed. Model BB3 is generated of stereo pair images with a base length which is already three times larger than suggested. Large parts of the models were not reconstructed (Fig. 62 (c)).

Model	B [m]	D [m]	Tolerance range for base length (D/8 - D/5) [m]
BB1	1.8	10.0	1.3 - 2.0
BB2	4.2	10.0	1.3 - 2.0
BB3	5.9	10.0	1.3 - 2.0
BB4	1.9	17.0	2.1 - 3.0
BB5	5.5	17.0	2.1 - 3.0
BB6	7.8	15.8	2.0 - 3.2

Table 6: Base lengths configurations for model B

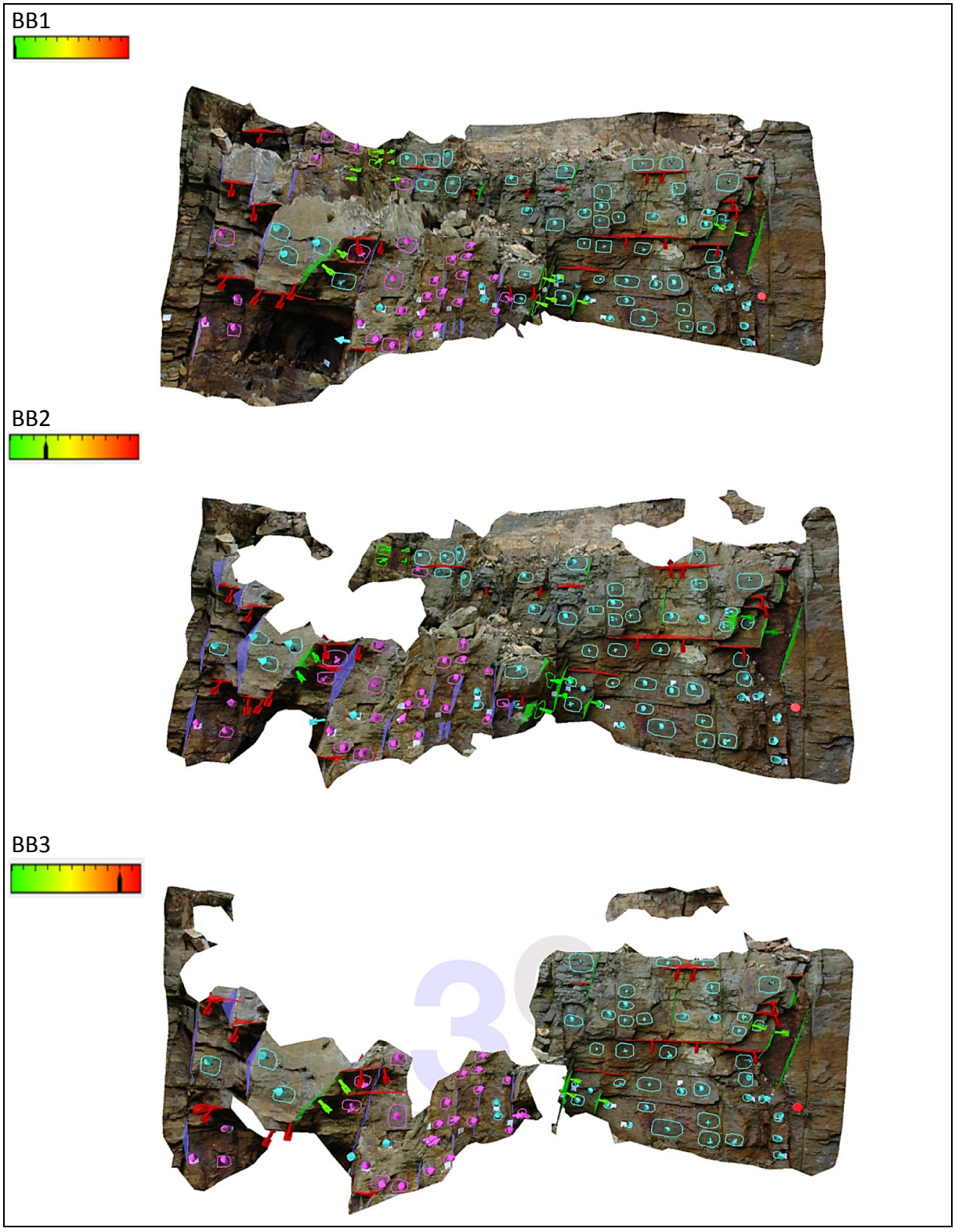

Figure 62: Rock face models for section B with variable base – lengths

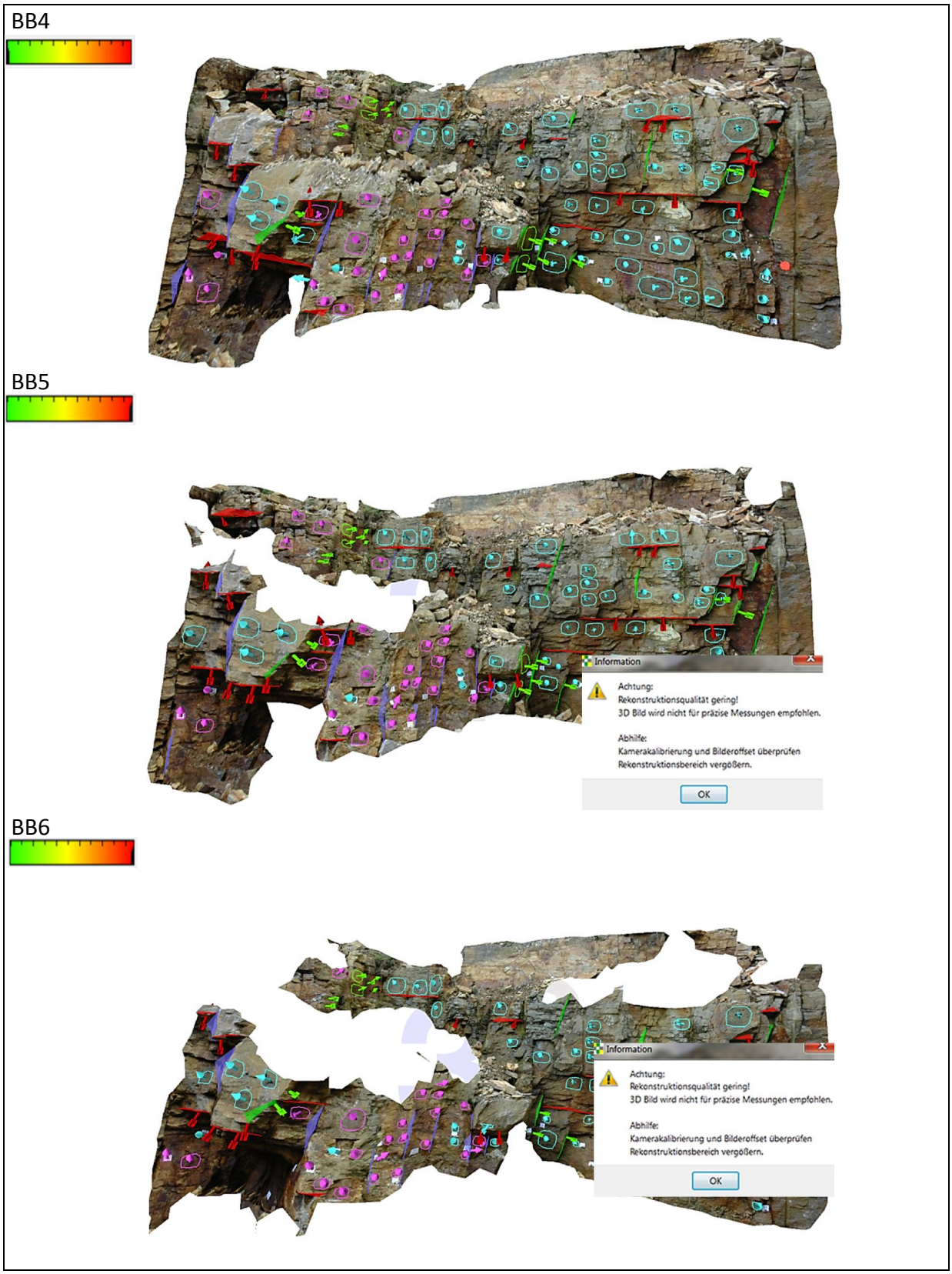

Figure 63: Rock face models for section B with variable base – lengths

5.4.2.3 DISCONTINUITY PLANE MEASUREMENTS (BB1 – BB6)

Orientation measurements performed on models BB1 – BB6 are shown in Fig. 64. Results of JS2 and JS3 show fewest variation with increasing base lengths. As the orientation of JS1 is not favorable orientated to camera line of sight the measurement number of orientation data is in general lower and the spread of orientation results is larger for JS1. With increasing base – length fewer orientation measurements are possible for JS1 and orientation becomes less accurate as dispersion increases.

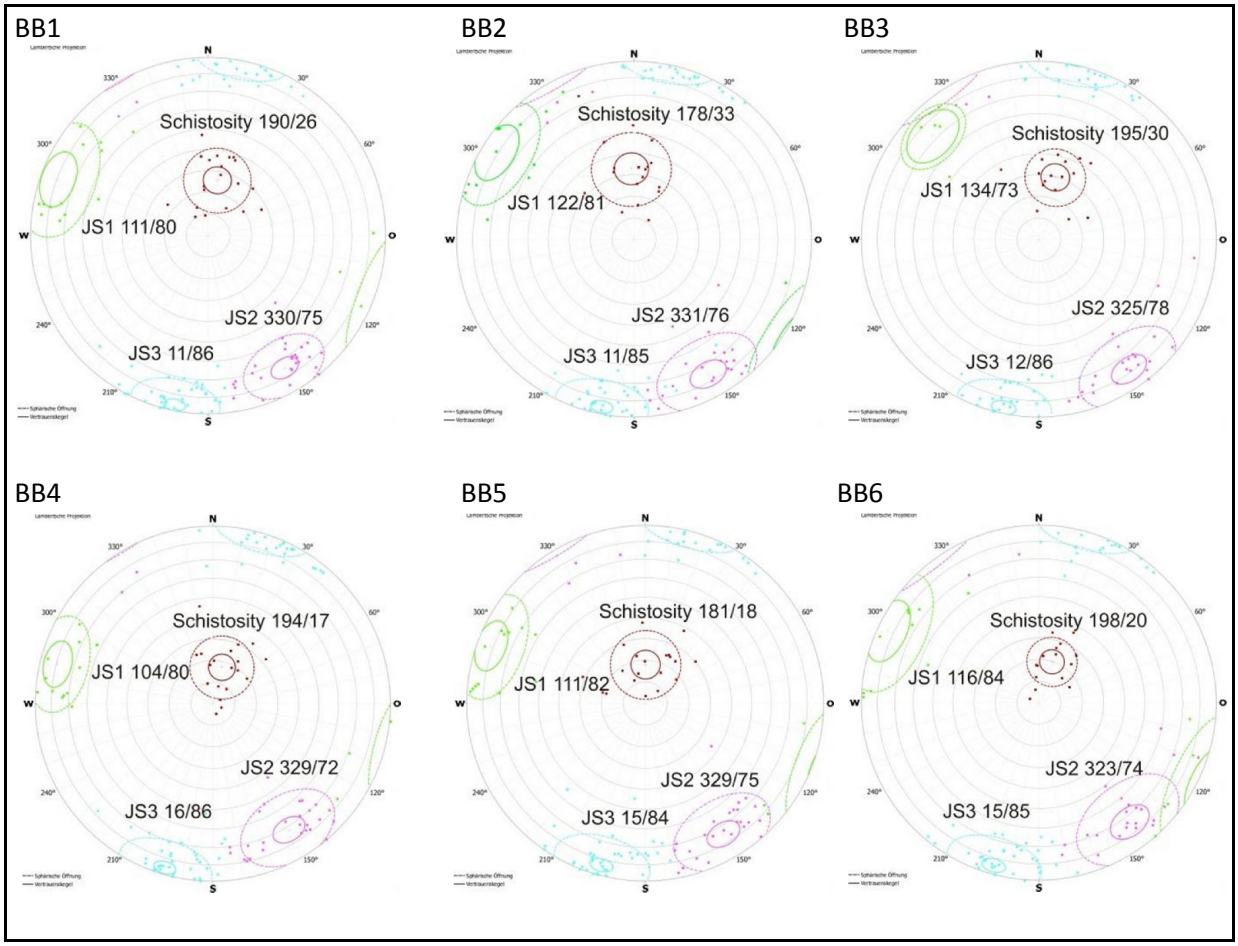

Figure 64: Lambert projection of discontinuity orientation data (poles with centers of gravity) of section B obtained by discontinuity plane measurements for variable base - lengths

5.4.2.4 DISCONTINUITY TRACE MEASUREMENTS (BB1 – BB6)

Orientation data for JS1 and schistosity planes obtained by trace measurements fluctuate less with increasing base – length (Fig. 65) compared to results obtained by discontinuity plane measurements (Fig. 64).

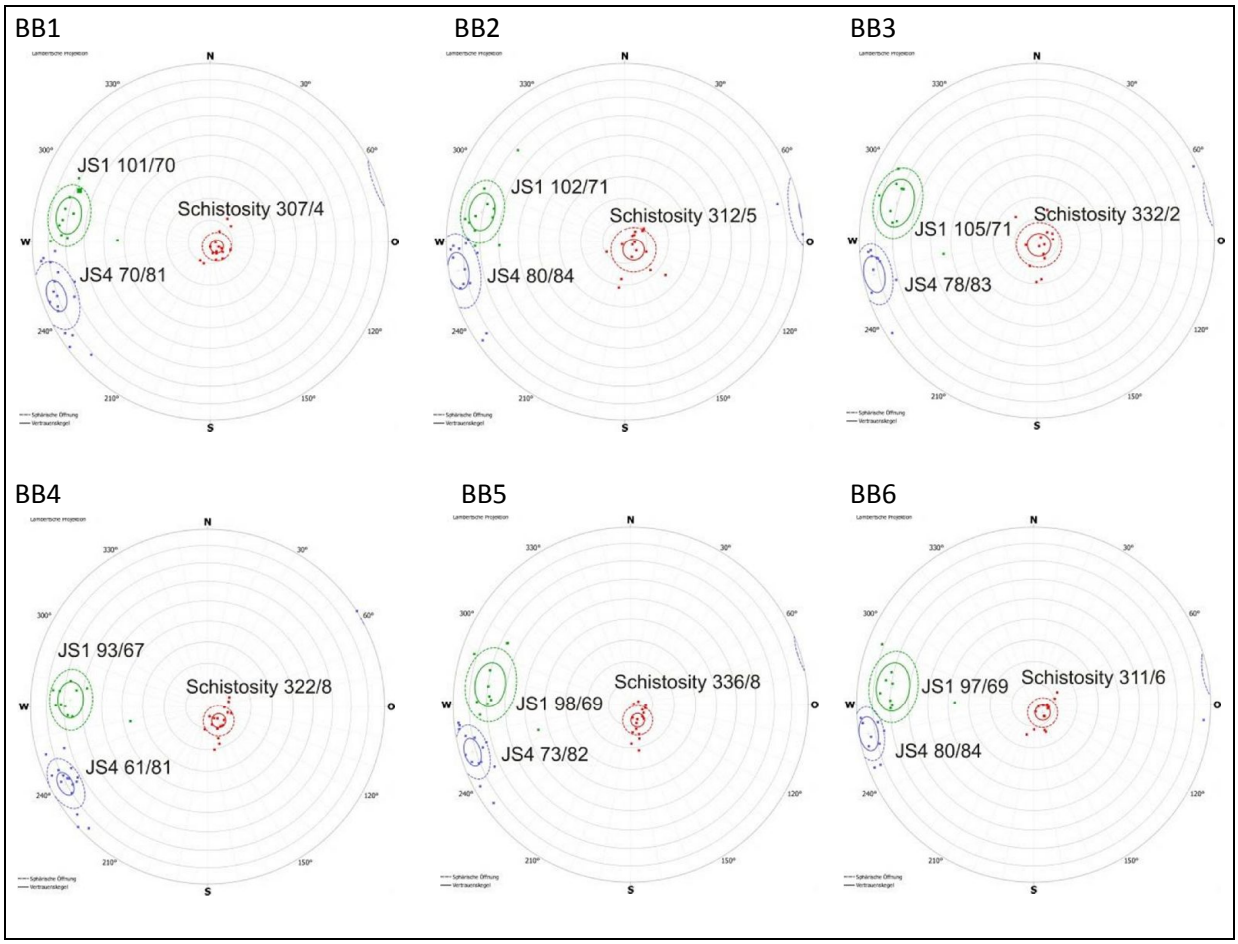

Figure 65: Lambert projection of discontinuity orientation data (poles with centers of gravity) of section B obtained by discontinuity trace measurements for variable base - lengths

5.4.3 VARIATION OF PERSPECTIVES (CAMERA ANGLE)

As a third aspect different imaging viewing directions were tested (Fig. 66).The choice of camera standpoints was limited to space in quarry. For AB1 image plane is approximately normal to rock face. This configuration is regarded as an “ideal case”. The viewing direction for AB2 deviates from AB1 21° (to the east). For the configuration AB3 the camera line of sight is out of the ideal 45° (to the west). Rock face models for configurations AB1 – AB3 are shown in Fig. 67. Model AB3 was not completely reconstructed due to the fact that these parts are not visible from this imaging perspective.

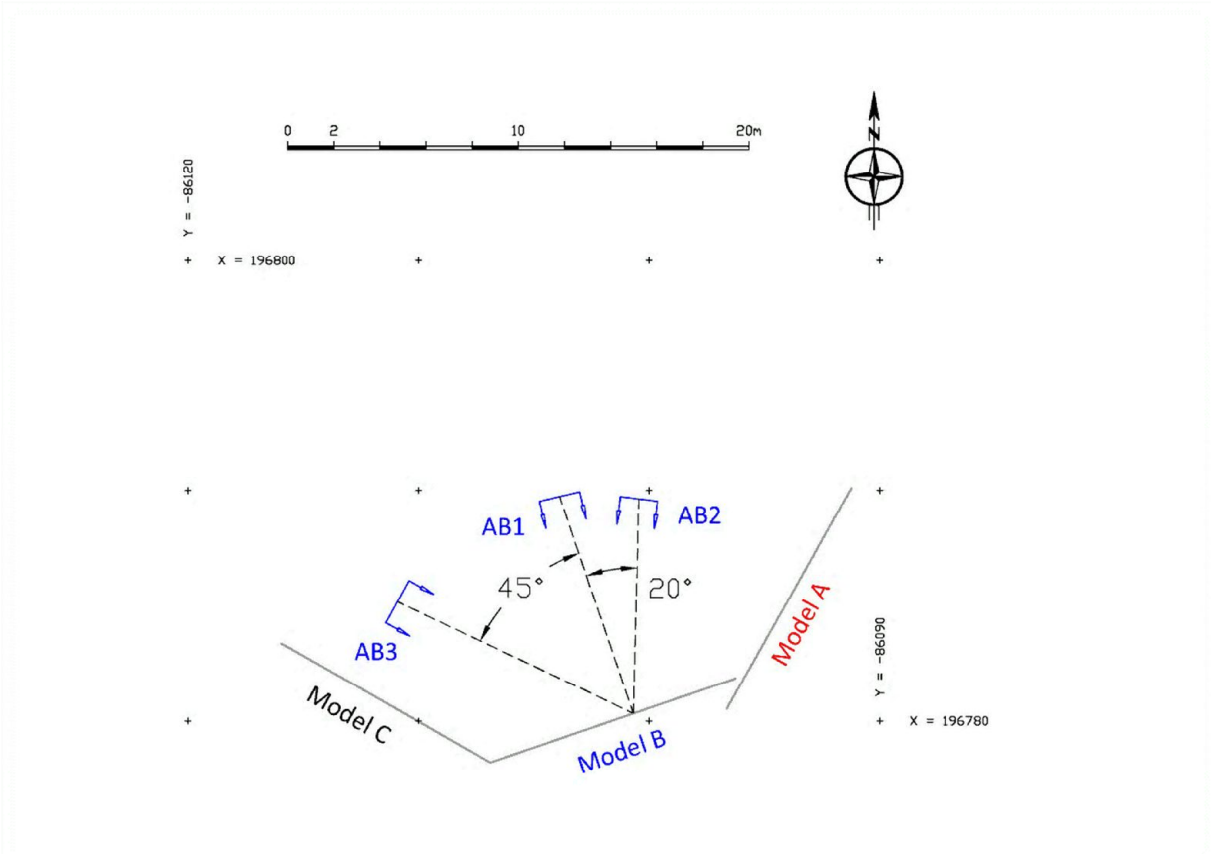

Figure 66: Location of camera standpoints for testing of variable intersecting angles (section B)

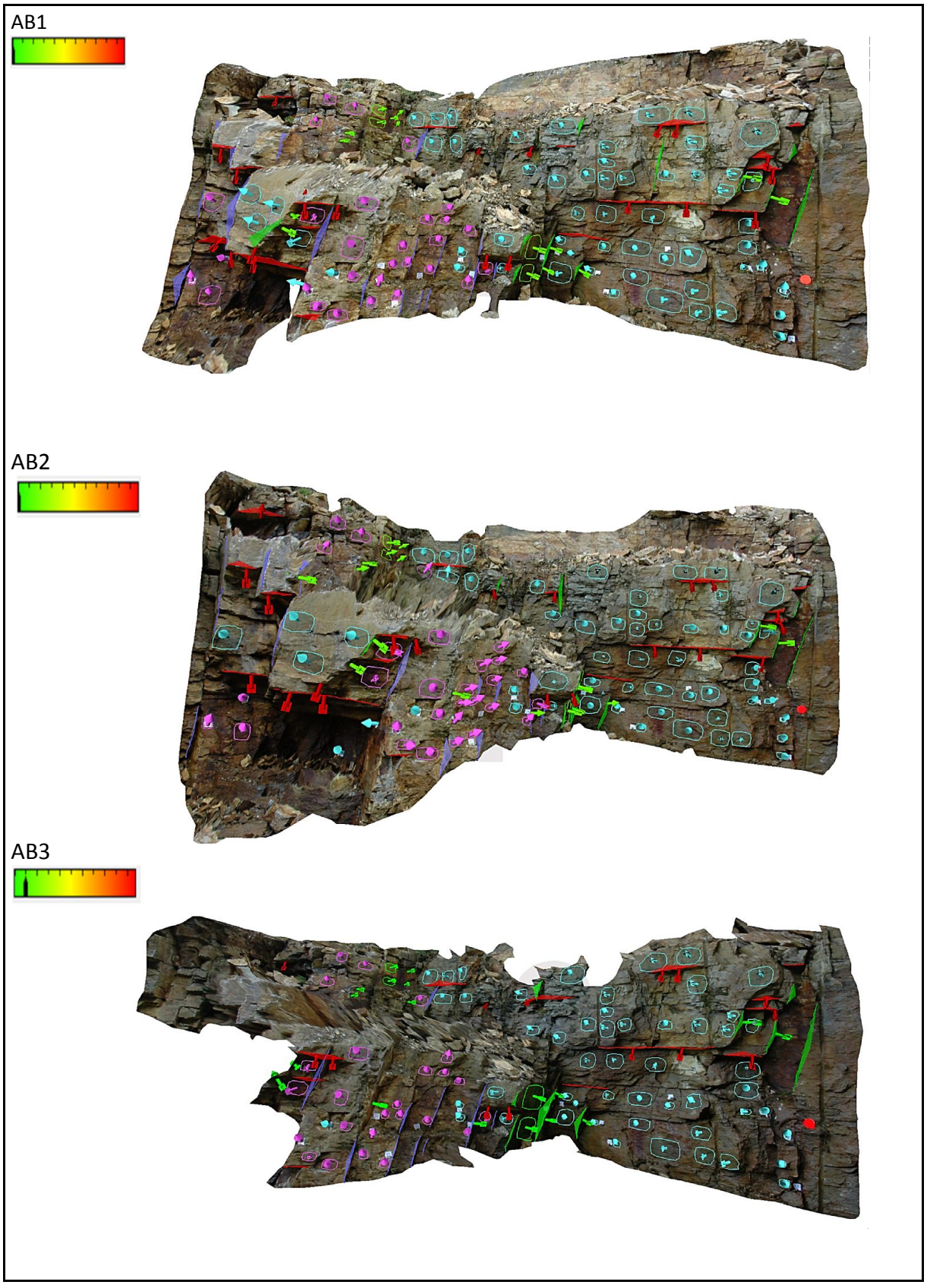

Figure 67: Rock face models for section B with variable camera angles

5.4.3.1 DISCONTINUITY PLANE MEASUREMENTS (AB1 – AB3)

Discontinuity plane measurements for configuration AB1 – AB3 are shown in Fig. 68 and orientation results of trace measurements are shown in Fig. 69. JS2 and JS3 show fewest variations for different imaging perspectives. Since most accurate orientation is measured for joints which are aligned normal or very nearby to image plane configuration AB3 is most suitable to measure orientation of JS1. The configuration gives the smallest orientation spread for JS1.

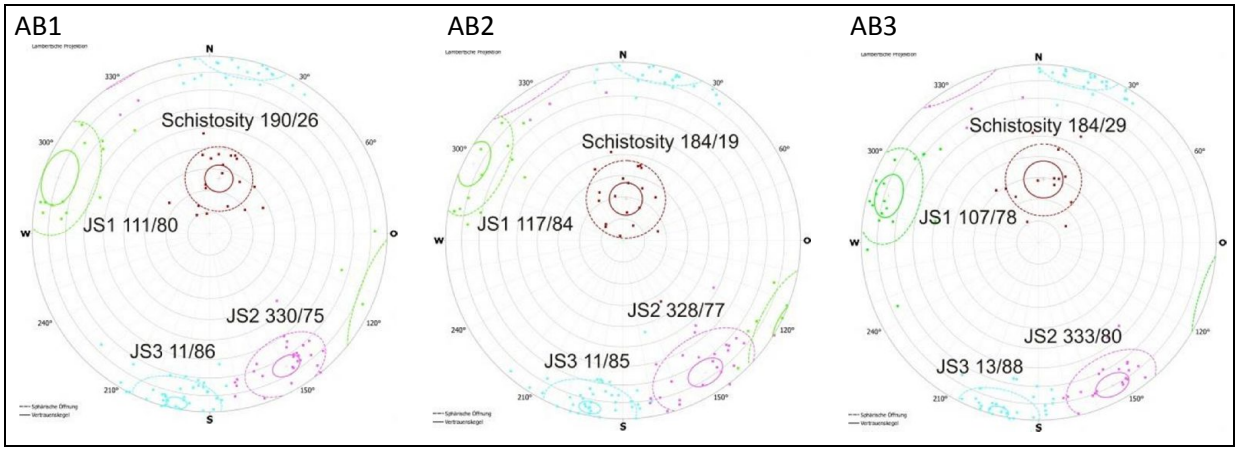

Figure 68: Lambert projection of discontinuity orientation data (poles with centers of gravity) of section B obtained by discontinuity plane measurements for variable camera angles

5.4.3.2 DISCONTINUITY TRACE MEASUREMENTS (AB1 – AB3)

Trace measurements deliver a close agreement of orientation results for JS1 for different imaging perspectives.

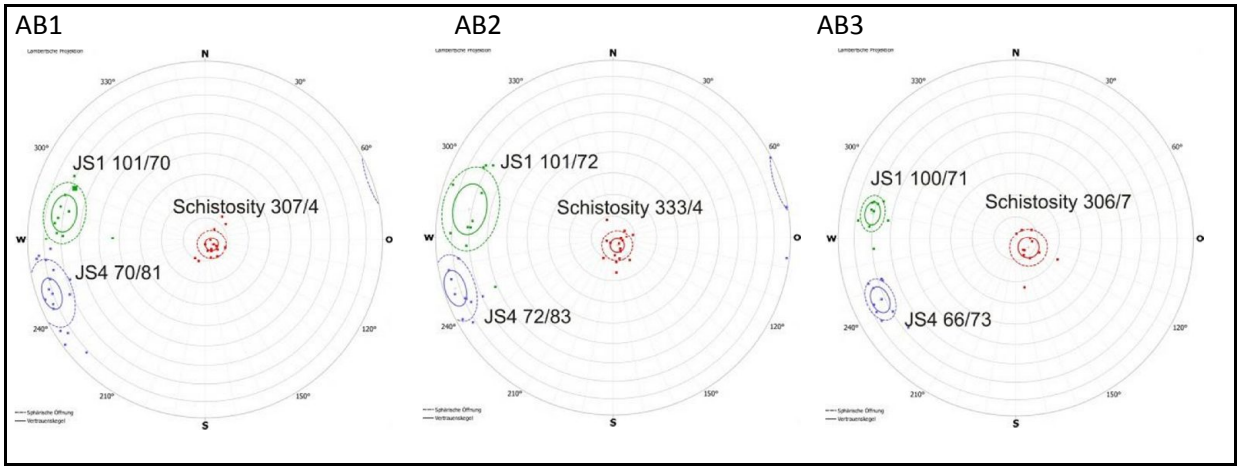

Figure 69: Lambert projection of discontinuity orientation data (poles with centers of gravity) of section B obtained by discontinuity trace measurements for variable camera angles

6. DISCUSSION AND CONCLUSION

Structural orientation data in the quarry area was obtained by manual field mapping using a geological compass and by digital rock face characterization. Although compass measurements are easy to perform in the field there are some drawbacks which may influence the quality of orientation measurements. With the compass only a minimum area at the exposed discontinuity surface is captured. When measuring on rough discontinuity surfaces orientation varies at different locations at the surface.

As there is no direct access to rock face in higher regions in investigated area orientation measurements in this parts are impossible. Furthermore compass measurements are slow and time consuming. The ShapeMetriX^{3D} system provides an ideal solution to overcome limitations of time and accessibility. Overlapping image pairs of rock face were combined with surveyed reference points to create digital 3D models of exposed rock face. Individual discontinuities were selected and manually outlined on 3D image to calculate an arbitrary number of orientations. Fig. 70 shows the number of orientation measurements obtained by manual and digital method.

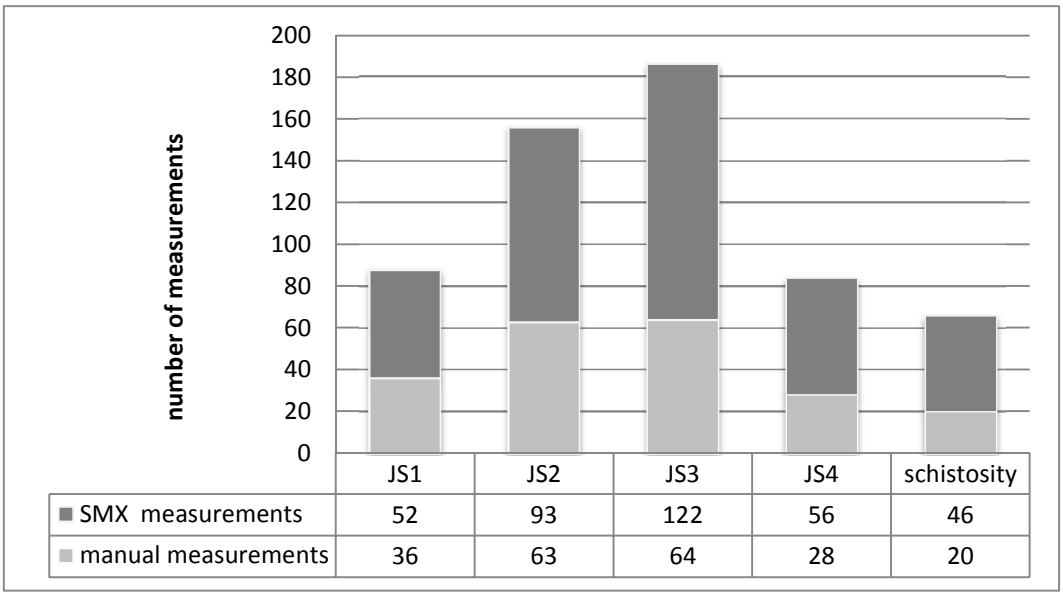

Figure 70: Number of manual and digital measured orientation data for each structure set

6.1 COMPARISON OF MANUAL AND DIGITAL ORIENTATION MEASUREMENTS

Manual and photogrammetric discontinuity orientations were compared. There is a close agreement in terms of discontinuity sets. Comparison of single individual orientations shows partly
larger deviations. There are different causes responsible for these deviations. As discontinuity planes are never perfectly planar a natural variability of discontinuity orientation has to be taken into account. Roughness measurements were carried out again manually and by the use of ShapeMetriX^{3D}. To obtain digital roughness information images were taken in close proximity to discontinuity surface using wide angle objective. A geometric image resolution of 0.1 mm/pixel was used to identify small scale surfaces features on the 3D image. Comparison of manually and digital measured roughness profile has shown that higher roughness amplitudes were obtained for digital profiles which is due to finer resolution of digital images in contrast to the manual roughness measurement device (carpenter comb). Investigations have shown that discontinuity roughness strongly influences orientation results. Depending on the position where orientation measurements are carried out on rough surfaces single orientation measurements can spread up to 16° for the investigated discontinuity surface. The largest deviations (up to 27°) between manually and digital measured discontinuity orientations are observed for obscured discontinuity surfaces representing shadow zones on the 3D image.

6.2 3D MODELS OF ROCK FACE AND DISCONTINUITY ORIENTATIONS

Several 3D models of rock face with different geometrical configurations have been evaluated. Models obtained from stereoscopic image pairs with different focal lengths deliver (f =18 – f=35) comparable orientation results. The quality of models generated from images with focal length of 45 mm gets worse (FB3). For ideal imaging configurations where base length are in the range of B= D/8 – D/5 models were fully reconstructed. Models with base lengths B ≥2/5 D (BA2, BA6, BB2, BB3, BB5 and BB6) were not completely reconstructed. For a configuration with a base length B > 3/5 D it was not possible to generate a model of the rock face (BA3) anymore.
Using a camera angle which deviates 45° from ideal imaging position the generated model is also incomplete (AB3).The use of digital photogrammetry to measure discontinuity orientation has shown that the orientation of discontinuity planes with respect to camera line of sight plays an important role. In Fig.71 and Fig.72 discontinuities with different orientations relative to an “ideal” imaging position almost parallel to exposed rock face sections are illustrated. The individual discontinuities shown below belong to different structure sets (Schistosity, JS1 – JS4). For simplified purposes discontinuity surfaces are represented as square surfaces with equal size. The delineated angles indicate the deviation of surface normals of joint planes to camera line of sight.

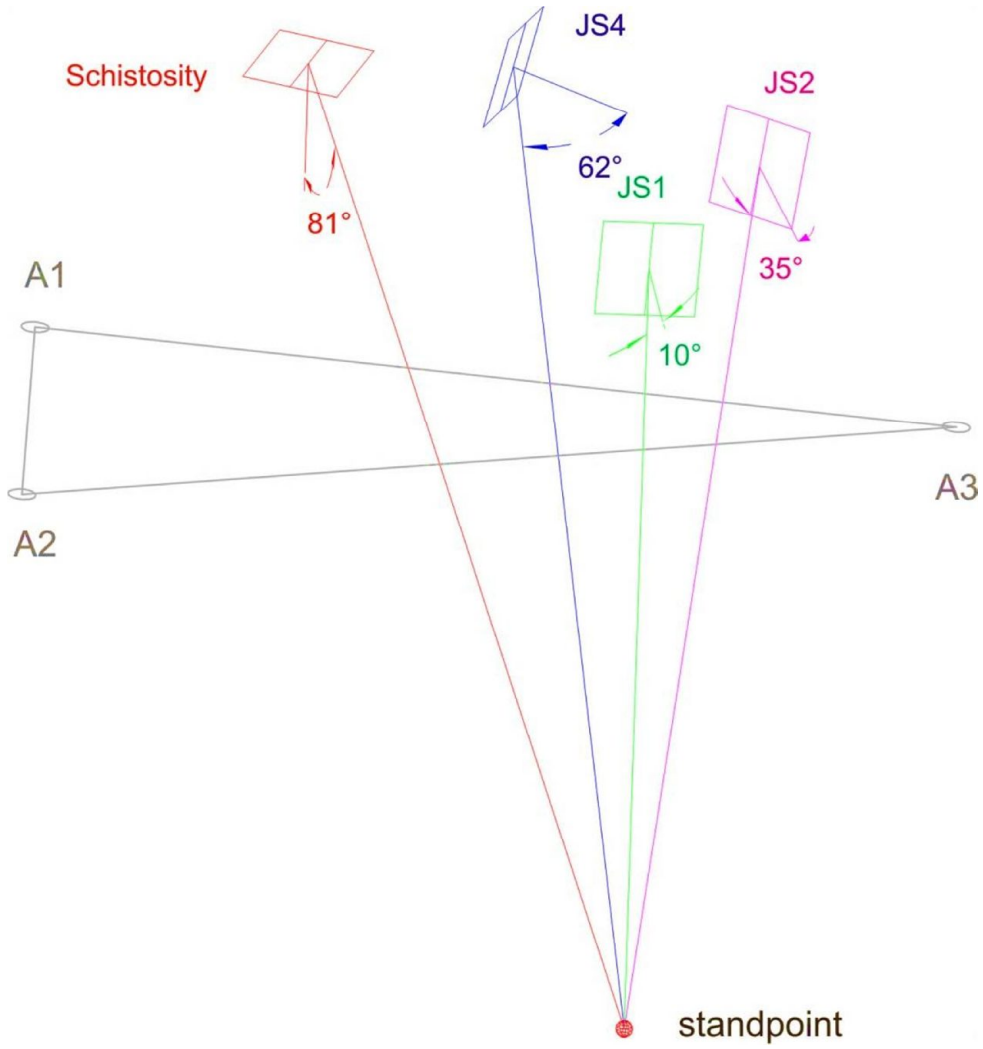

Figure 71: Orientation of individual joints with respect to camera line of sight in Model A (A1,A2 and A3 are reference points)

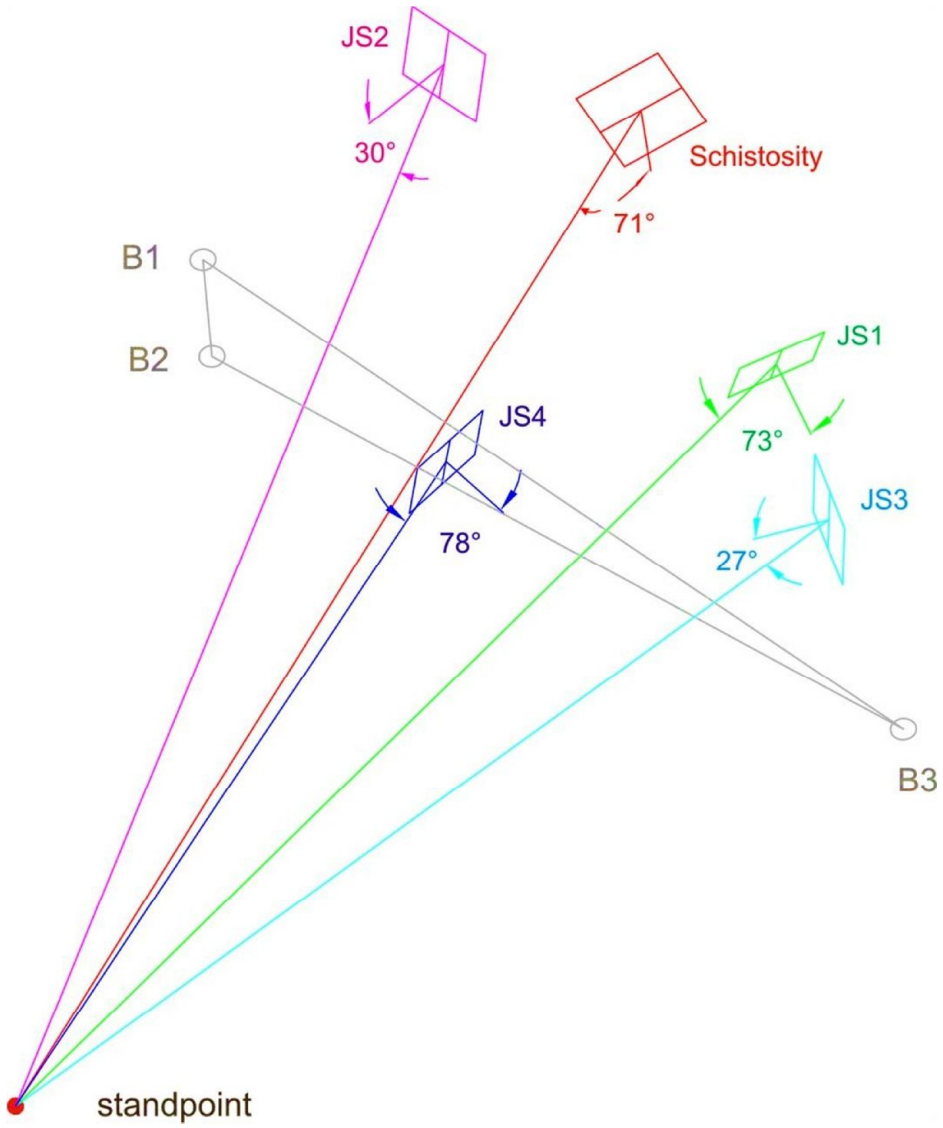

Figure 72: Orientation of individual joints with respect to camera line of sight in Model B (B1,B2,B3 are reference points)

Orientations of sub – horizontal inclined schistosity planes are difficult to measure with compass and as well with SMX measurements. There are only few planes those are day lightening and as these planes are very slightly inclined it is difficult to place the compass lid on the surface in some cases. In digital image sub – horizontal inclined schistosity planes cannot be fully sampled in digital images, thus leading to shadow zones on images. For only few day lighting surfaces the geometry for the reconstruction of points lying on horizontal planes is very poor. This explains the large spread of schistosity orientation results obtained by individual orientation measurements. For some configurations trace measurements deliver more reasonable results (FA2, FB2).

In Model A JS1 is orientated almost normal to camera line of sight. Therefore orientation results are very similar for the different configurations and are not affected by variation of distances (focal lengths) and base lengths. In contrast to this in model B orientation of JS1 is difficult to measure as the camera line of sight intersects joint surfaces in an acute angle for camera standpoints parallel to rock face. Fewer measurements were possible for this joint set and there is a larger spread in orientation results.

Joints of JS2 developed almost parallel to strike direction of the rock face. Numerous orientation measurements were possible to determine similar orientations for different configurations for both models.

Orientation of JS3 is only measureable in model B. Here joints approaching almost normal to camera line of sight. Like for JS2 similar orientation results were achieved for different configurations in model B.

Also sub – vertical inclined joint surfaces of JS4 have comparable orientation results for different configurations in model A. In model B there are almost no day lighting joint surfaces of JS4. As joint traces are visible in the model B only trace measurements were used to determine orientation.

Generally for joints with surface normals almost normal to camera line of sight, trace measurements deliver more reliable results if traces are clearly recognizable and trace measurements are carried out carefully.

BIBLIOGRAPHY

3G SOFTWARE AND MEASUREMENT GMBH, 2006. ShapeMetriX3D, User Manual for Version 3.5

BARTON, N.R. ,1973. Review of a new shear strength criterion for rock joints. *Eng. Geol.* 7, 287-332.

BARTON , N.R. and CHOUBEY, V. 1977. The shear strength of rock joints in theory and practice. *Rock Mech.* 10, 1-54.

BEER, A.J., STEAD, D., COGGAN, J.S., 2002. Estimation of the Joint Roughness Coefficient (JRC) by visual comparison. *Rock Mechanics and Rock Engineering* 35:65–74

FECKER, E., RENGERS, N., 1971. Measurement of large scale roughness of rock planes by means of profilograph and geological compass. *Proceedings symposium on rock fracture, Nancy, France*. pp. 1–18.

FENG, Q., FARDIN, N., JING, L., & STEPANSSON, O., 2003. A new method for in-situ non-contact roughness measurement of large rock fracture surfaces. *Rock Mechanics and Rock Engineering*, (36)1: 3-25.

FRANK W., GENSER J. & NEUBAUER F. 1992: Overview of the Eastern Alps. - ALCAPA Field Guide,IGP/KFU Graz: 7-16.

FRISCH, W., DUNKL, I. & KUHLEMANN, J. 2000: Post-collisional orogen-parallellarge-scale extension in the Eastern Alps. *Tectonophysics* 327, 239–265.

GAICH, A., POETSCH, M., and SCHUBERT, W., 2006. Acquisition and assessment of geometric rock mass feature by true 3D images, in: *Proceedings of the 41st U.S. Symposium on rock mechanics (USRNS), 17–21 June, Golden, Colorado, 2006*.

GIANNI, P., 1992: Rock Slope Stability Analysis. A.A. Balkema, Rotterdam

HOEK,E., and BRAY, J.W. 1981: Rock Slope Engineering. The Institution of Mining and Metallurgy, London, England.

ISRM Commission on Standardization of Laboratory and Field Tests, 1978: 'Suggested Methods for the Quantitative Description of Discontinuities', *International Journal of Rock Mechanics and Mining Sciences and Geomechanics*. Vol. 15, pp. 319-368.

KLICHE, A.C. (1999*). Rock slope stability*. *Society for Mining Metallurgy*. USA, 1999.

KURZ, W., FRITZ, H., TENCZER, V. and UNZOG, W., 2002. Tectonometamorphic evolution of the Koralm Complex (Eastern Alps): constraints from microstructures and textures of the 'Plattengneis' shear zone. *Journal of Structural Geology*, 24(12): 1957-1970.

PISCHINGER, G., KURZ, W., ÜBELEIS, M., EGGER, M., FRITZ, H., BROSCH, F. -J. and STINGL, K. 2008 (a) : Fault slip analysis in the Koralm Massif (Eastern Alps) and consequences for the final uplift of "cold spots" in Miocene times. *Swiss Journal of Geosciences* (2008) 101: 235-254.

PISCHINGER; G, BROSCH, F.-J., KURZ, W. & RANSTITSCH, G., 2008 (b): Normal faulting in a rigid basin boundary block– field evidence from the Koralm Complex (Eastern Alps).- Innsbruck University Press Conference Series, PANGEO Austria 2006, 250-251.

PRIEST, S.D., 1993. Discontinuity analysis for Rock Engineering. Chapman & Hall: London.

PRIEST, S.D., 1985. Hemispherical Projection Method in Rock Mechanics. Allen & Unwin: London

PRIEST, S.D. & J.A. Hudson 1976. Estimation of discontinuity spacing and trace length using scan line surveys. *Int. J. Rock Mech. Min. Sci and Geomech.*, Vol. 18, pp. 183-197.

PUTZ, M., STÜWE, K., JESSELL, M. and CALGANO, P., 2006. Three-dimensional model and late stage warping of the Plattengneis Shear Zone in the Eastern Alps. *Tectonophysics*, 412(1-2): 87-103.

REINECKER, J., 2000: Stress and Deformation: Miocene to present-day tectonics in the eastern alps. *Tübinger Geowissenschaftliche Arbeiten*, A(55): 128.

REINECKER, J. and LENHARDT, W.A., 1999. Present-day stress field and deformation in eastern Austria. *International Journal of Earth Sciences*, 88(3): 532-550.

SCHENK, T., and TOTH, Ch., 1992. "Conceptual Issues ofSoft copy Photogrammetric Workstations," *Photogrammet*ric *Engineering and Remote Sensing,* Vol. 58, No.1, pp.101-
110.

SEKER, D.Z. & TAVIL, A.Ü., 1996, Evaluation of Exterior Building Surface Roughness Degrees by Photogrametric Methods, *Building and Environment*,Vol.31,No.4.pp.393-398.

STURZENEGGER, M. and STEAD, D.: Close-range terrestrial digital photogrammertry and terrestrial laserscanning for discontinuity characterization on rock cuts, Eng. Geol., 106, 163–182, doi:10.1016/j.enggeo.2009.03.004, 2009.

THÖNI M. & JAGOUTZ E. 1992: Some new aspects of dating eclogites in orogenic belts: Sm-Nd, Rb-Srand Pb-Pb isotopic results from the Austroalpine Saualpe and Koralpe type-locality (Carinthia/Styria, SE Austria). - Geochim. Cosmochim. Acta 56: 347-368.

UNAL, M. 2000. *Modelling of discontinuity surface roughness and investigation of its effects on shear strength*, PhD thesis, Hacettepe University, Ankara, 219p.

UNAL, M., UNVER, B. & TERCZAN, A.E. 2000, Modelling ofdiscontinuity surface roughness by digital photogrammetry andgeostatistical methods, *Proc. of 9th Int. Symp. On MinePlanning and Equipment Selection*, Athens, Greece, pp. 391-396.

WALLBRECHER E. (1986): Tektonische und gefügeanalytische Arbeitsweisen.- 244 S., Stuttgart (Enke)

WYLLIE, D.C. and MAH, C.W. (2004): „Rock Slope Engineering" Fourth Edition. Spon Press, Taylor & Francis Group, New York, New York.

ZOBL, F., BRUNNER F.K., WIESER A. (2007): Development of a Digital Geological Compass, *Quarterly Journal of Engineering Geology and Hydrogeology* 2007; v. 40; p. 301-308.

LECTURE NOTES

ZHAO, J. (2008): Rock Mechanics. Course Lectures 2008, Part 3 – Properties of Rock Discontinuities

INTERNET SOURCES

http://www.breithaupt.de

http://www.leica-geosystems.com

http://www.zamg.ac.at/

A. APPENDIX

A1: COORDINATE TRANSFORMATION

Transformation DA-WALD - Zwangspunkte

2 - Stufen DatumstransformationHelmert 2d + 1d

Globale Parameter:

Drehpunkt im altem System (Y, X, H) (m)	0.000	0.000	0.000
Verschiebung (Y, X, H) (m)	-90.130	-577.330	-463.920
Drehung (Y, X, H) (gon)	0.000455	0.001585	0.001634
Maßstab	0.9999976		

Berechnete Parameter:

Lage		
Drehpunkt	-86170.432	196769.063
Verschiebung (Y, X) (m)	0.552	-0.353
Drehung (gon)	399.999673	
Maßstab	0.9999999	
Höhe		
Ebenen-Neigung (gon)	0.000000	0.000000
Verschiebung (m)	-1.136	

Mittlerer Fehler einer Koordinate	0.041
Mittlerer Fehler eines Punktes	0.070

Punkte	Code	Länge Y	Breite X	H H	Klaff	dy [m]	dx [m]	dh [m]	
989#132-189A1	F00	15.191448	46.903404	754.380			3D		**Zwangspunkt 1 Alt**
0#132-189A1	F11	-86919.230	196654.570	706.680	0.052	0.010	-0.010	-0.051	**Neu**
		inklusive Undulation von		0.000 m					
989#384-189A1	F00	15.212805	46.901103	619.076			3D		**Zwangspunkt 2 Alt**
0#384-189A1	F11	-85295.670	196375.200	571.500	0.059	-0.006	-0.007	0.059	**Neu**
		inklusive Undulation von		0.000 m					
989#73-189A1	F00	15.199524	46.909078	699.907			3D		**Zwangspunkt 3 Alt**
0#73-189A1	F11	-86294.740	197276.360	652.260	0.019	-0.004	0.017	-0.008	**Neu**
		inklusive Undulation von		0.000 m					

Transformation DA-WALD

2 - Stufen DatumstransformationHelmert 2d + 1d

Globale Parameter:

Drehpunkt im altem System (Y, X, H) (m)	0.000	0.000	0.000
Verschiebung (Y, X, H) (m)	-90.130	-577.330	-463.920
Drehung (Y, X, H) (gon)	0.000455	0.001585	0.001634
Maßstab	0.9999976		

Berechnete Parameter:

Lage		
Drehpunkt	-86170.432	196769.063
Verschiebung (Y, X) (m)	0.552	-0.353
Drehung (gon)	399.999673	
Maßstab	0.9999999	
Höhe		
Ebenen-Neigung (gon)	0.000000	0.000000
Verschiebung (m)	-1.136	

Punkte	Code	Länge Y	Breite X	H H	Undulation	
989#PP1	00	15.202759	46.905054	557.214		Alt
0#PP1	NN 11	-86054.770	196825.478	509.575	0.000	Neu
989#PP2	00	15.202379	46.904967	557.099		Alt
0#PP2	NN 11	-86083.835	196816.248	509.459	0.000	Neu
989#PP3	11	15.202122	46.904857	557.842		Alt
0#PP3	NN 11	-86103.607	196804.286	510.202	0.000	Neu

A2: POLAR CALCULATION AND COORDINATES OF REFERENCE POINTS

Satzorientierung

Zielpunkte	Code	Y	X	R	t	Ori	Dh Verb [Gon]		Perp [m]
0#PP3	**1**	**-86103.607**	**196804.286**		**Standpunkt**				
0#PP1	1	-86054.770	196825.478	0.0007	73.9359	73.9352	53.236	-0.0024	0.002
0#PP2	1	-86083.835	196816.248	391.4406	65.3609	73.9203	23.109	0.0125	0.005
						Satz =	**1**	**Ori =**	**73.9328**

Polarpunktberechnung

Punkte	Code	Y	X	H	zH	R	t	Z	D	dh Spkt
0#PP3	**11**	**-86103.607**	**196804.286**	**510.202**	**Standpunkt**		**Satz = 1**	**iH = 1.650**		**Ori = 73.9328**
0#PP1	11 Alt:	-86054.770	196825.478	509.575						
	Ber:	-86054.779	196825.476	509.577	1.285	0.0007	73.9336	101.1852	53.236	53.227
	Diff:	0.009	0.002	-0.001						
	AA11Neu:	-86054.770	196825.478	509.575						
0#PP2	11 Alt:	-86083.835	196816.248	509.459						
	Ber:	-86083.831	196816.246	509.468	1.285	391.4406	65.3734	103.0265	23.136	23.110
	Diff:	-0.004	0.003	-0.009						
	AA11Neu:	-86083.835	196816.248	509.459						
0#A1	NN11	-86091.240	196790.135	515.091	0.000	80.3463	154.2791	89.1356	19.070	18.793
0#A2	NN11	-86091.226	196790.103	512.940	0.000	80.3806	154.3135	96.3279	18.858	18.826
0#A3	NN11	-86096.642	196780.518	514.571	0.000	107.9208	181.8537	93.0408	24.917	24.768
0#C1	NN11	-86115.939	196783.370	516.814	0.000	159.9822	233.9150	87.1688	24.783	24.282
0#C2	NN11	-86115.938	196783.352	514.664	0.000	159.9563	233.8891	92.6668	24.459	24.297
0#C3	NN11	-86106.894	196778.205	515.421	0.000	134.0484	207.9813	91.4097	26.528	26.287
0#B1	NN11	-86096.262	196781.851	516.198	0.000	105.9264	179.8593	88.4120	24.004	23.607
0#B2	NN11	-86096.258	196781.829	514.047	0.000	105.9332	179.8660	94.1041	23.730	23.629
0#B3	NN11	-86106.892	196778.202	515.421	0.000	134.0429	207.9758	91.4119	26.531	26.290

A3: COMPASS ORIENTATION MEASUREMENTS

Structure set	Amount of data	Center of gravity [°/°]	Spherical aperture [°]	Parameter of concentration	Degree of orientation [%]	Cone of confidence [°]
Entire Model						
JS1	36	103/86	18.18	19.96	90.26	5.48
JS2	63	327/80	15.41	27.86	92.94	4.31
JS3	64	14/84	15.43	27.80	92.92	4.28
JS4	28	72/78	13.89	33.45	94.24	6.02
Schistosity	20	320/11	9.02	77.38	97.54	3.73
Model A						
JS1	22	285/88	17.03	22.25	91.42	8.50
JS2	40	325/81	14.73	30.17	93.54	5.24
JS4	14	66/80	9.84	63.59	97.08	5.02
Schistosity	12	315/9	8.50	83.93	97.82	4.77
Model B						
JS1	14	100/78	14.55	29.41	93.96	7.45
JS2	23	331/79	15.72	26.06	92.66	7.64
JS3	30	10/82	16.09	25.17	92.32	6.72
Schistosity	8	324/14	8.92	72.64	97.60	6.53
Model C						
JS3	33	17/86	13.90	33.62	94.23	4.38
JS4	13	79/76	13.98	31.64	94.17	7.49

Table 7: Statistics of orientation data for entire Model, Model A , Model B and Model C (compass measurements)

A4: ShapeMetriX ^{3D} ORIENTATION MEASUREMENTS

Structure set	Amount of data	Center of gravity [°/°]	Spherical aperture [°]	Parameter of concentration	Degree of orientation [%]	Cone of confidence [°]
Entire Model						
JS1	52	108/88	16.77	49.81	91.68	4.15
JS2	93	326/79	16.94	23.32	91.51	3.10
JS3	122	15/86	13.75	35.13	94.35	2.19
JS4	56	67/82	11.45	49.81	96.06	2.72
Schistosity	46	315/6	8.80	83.63	97.66	2.31
Model A						
JS1	38	289/85	14.46	31.22	93.76	4.22
JS2	77	328/76	16.42	24.70	92.01	3.31
JS4	22	62/83	8.00	98.60	98.06	3.14
Schistosity	28	320/4	8.08	97.69	98.03	2.77
Model B						
JS1	18	102/75	14.56	29.87	93.68	6.43
JS2	29	330/75	15.92	25.67	92.48	5.38
JS3	57	11/86	15.09	28.99	93.22	3.56
JS4	17	70/81	12.06	43.14	95.64	5.49
Model C						
JS3	60	21/89	11.19	52.19	96.23	2.56
JS4	20	74/79	10.39	58.44	96.75	4.31
Schistosity	4	314/4	2.10	1113.64	99.87	2.75

Table 8: Statistics of orientation data for entire Model, Model A , Model B and Model C (SMX measurements)

Structure set	Amount of data	Center of gravity [°/°]	Spherical aperture [°]	Parameter of concentration	Degree of orientation [%]	Cone of confidence [°]
FA1						
JS1	38	289/85	14.82	29.78	93.46	4.33
JS2	77	323/77	17.24	22.46	91.21	3.48
JS4	20	69/79	13.94	32.73	94.20	5.79
Schistosity	19	133/26	15.28	27.30	93.06	6.54
FA2						
JS1	38	289/84	14.46	31.22	93.76	4.22
JS2	77	328/76	16.42	24.70	92.01	3.31
JS4	20	65/79	11.83	45.17	95.79	4.91
Schistosity	19	141/14	14.28	31.14	93.92	6.11
FA3						
JS1	38	291/89	15.02	29.01	93.29	4.39
JS2	77	323/80	16.47	24.57	91.97	3.32
JS4	20	71/78	13.02	37.45	94.93	5.40
Schistosity	19	141/20	18.49	18.84	89.94	7.94
FA4						
JS1	38	291/88	13.51	35.70	94.55	3.94
JS2	77	322/82	16.50	24.48	91.94	3.33
JS4	20	73/79	13.42	35.27	94.61	5.57
Schistosity	19	146/27	17.41	21.16	91.05	7.47

Table 9: Statistics of orientation data for configuration with variable imaging distances for model A (discontinuity plane measurements)

Structure set	Amount of data	Center of gravity [°/°]	Spherical aperture [°]	Parameter of concentration	Degree of orientation [%]	Cone of confidence [°]
FA1						
JS4	16	64/87	10.53	56.17	96.66	4.96
Schistosity	29	5/5	8.46	89.28	97.84	2.85
FA2						
JS4	16	61/85	7.39	113.21	98.34	3.48
Schistosity	29	320/4	8.08	97.69	98.03	2.77
FA3						
JS4	15	60/84	9.14	73.92	97.47	4.48
Schistosity	27	348/4	6.68	142.20	98.65	2.34
FA4						
JS4	15	65/84	12.83	37.84	95.07	6.30
Schistosity	28	5/5	7.87	102.76	98.12	2.70

Table 10: Statistics of orientation data for configuration with variable imaging distances for model A (discontinuity trace measurements)

Structure set	Amount of data	Center of gravity [°/°]	Spherical aperture [°]	Parameter of concentration	Degree of orientation [%]	Cone of confidence [°]
FB1						
JS1	16	111/80	21.09	14.48	87.05	10.04
JS2	29	330/75	15.92	25.67	92.48	5.38
JS3	57	11/86	15.09	28.99	93.22	3.56
Schistosity	20	190/26	15.13	27.88	93.19	6.29
FB2						
JS1	16	104/80	17.47	20.80	90.99	8.28
JS2	29	329/72	18.90	18.41	89.51	6.41
JS3	57	16/85	15.95	22.43	91.55	7.25
Schistosity	20	194/17	14.56	30.05	93.68	6.05
FB3						
JS1	16	115/80	14.58	29.60	93.67	6.89
JS2	29	331/77	15.05	28.65	93.26	5.09
JS3	57	7/86	14.53	31.21	93.70	3.42
Schistosity	20	174/26	14.67	29.63	93.59	6.10

Table 11: Statistics of orientation data for configuration with variable imaging distances for model B (discontinuity plane measurements)

Structure set	Amount of data	Center of gravity [°/°]	Spherical aperture [°]	Parameter of concentration	Degree of orientation [%]	Cone of confidence [°]
FB1						
JS1	11	101/70	11.71	44.11	95.88	6.95
JS4	17	70/81	12.24	41.91	95.51	5.58
Schistosity	17	307/4	6.59	143.04	98.68	2.99
FB2						
JS1	11	93/67	11.79	43.58	95.83	6.99
JS4	17	61/81	9.44	69.97	97.31	4.29
Schistosity	17	322/8	7.06	124.50	98.49	3.21
FB3						
JS1	11	97/71	12.72	37.51	95.15	7.55
JS4	17	67/82	10.59	55.70	96.62	4.82
Schistosity	17	319/3	7.15	121.67	98.45	3.25

Table 12: Statistics of orientation data for configuration with variable imaging distances for model B (discontinuity trace measurements)

Structure set	Amount of data	Center of gravity [°/°]	Spherical aperture [°]	Parameter of concentration	Degree of orientation [%]	Cone of confidence [°]
BA1						
JS1	38	289/85	14.82	29.78	93.46	4.33
JS2	77	323/77	17.24	22.46	91.21	3.48
JS4	20	69/79	13.94	32.73	94.20	5.79
Schistosity	19	133/26	15.28	27.30	93.06	6.54
BA2						
JS1	38	291/87	14.59	30.71	93.66	4.26
JS2	76	325/79	17.24	22.48	91.22	3.51
JS4	20	70/81	15.33	27.17	93.01	6.38
Schistosity	18	126/29	21.70	13.82	86.33	9.65
BA3	no model	possible				
BA4						
JS1	38	289/84	14.46	31.22	93.76	4.22
JS2	77	328/76	16.42	24.70	92.01	3.31
JS4	20	65/79	11.83	45.17	95.79	4.91
Schistosity	19	141/14	14.28	31.14	93.92	6.11
BA5						
JS1	38	291/85	18.38	19.59	90.06	5.38
JS2	77	327/77	18.11	20.43	90.34	3.66
JS4	20	64/79	14.03	32.32	94.12	5.83
Schistosity	19	144/23	23.00	12.41	87.43	9.93
BA6						
JS1	37	291/86	16.98	22.82	91.47	5.04
JS2	71	324/77	19.76	17.26	88.57	4.17
JS4	37	65/79	15.29	27.32	93.04	6.36
Schistosity	18	140/36	24.62	10.88	82.64	10.98

Table 13: Statistics of orientation data for configuration with variable base lengths for model A (discontinuity plane measurements)

Structure set	Amount of data	Center of gravity [°/°]	Spherical aperture [°]	Parameter of concentration	Degree of orientation [%]	Cone of confidence [°]
BA1						
JS4	16	64/87	10.53	56.17	96.66	4.96
Schistosity	29	5/5	8.46	89.28	97.84	2.85
BA2						
JS4	16	67/86	12.51	39.93	95.30	5.91
Schistosity	30	3/4	9.17	76.07	97.46	3.09
BA3	no model	possible				
BA4						
JS4	16	61/85	7.39	113.21	98.34	3.48
Schistosity	29	320/4	8.08	97.69	98.03	2.77
BA5						
JS4	16	62/85	9.37	70.77	97.35	4.42
Schistosity	30	337/4	11.63	47.54	95.93	3.85
BA6						
JS4	15	57/83	7.31	115.41	98.38	3.57
Schistosity	26	2/3	8.06	97.84	98.03	2.88

Table 14: Statistics of orientation data for configuration with variable base lengths for model A (discontinuity trace measurements)

Structure set	Amount of data	Center of gravity [°/°]	Spherical aperture [°]	Parameter of concentration	Degree of orientation [%]	Cone of confidence [°]
BB1						
JS1	16	111/80	21.09	14.48	87.05	10.04
JS2	29	330/75	15.92	25.67	92.48	5.38
JS3	57	11/86	15.09	28.99	93.22	3.56
Schistosity	20	190/26	15.13	27.88	93.19	6.29
BB2						
JS1	13	122/81	19.76	16.15	88.57	10.64
JS2	26	331/76	19.50	17.26	88.86	7.03
JS3	56	11/85	15.79	26.53	92.60	3.76
Schistosity	19	178/33	17.57	20.79	90.89	7.54
BB3						
JS1	7	134/73	14.20	28.50	93.99	11.50
JS2	26	325/78	19.27	17.66	89.11	6.94
JS3	47	12/86	15.97	25.85	92.43	4.17
Schistosity	16	195/30	13.48	34.52	94.57	6.37
BB4						
JS1	16	104/80	17.47	20.80	90.99	8.28
JS2	29	329/72	18.90	18.41	89.51	6.41
JS3	57	16/85	15.95	22.43	91.55	7.25
Schistosity	20	194/17	14.56	30.05	93.68	6.05
BB5						
JS1	16	111/82	18.89	17.88	89.52	8.97
JS2	29	329/75	19.06	18.11	89.34	6.47
JS3	56	15/84	16.62	24.01	91.82	3.96
Schistosity	20	181/18	17.95	15.85	25.46	6.60
BB6						
JS1	14	116/84	21.67	13.62	86.36	11.18
JS2	24	323/74	21.22	14.63	86.90	8.01
JS3	52	15/85	16.37	24.68	92.05	4.06
Schistosity	15	198/20	11.36	48.12	96.12	5.57

Table 15: Statistics of orientation data for configuration with variable base lengths for model B (discontinuity plane measurements)

Structure set	Amount of data	Center of gravity [°/°]	Spherical aperture [°]	Parameter of concentration	Degree of orientation [%]	Cone of confidence [°]
BB1						
JS1	11	101/70	11.71	44.11	95.88	6.95
JS4	17	70/81	12.24	41.91	95.51	5.58
Schistosity	17	307/4	6.59	143.04	98.68	2.99
BB2						
JS1	11	102/71	11.91	42.72	95.74	7.07
JS4	15	80/84	12.80	38.01	95.09	6.28
Schistosity	16	312/5	10.23	59.43	96.84	4.82
BB3						
JS1	9	105/71	13.42	33.00	94.61	9.10
JS4	11	78/83	10.61	53.61	96.61	6.29
Schistosity	14	332/2	10.39	57.05	96.74	5.31
BB4						
JS1	11	93/67	11.79	43.58	95.83	6.99
JS4	17	61/81	9.44	69.97	97.31	4.29
Schistosity	17	322/8	7.06	124.50	98.49	3.21
BB5						
JS1	11	98/69	14.14	30.45	94.03	8.41
JS4	14	73/82	9.59	66.97	97.23	4.89
Schistosity	17	336(8	6.84	132.69	98.58	3.11
BB6						
JS1	9	97/69	13.62	32.05	94.45	9.23
JS4	10	80/84	9.26	69.51	97.41	5.83
Schistosity	14	311/6	6.88	129.35	98.56	3.51

Table 16: Statistics of orientation data for configuration with variable base lengths for model B (discontinuity trace measurements)

Structure set	Amount of data	Center of gravity [°/°]	Spherical aperture [°]	Parameter of concentration	Degree of orientation [%]	Cone of confidence [°]
AB1						
JS1	19	106/78	21.81	13.73	86.20	9.40
JS2	29	330/75	15.92	25.67	92.48	5.38
JS3	57	11/86	15.09	28.99	93.22	3.56
Schistosity	20	190/26	15.13	27.88	93.19	6.29
AB2						
JS1	18	117/84	18.44	18.88	89.99	8.17
JS2	29	328/77	20.20	16.20	88.08	6.86
JS3	57	11/86	15.84	26.37	92.55	3.70
Schistosity	20	184/19	18.44	18.88	89.99	8.17
AB3						
JS1	18	107/78	17.77	20.28	90.69	7.87
JS2	25	333/80	17.00	22.46	91.45	6.25
JS3	52	13/88	13.63	35.34	94.45	3.37
Schistosity	14	184/29	16.90	21.97	91.55	8.67

Table 17: Statistics of orientation data for configuration with variable camera angles for model B (discontinuity plane measurements)

Structure set	Amount of data	Center of gravity [°/°]	Spherical aperture [°]	Parameter of concentration	Degree of orientation [%]	Cone of confidence [°]
AB1						
JS1	11	101/70	11.71	44.11	95.88	6.95
JS4	17	70/81	12.24	41.91	95.51	5.58
Schistosity	17	307/4	6.59	143.04	98.68	2.99
AB2						
JS1	11	101/72	15.94	24.11	92.46	9.49
JS4	13	72/83	11.75	44.50	95.85	6.28
Schistosity	17	333/4	7.02	125.85	98.50	3.19
AB3						
JS1	10	100/71	6.80	128.54	98.60	4.28
JS4	10	66/73	7.95	94.20	98.09	5.00
Schistosity	12	306/7	8.58	82.36	97.77	4.81

Table 18: Statistics of orientation data for configuration with variable camera angles for model B (discontinuity trace measurements)

LIST OF FIGURES

LIST OF TABLES